DYNAMICAL APPROACH STUDY OF SPURIOUS STEADY-STATE NUMERICAL SOLUTIONS OF NONLINEAR DIFFERENTIAL EQUATIONS: II

H.C. Yee and P.K. Sweby

RNR Technical Report RNR-92-008, March 1992

NAS Applied Research Technical Report
RNR-92-008, March 1992, NASA Ames Research Center

DYNAMICAL APPROACH STUDY OF SPURIOUS STEADY-STATE NUMERICAL SOLUTIONS OF NONLINEAR DIFFERENTIAL EQUATIONS

II. *The Dynamics of Numerics of Systems of* 2×2 *ODEs and Its Connection to Finite Discretizations of Nonlinear PDEs*[1]

H.C. Yee[2]
NASA Ames Research Center, Moffett Field, CA 94035, USA
and
P.K. Sweby[3]
University of Reading, Whiteknights, Reading RG6 2AX, England

ABSTRACT

The objective of this paper is to study the dynamics of numerics of time discretizations for various 2×2 systems of first-order autonomous nonlinear ordinary differential equations (ODEs) with known analytic solutions. The main emphasis is to gain a basic understanding of the difference in the dynamics of numerics between the scalars and systems of nonlinear ODEs. It is found that in addition to the phenomenon of stable spurious steady-state numerical solutions occurring below and above the linearized stability limit of the exact steady states, more complex phenomena such as stable spurious limit cycles, stable spurious higher dimensional tori and the changing type and stability of numerical asymptotes were observed. With the aid of a parallel Connection Machine (CM2), the complex behavior and sometimes fractal like structure of the associated basins of attraction of the various widely used time discretizations in computational fluid dynamics (CFD) are revealed and compared. The underlying purpose of this study is to set the baseline global asymptotic solution behavior of the schemes so that one can use them more wisely in other more complicated settings such as when nonlinear systems of partial differential

---

[1] Part of the material appeared in the Proceedings of the 9th GAMM Conference on Numerical Methods in Fluid Mechanics, Lausanne, Switzerland, Sept. 25-27, 1991 and as an University of Reading numerical analysis report - 7/91, October 1991.

[2] Staff Scientist, Fluid Dynamics Division.

[3] Lecturer, Department of Mathematics; part of this work was performed as a visiting scientist at the NASA Ames Research Center; support of this visit was funded through the NAS Applied Research Branch of NASA Ames.

equations (PDEs) for which the exact solutions are not known are encountered in nonlinear sciences and in particular in CFD. This is especially important when there are no experimental data for comparison and/or when the numerical solution indicates a new flow structure not easily understood. The results of this investigation can be used as an explanation for possible causes of error, and slow convergence and nonconvergence of steady-state numerical solutions when using the time-dependent approach for nonlinear hyperbolic or parabolic PDEs. The knowledge gained can also aid the construction of appropriate iteration methods, relaxation procedures, or preconditioners for convergence acceleration strategies in numerically solved boundary-value problems of nonlinear PDEs, since most of these procedures can be viewed as approximations of time-dependent PDEs. It can also enhance the understanding of flow patterns in 2-D and 3-D flow visualizations of numerical data.

I. INTRODUCTION

The tool that is utilized for the current study belongs to a multidisciplinary field of study in numerical analysis, sometimes referred to as "The Dynamics of Numerics and The Numerics of Dynamics[4]". Here, to study the dynamics of numerics (dynamical behavior of a numerical scheme) means to study the local and global asymptotic behavior and bifurcation phenomena of the nonlinear difference equations resulting from finite discretization of a nonlinear differential equation (DE) subject to the variation of discretized parameters such as the time step, grid spacing, numerical dissipation coefficient, etc. In this paper, standard terminologies in nonlinear dynamics, chaotic dynamics [1-4] and computational fluid dynamics (CFD) are assumed. For an introduction to the dynamics of numerics and its impliciations for algorithm development in CFD, see [5,6] and references cited therein. To keep this paper somewhat self-contained, some of the ideas and logistics discussed in [5-8] that motivated the present study are repeated here.

1.1. Background

The phenomenon that a nonlinear DE and its discretized counterpart can have different dynamical behavior (asymptotic behavior) was not uncovered fully until recently. Aside from truncation error and machine round-off error, a more fundamental distinction between the DE (continuum) and its discretized counterparts for genuinely nonlinear behavior is extra solutions in the form of spurious stable and unstable asymptotes that can be created by the numerical method. Here we use the term "spurious asymptotic numerical solutions" to mean asymptotic solutions that satisfy the discretized counterparts but do not satisfy the underlying ordinary differential equations (ODEs) or partial differential equations (PDEs). Asymptotic solutions here include steady-state solutions (fixed points of period one), periodic solutions, limit cycles, chaos and strange attractors. See section III and [1-5] for definitions.

Iserles [9] showed that while linear multistep methods (LMMs) for solving ODEs possess only the fixed points (fixed points of period one) of the original DEs, popular Runge-Kutta methods may exhibit additional, spurious fixed points. It has been demonstrated (see for example [5,10,11] for the scalar case, and [7,8] for nonlinear reaction-convection model equations) that such spurious fixed points may be stable below the linearized stability limit of the scheme. More recently Iserles et al. [12,13], Hairer et al. [14] and Humphries [15] further advanced the theoretical understanding of the dynamics of numerics for ODE solvers. Iserles et al. and Hairer et al. classified and gave guidelines and theory on the types of Runge-Kutta methods that do not exhibit spurious period one or period two fixed points. Humphries [15] showed that under appropriate assumptions if stable spurious fixed points exist as the time-step approaches zero, then they must either approach a true fixed point or become unbounded. However, convergence in practical calculations involves a finite time step Δt as the number of integrations $n \to \infty$ rather than $\Delta t \to 0$, as $n \to \infty$. There appear to be missing links between theoretical development and practical scientific computation. Our aim is to provide some of these missing links. To be more precise, we want to study the global asymptotic behavior of ODE solvers for

[4] Named after the First IMA Conference on Dynamics of Numerics and Numerics of Dynamics, University of Bristol, England, July 31 - August 2, 1990

nonlinear ODEs when finite but not extremely small Δt is used.

One consequence of the existence of spurious asymptotes below or above the linearized stability limit of the schemes is that these spurious features may greatly affect the dynamical behavior of the numerical solution in practice due to the use of a finite time step. Indeed this will be the case not only for stable spurious asymptotes but also for unstable spurious asymptotic numerical solutions. More importantly, spurious fixed points other than period one and numerical chaos can be admitted by even the LMMs, including the simple Euler scheme. See [5,16] and section V for details. Thus, associated with the same (common) steady-state solution, the basin of attraction of the DEs (which initial conditions lead to which asymptotic states) might be very different from that of the basin of attraction of the discretized counterparts [5,8,16-18] due to the existence of spurious stable and unstable asymptotic numerical solutions. The result is a separate dependence on initial data for the individual DEs and their discretized counterparts. In other words, it is possible that for a given physical initial datum (associated with a particular steady state of the nonlinear DE) the numerical solution can converge to a wrong (but physical) steady state or a spurious asymptote. Here, a basin of attraction is the set of initial data whose solution curves all converge towards the same asymptote. As can be shown from our investigation, the difference in the basins of attraction between the continuum and its discretized counterparts occurs even when a linearized form of an implicit unconditionally stable LMM type of method is used (see also [8,18]). The difference is less pronounced if the resulting nonlinear algebraic equations are solved by a desired iteration procedure [9]. The various aspects that are addressed in this paper but not in [9] for different iteration procedures in solving the resulting nonlinear algebraic equations will be reported in a future paper.

1.2. Relevance and Motivations

Although the understanding of the dynamics of numerics of systems of nonlinear ODEs is important in its own right and has applications in the various nonlinear science fields, our main emphasis is CFD applications. Time-marching types of methods are commonly used in CFD because the steady PDEs of higher than one dimension are usually of the mixed type. When a time-dependent approach is used to obtain steady-state numerical solutions of a fluid flow or a steady PDE, a boundary value problem (BVP) is transformed into an initial-boundary value problem (IBVP) with unknown initial data. If the steady PDE is strongly nonlinear and/or contains stiff nonlinear source terms, phenomena such as slow convergence, nonconvergence or spurious steady-state numerical solutions can occur even though the time step is well below the linearized stability limit and the initial data are physically relevant. One of our goals is to search for logical explanations for these phenomena via the study of the dynamics of numerics. Here the term "time-dependent approach" is used loosely to include some of the iteration procedures (due to implicit time discretizations), relaxation procedures, and preconditioners for convergence acceleration strategies used to numerically solve steady PDEs. This is due to the fact that most of these procedures can be viewed as approximations of time-dependent PDEs (but not necessarily the original PDE that was under consideration). If one is not careful, numerical solutions other than the desired one of the underlying PDE can be obtained (in addition to spurious asymptotes due to the numerics).

It is a common practice in CFD to use fixed, variable or "local" time stepping in conjunction with standard relaxation procedures and preconditioners to accelerate convergence to steady-state numerical solutions. Usually these strategies consist of tuning parameters and are highly scheme and problem dependent. In addition, unlike ODE solvers, good error control in variable time step procedures for time-dependent PDEs has not been established. Moreover, for implicit time-marching schemes the use of a local time step procedure does not always perform better than a fixed time step procedure, depending on the type of implicit linearization, acceleration strategies and flow physics. See for example [19]. There appears to be no systematic generalized theory to guide in automating the tuning of these parameters or the choosing of time-stepping procedures. It is our belief that the understanding of the symbiotic relationship between the strong dependence on initial data and permissibility of spurious stable and unstable asymptotic numerical solutions at the fundamental level can guide the tuning of the numerical parameters and the proper and/or efficient usage of numerical algorithms in a more systematic fashion. It can also explain why certain schemes behave nonlinearly in one way but not another. Here strong dependence on initial data means that for a finite Δt that is not sufficiently small (approaching zero), the asymptotic numerical solution depends almost continuously on the initial data. Unlike nonlinear problems the asymptotic numerical solutions of linear or weakly nonlinear problems are independent of Δt as long as Δt is below a certain upper bound. We remark that strong dependence on initial data is different from sensitivity to initial data in chaotic phenomenon.

Due to the complexity of the subject matter, all of our study concerns fixed time step (and fixed grid spacing) time-marching methods. The fixed or variable time step study can also shed some light in identifying whether certain flow patterns are steady or unsteady. See [19-21] for some examples. Proper regulation of a variable time step to prevent the occurence of spurious steady-state numerical solutions will be a subject of future research. Also, we remark that in order to isolate the different causes and cures of slow convergence and nonconvergence of time-marching methods, our study concerns nonlinearity and stiffness that are introduced by DEs containing smooth solutions. Nonlinearity and stiffness that are introduced by the scheme, the coupling effect in the presence of a source term (terms) in coupled system of PDEs, the highly stretched nonuniform structured and unstructured grids, the discontinuities in grid interfaces and/or the discontinuities inherent in the solutions, and external flows that need special boundary condition treatment with a truncated finite computation domain are added factors and require additional treatment or different analysis. These are not considered at the moment. The reader is reminded that our attempt is to explain (besides the aforementioned factors) one of the basic causes of error, slow convergence and nonconvergence of time-marching methods in practical computations.

Nonunique steady-state solutions of nonlinear DEs vs. Spurious Asymptotes: The phenomenon of generating spurious steady-state numerical solutions (or other spurious asymptotes) by certain numerical schemes is often confused with the nonuniqueness (or multiple steady states) of the DE. In fact, the existence of nonunique steady-state solutions of the continuum can complicate the numerics tremendously (e.g., the basins of attraction) and is independent of the occurence of spurious asymptotes of the associated scheme. But, of course, a solid background

in the theory of nonlinear ODEs and PDEs and their dynamical behavior is a prerequisite in the study of the dynamics of numerics for nonlinear PDEs. Table 1.1 shows the possible stable asymptotic solution behavior for DEs and their discretized counterparts. See Yee et al. [5] for a discussion. It is noted that the approach and primary goal of our work is quite different from the work of e.g., Beam and Bailey [22] and Jameson [23]. The main goal of [22] and [23] is to study the nonunique steady-state solutions admitted by the PDE as the physical parameter is varied. Our primary interest is to establish some working tools and guidelines to help delineate the true physics from numerical artifacts via the dynamics of numerics approach. The knowledge gained from our series of studies [5,7,8] hopefully can shed some light on the controversy about the existence of multiple steady-state solutions through numerical experiments for certain flow types of the Euler and/or Navier-Stokes equations.

Linearized Analysis vs Nonlinear Solution Behavior: Another phenomenon is that the use of linearized analysis as a guide to numerically studying strongly nonlinear DEs (ODEs or PDEs) may be insufficient and may lead to misleading results. Linearized stability analysis (with the inital data sufficiently close to the exact solution) sometimes can only supply part of the nonlinear stability behavior, e.g., before a bifurcation point occurs [1-4], since linearized stability is a local phenomenon. If it is possible, performing a global bifurcation analysis would elucidate a more complete nonlinear stability behavior. To obtain a global picture of the nonlinear stability of the bifurcation part of the analysis, one has to resort to more sophisticated mathematical tools such as local and global bifurcation theories [1-4]. This distinction between linearized stability and nonlinear stability analysis is carried over to the discretized counterparts as well and is used in the discussion throughout the paper. The distinction between linearized analysis and nonlinear analysis was discussed and illustrated in [5,7,8,17]. For the discretized counterpart, the situtation is further compounded in practical computations for highly coupled nonlinear systems of PDEs where the exact linearized stability limit is usually not computed, but rather a frozen coefficient procedure at each time step with a fixed grid spacing is used to approximate the stability limit. Thus, if one is not careful, it is possible that erroneous results can be achieved unknowingly in practical computations.

Depending on the initial data and the scheme, the possible asymptotic solution behavior of numerical schemes operating at time steps below or above the von Neumann limit, CFL limit or linearized stability limit for nonlinear ODEs and/or time-dependent nonlinear PDEs is summarized in Table 1.2. Here, the CFL limit is different from the linearized stability limit. Note that strictly speaking von Neumann and CFL limits are different but their limits may be the same. In Tables 1.2 and 1.3 we have grouped them in the same category. The definition of linearized stability is stated in Table 1.3. Each of the phenomena listed in Table 1.2 can be supported by simple model DEs with commonly used finite discretizations in CFD (cf. [5,8,16,17] and the present paper). Table 1.3 compares the various guidelines, assumptions, usage and applicability of four different methods in obtaining stability criterion for time step constraints for the time-dependent approach to the steady-state numerical solutions. Note that the third row under the assumption and usage heading (concerning inside and outside the stability interval) reflects some of the conventional practice in CFD rather than a statement of truth. A high percentage of the current computer codes in CFD are operated under the guidelines of the first stability

criterion. Without the source term, the first three stability procedures are equivalent for 1-D linear initial value problems. In the absence of source terms in nonlinear problems, the first three procedures are equivalent when the iterated solutions are very near the exact steady-state solution, since perturbing around the iterated solution at the "frozen coefficient or time level n" is approximately equal to perturbing around the exact steady state. When multiple steady states of the governing DE and/or spurious asymptotes exist and/or in the presence of source terms, these procedures are different. Although the last three stability procedures cannot be realized in practice, they are in the order of increasing importance in providing closer stability behavior for strongly nonlinear problems.

1.3. Primary Goal of This Series of Four Papers

The primary goal of this series of papers has been expanded since part I was published. The underlying purpose of this paper and the companion papers [5,7,8] (under the assumptions stated in the second and third paragraphs of section 1.2) is to lay the foundation for the utilization of the dynamics of numerics in algorithm development for computational sciences in general and CFD in particular. The intent of these papers is (a) to reveal the logistics, methodology, and usages of nonlinear dynamics for CFD, (b) to complement the commonly used linearized stability theory in CFD, (c) to search for possible explanations on the causes of errors and slow convergence and nonconvergence of steady-state numerical solutions when using the time-dependent approach to the steady states, (d) to guide the construction of appropriate iteration methods, relaxation procedures, or preconditioners for convergence acceleration strategies in numerically solved BVPs of nonlinear PDEs and (e) to enhance the understanding of flow visualization of numerical data such as lines of separation and re-attachment points, etc. Referring to the last issue, if the governing PDE and/or its discretized counterparts possess higher than three-dimensional (or infinite dimensional) dynamical behavior, the projections of these higher dimensional dynamics onto a 2-D or 3-D topology can lead to misinterpretation of flow types. As can be seen later, depending on the scheme, initial data and discretized values, the numerics can alter the true flow type. See Refs. [24-32] for some investigations and issues on the study of flow visualizations. Referring to the third and fourth issues above, in many CFD computations the steady-state equations are PDEs of the mixed type and a time-dependent approach can avoid the complication of dealing with elliptic-parabolic or elliptic-hyperbolic types of PDEs.

This is part II of a series of papers on the same topic. Part I [5] concentrated on the dynamical behavior of time discretizations for scalar nonlinear ODEs. The intent of part I was to serve as an introduction to motivate this concept to researchers in the field of CFD and to present new results for the dynamics of numerics for first-order scalar autonomous ODEs. The present paper, the second of this series, is devoted to the study of the dynamics of numerics for 2×2 systems of ODEs. Lafon and Yee [7], the third of this series, was devoted to the study of the dynamics of numerics of commonly used numerical schemes in CFD for a model reaction-convection equation. Part III addressed four different numerical aspects of a model reaction-convection equation. It can be shown that (1) stable and unstable spurious steady-state numerical solutions can be independently introduced by spatial and temporal discretizations satisfying the same

boundary condition and initial data, (2) the various ways of discretizing (spatial and/or temporal) the reaction term can affect the stability of the spurious as well as the exact steady-state solutions, and (3) the numerical phenomenon of incorrect propagation speeds of discontinuities can be linked to the existence of some stable spurious steady-state numerical solutions. The possible cause of convergence to a spurious steady state and a suggestion to avoid spurious steady states were also discussed in part III. Lafon and Yee [8], the fourth of this series was devoted to a more detailed study of the effect of numerical treatment of nonlinear source terms on nonlinear stability of the steady-state numerical solution for the same model nonlinear reaction-convection BVP. The symbiotic relationship between the strong dependence on initial data and the permissibility of spurious stable and unstable asymptotic numerical solutions for implicit numerical treatment of the source terms with linearization, as well as more detailed nonlinear analysis than [7] of explicit numerical treatment of the source terms were considered. A summary of [7,8] can be found in [33]. A summary of the four parts and the logistics and the methodology for the dynamics of numerics in numerical algorithm development for CFD were summarized in [6]. Reference [6] also revealed the difficulties behind the construction of suitable numerical schemes and discussed preliminary ideas for constructing numerical schemes for hypersonic reacting flows and combustion related problems. In our companion papers [10,11], a theoretical bifurcation analysis of a class of explicit Runge-Kutta methods was presented.

1.4. Objectives

The symbiotic relationship between the strong dependence on initial data and the permissibility of spurious stable and unstable asymptotic numerical solutions for commonly used time discretizations in CFD is illustrated for four different nonlinear model ODEs with known analytic solutions. This is an attempt to understand the global asymptotic behavior of time discretizations for highly nonlinear and stiff DEs. The objective is to gain a basic understanding of the difference in the dynamics of numerics between scalars and systems of strongly nonlinear ODEs. A primary distinction between the dynamics of scalars and systems of first-order autonomous ODEs is that there is no limit cycle or higher dimensional tori counterparts for the scalar case. Consequently, spurious limit cycles, higher dimensional tori or the changing type and stability of fixed points can be introduced by the numerics when solving systems of ODEs [16]. For example, saddle points can become stable or unstable nodes even though the flow type of the DE remains unchanged. As can be seen from the present study, these phenomena are independent of whether the schemes are explicit or implicit and/or LMMs. We conjecture that the existence of stable spurious limit cycles might be one of the contributing factors in nonconvergence of the time-dependent approach to the steady state. Also the various spurious features of the numerics can contribute to the misinterpretation of flow types in flow visualizations of numerical data. The underlying goal is to investigate the effect of time discretizations on the existence and stability of spurious asymptotic numerical solutions of PDEs when time splitting [34], method of lines (MOL) [35], finite element methods, and inertial manifold (IM) [36-44] and approximate inertial manifold (AIM) [45,46] approaches are used to numerically approximate certain types of hyperbolic and parabolic PDE solutions. Referring to the second approach, depending on the number of grid points "J" used, the dimensions of the resulting

system of semi-discrete approximations of ODEs can be very large. From the theory of nonlinear dynamics for ODEs, it is well known that much of the established theory and known behavior of nonlinear dynamics are restricted to lower dimensional first-order ODEs (or for problems that exhibit lower dimensional dynamical behavior). In addition, if higher than two time levels of ODE solvers are used, the dynamics of these discretized counterparts usually are richer in structure and more complicated to analyze than their one or two time-level ODE solver cousins. Therefore, in order to gain a first hand understanding of the subject we restrict our study to 2×2 systems of first-order autonomous ODEs and two time-level ODE solvers with a fixed time step. See sections IV - VI for more details.

Outline: The outline of this paper is as follows. Section II discusses the connection of the dynamics of numerics for systems of ODEs and numerical approximations of time-dependent PDEs. We also discuss in what manner the study of the dynamics of numerics can enhance the understanding of flow patterns in 2-D and 3-D flow visualization of numerical data obtained from finite discretization of a PDE. Section III reviews background material for nonlinear ODEs and ODE solvers. Section IV describes four 2×2 systems of nonlinear first-order autonomous model ODEs. Section V describes the 11 time discretizations (ODE solvers) and the associated bifurcation diagrams for the four model ODEs. Section VI discusses the combined basins of attraction and bifurcation diagrams for the underlying schemes for the four model equations. Comparison between a linearized implicit Euler and Newton method is briefly discussed in section 6.5. The paper ends with some concluding remarks in section VII.

II. CONNECTIONS BETWEEN THE DYNAMICS OF NUMERICS OF SYSTEMS OF ODEs AND NUMERICAL APPROXIMATIONS OF TIME-DEPENDENT PDEs

For finite discretizations of PDEs, spurious asymptotes and especially spurious steady states can be independingly introduced by time and spatial discretizations [7,8,18]. The interaction between temporal and spatial dynamical behavior is more complicated when one is dealing with the nonseparable temporal and spatial finite-difference discretization such as the Lax-Wendroff type. Also, the analysis would be more complex if the governing nonlinear PDE possessed more than one stable steady-state solution in addition to the spurious ones that are purely due to the numerical method.

In order to gain a first hand understanding of the dynamics of numerics for time-dependent PDEs, separable temporal and spatial finite difference methods (FDM) should be studied first since the analysis and the different features of the numerics due to temporal and spatial discretizations can become more apparent by this type of FDM. A standard method for obtaining such a FDM is the method of lines procedure where the time-dependent PDE is reduced to a system of ODEs (by replacing the spatial derivatives by finite difference approximations). The resulting approximation is called semi-discrete, since the time variable is left continuous. The semi-discrete system in turn can be solved by the desired ODE solvers. Similar semi-discrete systems can be obtained by finite element methods except in this case an additional mass matrix is involved. Besides the MOL approach, coupled nonlinear ODEs can arise in many other ways when analyzing nonlinear PDEs. See for example [24-32,36-50]. Among these possibilities, the idea of IM and AIM for incompressible Navier-Stokes [36-46], the relationship between shock waves, heteroclinic orbits of systems of ODEs [49,50], and flow visualization of numerical data [24-32] are touched upon in sections 2.3 - 2.5.

2.1. Bifurcation Study by the Method of Lines Approach
(For Time-Dependent Approach to the Steady-State Numerical Solutions)

With the MOL procedure the analysis of the occurrence of spurious asymptotes for the FDM can be split into five separate stages. First, the fixed points or the steady solutions for each of the associated systems of ODEs are solved. Second, the types of bifurcation phenomena in terms of variation of system parameters as well as the discretized parameters such as grid spacing, coefficient of numerical dissipation, etc. are identified. Third, the linearized stability and nonlinear stability (in terms of bifurcation theory) around these fixed points are analyzed. Fourth, a bifurcation analysis similar to the fourth stage for the fully discretized set of nonlinear finite difference equations is performed. Fifth, time discretizations are applied to the semi-discrete system of ODEs and linearized stability is performed to investigate in what manner the time discretization can destabilize the stable spurious steady states or vice versa. Note that the order of stages (4) and (5) is not important. Stages one to three involves spurious asymptotes strictly introduced by the spatial discretizations. Stages four and five involves spurious asymptotes introduced by both the time and spatial differencings. See [7] for the five stages of analysis for a model reaction-convection equation.

Some global solution behavior of these fixed points can be obtained by the pseudo arclength continuation method devised by Keller [51], a standard numerical method for obtaining bifurcation curves in bifurcation analysis. A popular bifurcation computer program AUTO [52] (which contains the pseudo arclength continuation method) can be modified to cater to the PDE study. As can be seen from our study [7,8], one deficiency of the pseudo arclength continuation method (AUTO) is that it cannot provide the complete bifurcation diagram since a known solution for each of the main bifurcation branches is needed before one can continue the solution along a specific main branch. For spurious asymptotes that are due to the numerics, it is usually not easy to even locate just one solution on each of these branches. To obtain the complete global asymptotic numerical solution behavior, knowledge of the associated basins of attraction is necessary. Due to the size of the problem, our approach, in addition to using the pseudo arclength continuation method to obtain selected cases of the bifurcation diagrams and analytical means (if possible), is to obtain the majority of the cases by a large number of numerical integrations on the NASA Ames CM2. The CM2 enables us to obtain a detailed picture of the global dynamical behavior of the discretizations which would have been impossible using scalar or vector machines.

The results of this paper indirectly can provide a basic background for the last two stages of bufurcation study by the MOL approach. The authors feel that this is the most straight-forward way of gaining a complete understanding of what 'really' is happening at the fundamental level. But the key point is that if the ODEs are obtained from some kind of semi-discrete approximations of PDEs, the resulting system of ODEs should contain additional system parameters and discretized parameters as opposed to physical problems governed by ODEs. Depending on the differencing scheme the resulting discretized counterparts of a PDE can be nonlinear in Δt, the grid spacing Δx and the numerical dissipation parameters, even though the DEs consist of only one parameter or none. It is the introduction of new parameters due to the finite discretization that add a new dimension to the implication and interpretation of accuracy, stability and convergence rate of asymptotic numerical solutions of strongly nonlinear PDEs. Furthermore, it is important to distinguish between the complexity involved in the analysis of the dynamics of numerics for ODEs and PDEs. The dynamics of numerics for PDEs involves spatial as well as temporal dynamical behavior. Spurious asymptotes exist even for nonlinear hyperbolic conservation laws containing zero source terms (cf. [17] and section V). Also, one might be able to choose a "safe" ODE solver to avoid spurious stable steady states due to time discretizations. However, spurious steady states introduced by spatial discretizations in nonlinear hyperbolic and parabolic PDEs for CFD applications appear to be more difficult to avoid. In the case of MOL approach, if spurious steady states due to spatial discretizations exist, the resulting ODE system has already inherented this spurious feature as part of the exact solutions of the semi-discrete case. We remark that spurious stable and unstable asymptotes other than the steady states due to time and/or spatial discretizations are even more difficult to avoid than spurious steady states. See sections V and VI for some illustrations. Taking for example the nonlinear ODE models that are considered, it is relatively easy to avoid spurious steady states since if a numerical steady state U^* for the ODE $dU/dt = S(U)$ is spurious, then $S(u^*) \neq 0$. This is not the case for spurious asymptotes such as limit cylces.

Note that nonlinearity can also be introduced by nonlinear schemes (in space) themselves.

Schemes such as the total variation diminishing (TVD) and essentially nonoscillatory (ENO) schemes can introduce nonlinearity into the discretized equation even though a linear constant hyperbolic equation is used. See reference [53] for a background on this subject. This aspect requires a separate investigation. Nonlinearities and stiffness that are introduced by other sources as stated at the end of section 1.2 are a subject of future research. What is of concern in this paper and the companion papers deals with nonlinearity and stiffness that are introduced by the DE.

2.2. Possible Stable Asymptotic Solution Behavior for DEs and Their Discretized Counterparts

Recall that Table 1.1 gives a comparison of the possible stable asymptotic solution behavior of DEs (ODEs or PDEs) and their discretized counterparts. To be precise, consider a nonlinear scalar reaction-convection-diffusion model equation

$$\frac{\partial u}{\partial t} + \frac{\partial f(u)}{\partial x} = \varepsilon \frac{\partial^2 u}{\partial x^2} + \alpha S(u) \qquad \varepsilon, \alpha \text{ system parameters} \tag{2.1}$$

where $f(u)$ is a linear or nonlinear function of u. The nonlinear source term (or the reaction term) $S(u)$ can be very stiff. Equation (2.1) can be viewed as a model equation in combustion or as one of the species continuity equations in nonequilibrium flows (except in this case, the source term is coupled to other species mass fractions). Table 2.1 shows the classification of the types of one-dimensional scalar time-dependent PDEs that are considered with time and space variables that do not explicitly appear in the coefficients or nonlinear terms of the equations. Also, the considered PDEs are conservation laws if the source term is not present in the hyperbolic PDEs. Tables 2.2 and 2.3 show the possible existence of spurious asymptotic numerical solutions for the MOL (or separable time and spatial discretizations) approach of obtaining the full discretization for the type of scalar one-dimensional PDEs shown in Table 2.1. Tables 2.2 and 2.3 assume the use of conservative schemes for the convection term. One can see the drastic difference in the dynamics of numerics on linear and nonlinear time-dependent PDEs. Depending on the types of PDEs and the associated numerical methods, the interplay between the spatial and time discretizations on the permissibility of spurious asymptotes can be very complex. The majority of the phenomena shown in Tables 1.1, 2.2 and 2.3 are supported by simple examples in Refs. [5,7,8] and the present paper. If implicit LMMs are used for the time discretization and if the resulting nonlinear alegbraic systems are solved exactly, some of the results stated in tables 2.2 and 2.3 can be avoided. However, if the nonlinear algebraic systems are solved iteratively, some of the results stated in Tables 2.2 and 2.3 are also possible. In addition, if nonlinear spatial discretization such as TVD or ENO schemes is used, some of the results stated in tables 2.2 and 2.3 might not be valid since nonlinear spatial discretizations can introduce nonlinearities into the discretized counterpart even if the PDE is linear. In other words, columns with the words "NO" in Tables 2.2 and 2.3 can be replaced with a "YES". Tables 1.1, 2.2 and 2.3 reveal much of the nonlinear effects which cannot be explained fully by linearized analysis except in unique cases or in weakly nonlinear problems.

2.3. Inertial Manifold (IM) and Approximate Inertial Manifold (AIM)

The concept of IMs was introduced by Foias, Sell and Temam [36] in 1985. See Refs. [36-44] for details of the subject. The key idea of IMs and AIM is to establish theories to aid in better understanding of nonlinear phenomena and turbulence via the study of the interaction of short and long wavelengths of dissipative systems. In summary, an IM is a finite-dimensional submanifold that contains all the attractors and invariant sets of an infinite-dimensional dynamical system described by some dissipative PDEs. The principal objective of the theory is to reduce the description of the long-term dynamics of the infinite-dimensional problem to a finite system of ODEs. An attractive feature is that the reduction introduces no error in the problem. That is, the IM contains all pertinent information about the long-term dynamics of the original system. One of the key objectives of AIMs is to handle cases where the IM is not known to exist. AIM also can help to find good algorithms for dealing with the IMs that are known to exist. Moreover, AIM may also help reduce finite but extremely large systems of ODEs to lower-dimensional problems. In a nut shell, the derivation of exact and approximate IMs is based on the decomposition of the unknown function into large-scale and small scale components. In the case of fluid dynamics, those structures can be identified as large and small eddies. Thus IM or AIM corresponds to an exact or approximate interaction law between the short and long wavelengths.

More recently, Kwak [43] has shown that the long-term dynamics of the two-dimensional incompressible Navier-Stokes equations can be completely described by a finite system of ODEs. Kwak does so by finding a nonlinear change of variable that embeds the incompressible Navier-Stokes equations in a system of reaction-diffusion equations that possess an IM. All of the theories of IMs and AIMs are very involved and interested readers are encouraged to read [36-46] and the references cited therein. The main purpose of this section is to show another aspect of the importance of the study of the dynamics of numerics for nonlinear ODEs in relationship to CFD.

2.4. Relationship Between Shock Waves and Heteroclinic Orbits of Systems of ODEs

Another example of the importance of understanding the "dynamics" and the "dynamics of numerics" of systems of ODEs is related to the study of shocks using equilibrium bifurcation diagrams of associated vector fields. This was introduced by Shearer et al. [50]. The authors find of great interest how one can reduce the study of admissible shock wave solutions of a 2×2 hyperbolic conservation laws to the study of heteroclinic orbits of a system of nonlinear ODEs. Further development in this area can help in constructing suitable approximate Riemann solvers in numerical computations. The following material on the work of Shearer et al. on this subject is excerpted from [49].

Consider a 2×2 system of hyperbolic conservation laws

$$\frac{\partial U}{\partial t} + \frac{\partial F(U)}{\partial x} = 0. \tag{2.2}$$

A shock wave solution of (2.2) with speed s is a piecewise constant function

$$U(x,t) = \begin{cases} U_- & \text{if} \quad x < st \\ U_+ & \text{if} \quad x > st \end{cases} \tag{2.3}$$

that satisfies the Rankine-Hugoniot condition

$$F(U_+) - F(U_-) - s(U_+ - U_-) = 0. \tag{2.4}$$

Such a shock wave is admissible if it possesses a viscous profile; i.e., a traveling wave solution

$$U = U((x - st)/\epsilon) \tag{2.5}$$

of the parabolic system

$$\frac{\partial U}{\partial t} + \frac{\partial F(U)}{\partial x} = \epsilon \frac{\partial^2 U}{\partial x^2}; \qquad \epsilon > 0 \tag{2.6}$$

with boundary conditions

$$U(\pm\infty) = U_\pm, \quad U'(\pm\infty) = 0. \tag{2.7}$$

Substitution of (2.5) into (2.6) and one integration, using the left-hand boundary condition from (2.7), leads to the system of ordinary differential equations

$$\frac{dU}{d\xi} = F(U) - F(U_-) - s(U - U_-), \tag{2.8}$$

where $\xi = (x - st)/\epsilon$, and U_- and s are parameters. One equilibrium (fixed point) of (2.8) is U_-. The triple (U_-, U_+, s) satisfies the Rankine-Hugoniot condition (2.4) if and only if U_+ is also an equilibrium of (2.8). In this case, the shock wave (2.3) has a viscous profile if and only if there is an orbit (trajectory) of (2.8) from U_- to U_+. An orbit that goes from one equilibrium to another is called a heteroclinic orbit or a connection. Thus one has reduced the study of admissible shock wave solutions of (2.2) to the study of heteroclinic orbits of the nonlinear ODE (2.8).

One refers to a shock (2.3) as a Lax shock if U_- is an unstable node and U_+ is a saddle (a slow shock), or U_- is a saddle and U_+ is a stable node (a fast shock). The connection between this interpretation of the Lax condition and the usual one relating shock speeds to characteristic speeds is made by noting that the eigenvalues of an equilibrium U are eigenvalues of $-sI + \frac{\partial F(U)}{\partial U}$, while the characteristic speeds are eigenvalues of $\frac{\partial F(U)}{\partial U}$. A Lax shock (2.3) is called a compressive shock if it is admissible; i.e., if there is a heteroclinic orbit from U_- to U_+. Since node-to-saddle and saddle-to-node heteroclinic orbits are stable to perturbation, compressive shocks come in one-parameter families: for fixed U_-, as s varies in some interval, there exists a corresponding U_+ connected to U_-.

An admissible shock wave is undercompressive if both U_- and U_+ are saddle points. The trajectory from U_- to U_+ is then a saddle-to-saddle connection. Such heteroclinic orbits are

not stable to perturbation; for fixed U_-, they are expected to occur only for isolated values of s. Undercompressive shocks were not considered classically, but they arise naturally in solving the Riemann problem near an umbilic point such as problems in elasticity and oil recovery.

In [49] Schecter and Shearer studied undercompressive shocks for nonstrictly hyperbolic conservation laws by adding information to the equilibrium bifurcation diagrams (introduced by Shearer et al.) about heteroclinic orbits of the vector fields. The augmented equilibrium bifurcation diagrams are then used in the construction of solutions of Riemann problems.

2.5. Dynamics of Numerics and Flow Visualizations of Numerical Data

The use of flow visualization of numerical data (numerical solutions of finite discretizations of e.g., fluid flow problems) in an attempt to understand the true flow physics has become increasingly popular in the last decade. See, for example Refs. [24-32]. Many of the techniques rely on the extraction of the boundary surfaces by analyzing a set of appropriate vector fields. Approximations are then performed based on this set of vector fields. The study of the topological features of certain flow physics based on the numerical data is then related to the study of fixed points of the associated systems of ODEs. Fluid problems with known flow physics can be used to reveal how well the associated vector fields of the numerical data can mimic the true physics. It can also help to delineate spurious flow patterns that are solely due to the numerics.

However, we are entering into the regime where CFD is extensively used to aid the understanding of complicated flow physics that is not amenable to analysis otherwise. In the situation where the numerical data indicate flow structures which are not easily understood, a good understanding of the spurious dynamics that can be introduced by the numerics is needed. See Refs. [24-32] and references cited therein on the various aspects of flow visualizations of numerical data. Another aspect is that if the governing DE and/or its discretized counterparts possess higher than three-dimensional (or infinite dimensional) dynamical behavior, the projections of these higher dimensional dynamics onto a 2-D or 3-D topology can lead to misinterpretation of flow types.

III. PRELIMINARIES FOR ODEs AND ODE SOLVERS

Consider a 2×2 system of first-order autonomous nonlinear ODEs of the form

$$\frac{dU}{dt} = \alpha S(U), \tag{3.1}$$

where U and S are vector functions of dimension 2, α is a parameter and $S(U)$ is nonlinear in U. For simplicity of discussion we consider only autonomous ODEs where α is linear (constant scalar factor) in (3.1); i.e., α does not appear explicitly in S. Other types of system parameters may be included in S but are not explicitly stated at this point. See section IV for more details.

A fixed point U_E of an autonomous system (3.1) is a constant solution of (3.1); that is

$$S(U_E) = 0, \tag{3.2}$$

where the subscript "E" stands for "exact" and U_E denotes the fixed points of the ODE as opposed to the additional fixed points of the discretized counterparts (spurious fixed points) due to the numerical methods which we will encounter later. Note that the terms "equilibrium points", "critical points", "singular points", "stationary points", "fixed points" and even "steady-state solutions" are sometimes used interchangeably in the literature and we adopt these nomenclatures in the rest of this text.

Let the eigenvalues of $J(U_E) = \frac{\partial S}{\partial U}|_{U_E}$ (the Jacobian matrix of $S(U)$ evaluated at U_E) be λ_1 and λ_2. Here $J(U_E)$ is assumed to be nonzero. The fixed point U_E is hyperbolic if $\mathrm{Re}(\lambda_i) \neq 0$, i =1,2. If both λ_i are real, U_E is a saddle if $\lambda_1\lambda_2 < 0$ and a node if $\lambda_1\lambda_2 > 0$. If exactly one $\lambda_i = 0$, then U_E is semihyperbolic. If the eigenvalues are complex, then U_E is a spiral. The "tightness" of the spiral is governed by the magnitude of the imaginary part of the eigenvalues. If the eigenvalues both have a zero real part, then U_E is non-hyperbolic. Such a fixed point is called a center. Under this situation, more analysis is needed to uncover the real behavior of (3.1) around a non-hyperbolic fixed point. The fixed point U_E is stable if both λ_1 and λ_2 have negative real parts. U_E is unstable if a λ_i has a positive real part. In the non-hyperbolic case the fixed point is neutral.

If due to a variation of a parameter of the ODE a fixed point becomes unstable, then, if at the point of instability the eigenvalues are distinct and real, the resulting bifurcation will be to another fixed point. Such bifurcation is called a steady bifurcation. If, however, the eigenvalues are complex, then the bifurcation will be of a Hopf type. This is a slightly simplified classification, since our main concern in this work is not on the variation of the ODE parameter. Detailed background information can be found, e.g., in [1-4].

Consider a nonlinear discrete map from a finite discretization of (3.1)

$$U^{n+1} = U^n + D(U^n, r), \tag{3.3}$$

where $r = \alpha\Delta t$ and $D(U^n, r)$ is linear or nonlinear in r depending on the ODE solver. Here r is used to represent the time step Δt which may include any constant scalar factors α present in

(3.1). In most of the ODE models considered later, $\alpha = 1$. A fixed point U_D of (3.3) is defined by $U^{n+1} = U^n$, or

$$U_D = U_D + D(U_D, r) \tag{3.4a}$$

or

$$D(U_D, r) = 0. \tag{3.4b}$$

In the context of discrete systems, the term "fixed point" without indicating the period means "fixed point of period 1" or the steady-state solution of (3.3). Here we use the term asymptote to mean a fixed point of any period, a limit cycle, chaos, or a strange attractor.

The type of finite discretization of (3.1) represented in (3.3) assumed the use of two-time level schemes. Otherwise the vector dimension of (3.3) would be 2(k-1) instead of 2 where k is the number of the time level of the scheme. Here the vector function D is assumed to be consistent with the ODE (3.1) in the sense that fixed points of the ODE are fixed points of the scheme; however, the reverse need not hold. It is this feature, that the discretized counterparts of the underlying ODE possess a much richer dynamical behavior than the original ODE, which forms the core of this study. Thus the fixed points U_D of $D(U_D, r) = 0$ may be true fixed points U_E of (3.1) or spurious fixed points U_S. The spurious fixed points U_S are not roots of $S(U) = 0$. That is $S(U_S) \neq 0$.

Letting $U^n = U_D + \delta^n$, then a perturbation analysis on (3.3) yields

$$\delta^{n+1} = \left(I + \frac{\partial D(U_D, r)}{\partial U} \right)^{n+1} \delta^0. \tag{3.5}$$

Assuming $\frac{\partial D(U_D, r)}{\partial U} \neq 0$, then the numerical fixed point U_D is stable if the eigenvalues of

$$J_D = I + \frac{\partial D(U_D, r)}{\partial U} \tag{3.6}$$

lie inside the unit circle. If both eigenvalues are real and both lie inside (outside) the unit circle, then the fixed point is a stable (unstable) node. If one is inside the unit circle and the other outside, then the fixed point is a saddle. If both eigenvalues are complex, then the fixed point is a spiral. If the eigenvalues lie on the unit circle, then the fixed point of (3.3) is indeterminant and additional analysis is required to determine the true behavior of (3.3) around this type of fixed point. For a more refined definition and the difference in fixed point definition between ODEs and discrete maps, see [54-58] and references cited therein. A similar definition (with additional classification) for steady and Hopf bifurcation as the ODE holds true for (3.3). However, we now are concerned with the manner in which the real or complex eigenvalues cross the unit circle when a fixed point becomes unstable. The reader is referred to [1-4,59,60] for full details on the subject of bifurcation theory.

An important feature which can arise (for both system of ODEs (3.1) and their discretizations) as the result of a Hopf bifurcation is a limit cycle where the trajectory traverses a closed curve in phase space. In all but a few simple cases such limit cycles are beyond analysis.

IV. MODEL 2×2 SYSTEMS OF NONLINEAR FIRST-ORDER AUTONOMOUS ODEs

Four 2×2 systems of nonlinear first-order autonomous model ODEs are considered. The purpose of choosing one of the models is to illustrate the numerical accuracy of computing a limit cycle for the various ODE solvers. Two of these systems arise from the mathematical modelling of physical and biological processes, namely, a damped pendulum and a simple model of predator-prey interaction in population dynamics. The fourth system arises as a gross simplification of finite discretization of a PDE. Since the purpose of the present study is to illustrate the dynamics of numerics of ODE solvers, we do not treat any system parameter present in the differential equations as a bifurcation parameter, but instead keep it constant throughout each numerical calculation so that only the discretization parameters come into play. The systems considered with $U = (u, v)$ or $z = u + iv$ are

1. A **Dissipative complex** model:

$$\frac{dz}{dt} = z(i + \epsilon - |z|^2) \tag{4.1}$$

2. A **Damped Pendulum** model:

$$\begin{aligned} \frac{du}{dt} &= v \\ \frac{dv}{dt} &= -\epsilon v - \sin(u) \end{aligned} \tag{4.2}$$

3. A **Predator-Prey** model:

$$\begin{aligned} \frac{du}{dt} &= -3u + 4u^2 - 0.5uv - u^3 \\ \frac{dv}{dt} &= -2.1v + uv \end{aligned} \tag{4.3}$$

4. A **Perturbed Hamiltonian system** model:

$$\begin{aligned} \frac{du}{dt} &= \epsilon(1 - 3u) + \frac{3}{4}\Big[1 - 2u + u^2 - 2v(1 - u)\Big] \\ \frac{dv}{dt} &= \epsilon(1 - 3v) - \frac{3}{4}\Big[1 - 2v + v^2 - 2u(1 - v)\Big] \end{aligned} \tag{4.4}$$

Here ϵ is the system parameter for (4.1), (4.2) and (4.4).

Before investigating the fixed points of these ODEs, we show the perturbed Hamiltonian system's relationship with the numerical solution of a PDE. Consider the viscous Burgers' equation with no source term

$$\frac{\partial u}{\partial t} + \frac{1}{2}\frac{\partial (u^2)}{\partial x} = \beta \frac{\partial^2 u}{\partial x^2} \qquad \beta > 0. \tag{4.5}$$

Let $u_j(t)$ represent an approximation to $u(x_j, t)$ where $x_j = j\Delta x$, $j = 1, ..., J$, with Δx the uniform grid spacing. Consider the three-point central difference in space with periodic condition $u_{J+j} = u_j$, and assume $\sum_{j=1}^{J} u_j =$ constant, which implies that $\sum_{j=1}^{J} \frac{du_j}{dt} = 0$. For simplicity, take $J = 3$ and $\Delta x = 1/3$. Then, with $\epsilon = 9\beta$,

$$\frac{du_1}{dt} + \frac{3}{4}\left(u_2^2 - u_3^2\right) = \epsilon(u_2 - 2u_1 + u_3) \tag{4.6a}$$

$$\frac{du_2}{dt} + \frac{3}{4}\left(u_3^2 - u_1^2\right) = \epsilon(u_3 - 2u_2 + u_1) \tag{4.6b}$$

$$\frac{du_3}{dt} + \frac{3}{4}\left(u_1^2 - u_2^2\right) = \epsilon(u_1 - 2u_3 + u_2) \tag{4.6c}$$

$$\sum_{j=1}^{3} \frac{du_j}{dt} = 0. \tag{4.6d}$$

This system can be reduced to a 2×2 system of first-order nonlinear autonomous ODEs (4.4). In this case, the nonlinear convection term is contributing to the nonlinearity of the ODE system (4.4).

These four equations were selected to bring out the dynamics of numerics for four different types of solution behavior of the ODEs. The dissipative complex system (4.1) possesses either a unique stable fixed point or limit cycle with an unstable fixed point depending on the value of ϵ. This is the rare situation where the analytical expression of a limit cycle can be found. The damped pendulum (4.2) exhibits a periodic structure of an infinite number of fixed points (nonunique stable and unstable fixed points). The predator-prey model (4.3) exhibits multiple stable fixed points without a periodic pattern as model (4.2). As stated earlier, the perturbed Hamiltonian model (4.4) which arises as a gross simplification of finite discretization of the viscous Burgers' equation, exhibits an unique stable fixed point. Following the classification of fixed points of (3.1) in section III, one can easily obtain the following:

Fixed Point of (4.1): The dissipative complex model has a unique fixed point at (0,0) for $\epsilon \leq 0$. The fixed point is a stable spiral if $\epsilon < 0$. It is a center if $\epsilon = 0$. For $\epsilon > 0$, the fixed point (0,0) becomes unstable with the birth of a stable limit cycle with radius equal to $\sqrt{\epsilon}$ centered at (0,0). Figure 4.1 shows the phase portrait (u - v plane) of system (4.1) for $\epsilon = -1$ and $\epsilon = 1$ respectively. Here the entire (u, v) plane belongs to the basins of attraction of the stable fixed point (0,0) if $\epsilon < 0$. On the other hand, if $\epsilon > 0$, the entire (u, v) plane except the unstable fixed point (0,0) belongs to the basins of attraction of the stable limit cycle centered at (0,0).

Fixed Points of (4.2): The damped pendulum (4.2) has an infinite number of fixed points, namely $(k\pi, 0)$ for integer k. If k is odd, the eigenvalues of the Jacobian $J(U_E)$ are of opposite sign and these fixed points are saddles. If k is even, however, two cases must be considered, depending on the value of ϵ. If $\epsilon < 2$ and positive, the eigenvalues are complex with negative real part and the fixed points are stable spirals. If $\epsilon \geq 2$, the eigenvalues are real and negative and the fixed points are nodes. If $\epsilon = 0$, the spirals become centers. Figure 4.2 shows the phase portrait and their corresponding basin of attraction for system (4.2). The different shades of grey regions represent the various basins of attraction of the respective stable fixed points for $\epsilon = 0.5$ and $\epsilon = 2.5$.

Fixed Points of (4.3): The fixed points of the predator-prey equation are less regular than those for the damped pendulum equation. System (4.3) has four fixed points (0,0), (1,0), (3,0) and (2.1,1.98). By looking at the eigenvalues of the Jacobian of S, one finds that (0,0) is a stable node, (2.1,1.98) is a stable spiral, and (1,0) and (3,0) are saddles. Figure 4.3 shows the phase portrait and their corresponding basins of attraction for system (4.3). The different shades of grey regions represent the various basins of attraction of the respective stable fixed points. The white region represents the basin of divergent solutions.

Fixed Points of (4.4): The perturbed Hamiltonian (semi discrete system of the viscous Burgers' equation with three-point central difference in space) has four steady-state solutions of which three are saddles and one is a stable spiral at (1/3, 1/3) for $\epsilon \neq 0$. For $\epsilon = 0$ the stable spiral becomes a center. Figure 4.4 shows the phase portrait and their corresponding basins of attraction for system (4.4). The shaded region represents the basins of attraction for the fixed point (1/3, 1/3) for $\epsilon = 0$ and $\epsilon = 0.1$. The white region represents the basin of divergent solutions. From here on we refer to (4.4) also as a viscous Burgers' equation with central difference in space.

V. ODE SOLVERS AND BIFURCATION DIAGRAMS

This section describes the 11 time discretizations and their corresponding bifurcation diagrams for the four model ODEs (4.1)-(4.4). The 11 ODE solvers are listed in section 5.1. Section 5.2 discusses the stability of selected fixed points of the discretized counterparts of three of the model ODEs ((4.1), (4.2) and (4.4)) as functions of system parameters. Section 5.3 discusses the nonlinear stability (bifurcation diagrams) of the discretized counterparts as a function of the discretized parameter ϵ (with the system parameter held fixed).

5.1. ODE Solvers

The ODE solvers considered are the explict Euler, two second-order Runge-Kutta, namely, the modified Euler (R-K 2) and the improved Euler (R-K 2), a third-order Runge-Kutta (R-K 3), the fourth-order Runge-Kutta (R-K 4), the two and three-step predictor-corrector [61-63], and noniterative linearized forms of the implicit Euler and the trapezoidal methods.

(1) Explicit Euler (R-K 1):

$$U^{n+1} = U^n + rS^n; \qquad S^n = S(U^n), \tag{5.1}$$

(2) Modified Euler (R-K 2):

$$U^{n+1} = U^n + rS\left(U^n + \frac{r}{2}S^n\right), \tag{5.2}$$

(3) Improved Euler (R-K 2):

$$U^{n+1} = U^n + \frac{r}{2}\left[S^n + S(U^n + rS^n)\right], \tag{5.3}$$

(4) Heun (R-K 3):

$$\begin{aligned} U^{n+1} &= U^n + \frac{r}{4}\left(k_1 + 3k_3\right) \\ k_1 &= S^n \\ k_2 &= S\left(U^n + \frac{r}{3}k_1\right) \\ k_3 &= S\left(U^n + \frac{2r}{3}k_2\right), \end{aligned} \tag{5.4}$$

(5) Kutta (R-K 3):

$$
\begin{aligned}
U^{n+1} &= U^n + \frac{r}{6}\Big(k_1 + 4k_2 + k_3\Big) \\
k_1 &= S^n \\
k_2 &= S\Big(U^n + \frac{r}{2}k_1\Big) \\
k_3 &= S\Big(U^n - rk_1 + 2rk_2\Big),
\end{aligned} \tag{5.5}
$$

(6) R-K 4:

$$
\begin{aligned}
U^{n+1} &= U^n + \frac{r}{6}\Big(k_1 + 2k_2 + 2k_3 + k_4\Big) \\
k_1 &= S^n \\
k_2 &= S\Big(U^n + \frac{r}{2}k_1\Big) \\
k_3 &= S\Big(U^n + \frac{r}{2}k_2\Big) \\
k_4 &= S\Big(U^n + rk_3\Big),
\end{aligned} \tag{5.6}
$$

(7) Predictor-corrector for m=2,3 (PC2, PC3):

$$
\begin{aligned}
U^{(0)} &= U^n + rS^n \\
U^{(k+1)} &= U^n + \frac{r}{2}\Big[S^n + S^{(k)}\Big], \qquad k = 0, 1, ..., m-1 \\
U^{n+1} &= U^n + \frac{r}{2}\Big[S^n + S^{(m-1)}\Big],
\end{aligned} \tag{5.7}
$$

(8) Adam-Bashforth (2nd-order):

$$
U^{n+1} = U^n + \frac{r}{2}\Big[3S(U^n) - S(U^{n-1})\Big], \tag{5.8}
$$

(9) Linearized Implicit Euler:

$$
U^{n+1} = U^n + r(I - rJ^n)^{-1}S^n \tag{5.9}
$$

$$J^n = \left(\frac{\partial S}{\partial U}\right)^n \qquad \text{and} \quad \det(I - rJ^n) \neq 0,$$

(10) Linearized Trapezoidal:

$$U^{n+1} = U^n + r(I - \frac{r}{2}J^n)^{-1} S^n \tag{5.10}$$

$$J^n = \left(\frac{\partial S}{\partial U}\right)^n \qquad \text{and} \quad \det\left(I - \frac{r}{2}J^n\right) \neq 0,$$

where the numeric identifier after the "**R-K**" indicates the order of accuracy of the scheme and $r = \Delta t$ with $\alpha = 1$ in (3.1) and det( ) means the determinant of the quantity inside the ( ). See Beam and Warming [64,65] for the versatility of the linearized implicit Euler and linearized trapezoidal methods in CFD applications. Studies on Newton method and some iteration procedures other than the noniterative forms (5.9) and (5.10) for the Implicit Euler and Trapezoidal methods will be reported in a separate paper. A comparison between Newton method and the linearized implicit method (5.9) for model (4.4) is included in section 6.5. Although the explicit Euler can be considered as an R-K 1, it is also a LMM. All of the R-K methods (higher than first order) are nonlinear in the parameter space Δt (or r). As discussed in [5], a necessary condition for an ODEs solver to produce spurious fixed points is the introduction of nonlinearity in the parameter space r. For simplicity in referencing, hereafter we use "implicit Euler" and "trapezoidal" to mean the linearized forms (5.9) and (5.10), respectively, unless otherwise stated.

5.2. Stability of Fixed Points of Numerical Methods as a Function of System Parameters

As mentioned at the beginning of section IV, our study assumes a fixed system parameter so that only the discretized parameter comes into play. However, in order to get a feel for the numerical stability around selected stable fixed points U_E as a function of the system parameter ϵ, Figs. 5.1 - 5.3 show the stability regions of the schemes as a function of the system parameter ϵ for the ODE models (4.1), (4.2) and (4.4) around a selected fixed point for each of the models. The linearized stability regions for the R-K methods of the same order behave in exactly the same manner, and the linearized stability regions around stable U_E of the linearized implicit methods are not interesting, since they have the same regions of stability as the ODEs.

The stability diagrams presented were obtained by numerically solving the absolute stability polynomials for the various methods, in most cases using Newton iteration.

For the Runge-Kutta schemes (of order $p \leq 4$) the stability [60] condition is that

$$\left|1 + \lambda r + \frac{\lambda^2 r^2}{2} + \ldots \frac{\lambda^p r^p}{p!}\right| < 1, \tag{5.11}$$

where λ are the eigenvalues of the Jacobian of $S(U)$.

For Predictor-Corrector of steps $p = 2, 3$ the stability condition is that

$$\left| 1 + \lambda r + ... + \frac{\lambda^p r^p}{2^p} \right| < 1, \tag{5.12}$$

and for the Adams-Bashforth method the roots μ of

$$\mu^2 - (1 + \frac{3\lambda r}{2})\mu + \frac{\mu}{2} = 0 \tag{5.13}$$

satisfy $|\mu| < 1$. Note that all of these expressions only hold for the U_E fixed points of the system.

In all cases the boundary of the stability region is when unit modulus is attained. The linearized implicit Euler and trapezoidal methods are unconditionally stable for the stable exact fixed points U_E of the ODE systems we are considering.

These stability regions can be used to isolate the key regions of the ϵ parameter to be considered for the study of dynamics of numerics later. Due to the enormous number of possibilities, detailed study can only concentrate on one to two representative system parameters. Even with such a restriction, as can be seen later, computing the corresponding bifurcation diagrams and basins of attraction is very CPU intensive. Fortunately the computation can be made highly parallel. Figures 5.1 - 5.3 also can serve as a spot check on the numerical results presented in the next section.

5.3. Bifurcation Diagrams

In this section, we show the bifurcation diagrams of selected R-K methods and summarize the spurious dynamical behavior of the 11 ODE solvers based on a selected domain of initial data and ranges of the discretized parameter Δt. The key point is to illustrate the many ways in which the dynamics of a numerical discretization of 2×2 first-order autonomous nonlinear system of ODEs can differ from the system itself. Another point is to gain some basic understanding of the difference in the dynamics of numerics between the scalar and systems of nonlinear ODEs. Due to the fact that there is no limit cycle or higher dimensional tori counterparts for the scalar first-order autonomous ODEs, spurious limit cycles and higher dimensional tori can only be introduced by the numerics when solving nonlinear ODEs other than scalar first-order autonomous ODEs (if 2 time-level schemes are used) and/or by using a scheme with higher than two time levels for the scalar first-order autonomous ODEs. Later we contrast these results with the combined basins of attraction and bifurcation diagrams presented in section VI. We purposely present our results in this order (not showing the basins of attraction) in order to bring out the importance of basins of attraction for the time-dependent approach in obtaining steady-state numerical solutions.

Although we purposely selected the model equations with known analytical solutions, depending on the scheme, the dynamics of their discretized counterparts might not be that easy to analyze. We found that mathematical analysis of the dynamics of numerics for higher-order

schemes is not practical, even with the aid of algebraic manipulators such as DERIVE [66], MAPLE [67], or MATHEMATICA [68]. Only some analysis is possible for the lower order schemes for a few of the models. In particular, some analytical linearized analysis (without numerical computations) of fixed points of periods one and two is possible for the predator-prey and the damped pendulum case. However, analytical analysis for the dissipative complex model and the perturbed Hamiltonian is not practical. For a detailed analysis of these selected cases, readers are referred to Sweby and Yee [16]. For the majority of the cases where rigorous analysis is impractical we have still been able to investigate the dynamics of numerics using numerical experiments.

As stated in section 2.1, some global solution behavior of fixed points of the discretized counterpart of ODE solvers (5.1) - (5.10) for (4.1) - (4.4) can be obtained by the pseudo arclength continuation method devised by Keller [51], a standard numerical method for obtaining bifurcation curves in bifurcation analysis. One deficiency of the pseudo arclength continuation method is that for problems with complicated bifurcation patterns, it cannot provide the complete bifurcation diagram since a known solution for each of the main bifurcation branches is needed before one can continue the solution along a specific main branch. For spurious asymptotes it is usually not easy to locate even just one solution on each of these branches.

The nature of our calculations requires thousands of iterations of the same equation with different ranges of initial data on a preselected (u, v) domain and ranges of the discretized parameter space Δt. Since the NASA Ames CM2 allows vast numbers (typically 65,536) of calculations to be performed in parallel, our problem is perfect for computation on the CM2. With the aid of the CM2 it was possible to obtain both full bifurcation diagrams in a (r, u) plane and orbits with their basins of attraction in the phase plane (u, v). This provided a detailed picture of the dynamical behavior of the discretizations which would have been almost impossible (within a reasonable time frame) using scalar or vector computers.

To obtain a "full" bifurcation diagram, the domain of initial data and the range of the Δt parameter are typically divided into 512 equal increments. For each initial datum and Δt, the discretized equations are preiterated 1,000 - 5,000 before the next 5,000 - 9,000 iterations are plotted. The preiterations are necessary in order for the trajectories to settle to their asymptotic value. Since the results are a three dimensional graph $((r, u, v))$, we have taken slices in v = constant planes in order to enhance viewing and decrease CPU computations. Bear in mind that with this method of computing the bifurcation diagrams, only the stable branches are obtained. That is, unstable fixed points and unstable asymptotes are not present on our bifurcation diagrams. Some of the bifurcation diagrams in a v = constant plane for the four model ODEs and for the modified Euler, improved Euler, Kutta and R-K 4 methods are shown in Figs. 5.4 - 5.8. Figure 5.4 shows a typical example of spurious stable fixed points occurring below the linearized stability by the modified Euler method. It also shows the existence of spurious asymptotes such as limit cycles, higher order periodic solutions and possibly numerical chaos. See later sections and subsections for further details. Bifurcation diagrams for the rest of the ODE solvers are illustrated in section VI with basins of attraction superimposed (see Figs. 6.5 - 6.7, 6.12 - 6.14, 6.19 - 6.21, 6.27 - 6.29, and 6.31). Due to the plotting package, the labels (u_n, v_n) on all of the figures are the same as (u^n, v^n).

The term "full bifurcation" as defined in Yee et al. [5] is used to mean bifurcation diagrams obtained with a proper choice of initial data to cover the essential lower-order periods in such a way as to closely mimic the exact or "true" bifurcation diagram of the underlying discrete map. This is necessary since solutions with different initial conditions will converge to different asymptotic limits. It is noted that except in rare situations, it is not possible to get the "true" bifurcation diagram of the underlying discrete map numerically.

The following summarizes the spurious dynamical behavior of the 11 ODE solvers based on selected domains of initial data and ranges of the discretized parameter Δt. Numerical results agree with some of the analytical linearized analysis (without numerical computations) reported in Sweby and Yee [16].

Bifurcation Diagrams of ODE Solvers for Model (4.1): Recall from section IV that the dissipative complex model (4.1) possesses a unique fixed point at $(u, v) = (0, 0)$ (stable spiral or center) if $\epsilon \leq 0$. For $\epsilon > 0$ the stable fixed point at (0,0) becomes unstable, whereas the birth of a unique stable limit cycle with radius $\sqrt{\epsilon}$ centered at (0,0) is encountered. Note also that for $\epsilon = 0$, the system is nondissipative (or a Hamiltonian system), and all of the 11 ODE solvers converge quite slowly to the fixed point (0,0). We think that schemes such as the simplectic type [69] can do a better job for this type of ODE. For sufficiently small negative (positive) ϵ, all of the studied schemes converge extremely slowly to the stable spiral (limit cycle). This is a typical example of slow convergence of the numerical solution due to the stiffness of the system parameter. While the bifurcation diagrams for $\epsilon \leq 0$ for the various ODE solvers are not too interesting, the bifurcation diagrams for $\epsilon > 0$ are very instructive. Figure 5.5 shows the bifurcation diagrams for the four R-K methods for $\epsilon = 1$. Note that the labels "$r = aDt$" on these figures is equivalent to "$r = \Delta t$" with "$a = 1$". The trapezoidal method produces no spurious steady states. However, the implicit Euler method in additon to maintaining an unconditionally stable feature of the exact limit cycle, also turns the unstable fixed point $U_E = (0, 0)$ (the exact unstable fixed point of the ODE (4.1) for $\epsilon > 0$) into a stable fixed point. See Figs. 6.7, 6.10 and 6.11 for additional details.

Note also that R-K 4 method gives the most overall accurate numerical approximations of the true limit cycle with radius $\sqrt{\epsilon}$ centered at (0,0). The Adam-Bashforth, implicit Euler and trapezoidal methods give the least accurate numerical approximation of the limit cycle for r closer to the linearized stability. The R-K 4 and Heun methods produce spurious higher-order limit cycles. See section IV and Figs. 6.8 and 6.10 for more details. These diagrams illustrate the unreliability of trying to compute a true limit cycle with any sizable r. This should not be surprising since the scheme only gives an $O(r^p)$ approximation to the solution trajectories, and, since the limit cycle is not a fixed point, we would expect inaccuracies to be introduced. However, it would not be easy to detect in practice, especially when a numerical solution produces the qualitative features expected. See section VI and Figs. 6.5 - 6.11 for additional details. All of the studied explicit methods produce spurious asymptotes.

Bifurcation Diagrams of ODE Solvers for Model (4.2): All of the studied 11 explicit and implicit methods produce spurious asymptotes. In particular, some of the explicit methods (even explicit Euler) produce spurious limit cycles for certain ϵ values. For certain ranges of Δt and

ϵ values the implicit Euler and trapezoidal methods turn the saddle points (fixed points of (4.2)) into an unstable fixed point of different type (see Figs. 6.14, 6.17 and 6.18). For the modified Euler method, spurious steady states occur below the linearized stability limit of the scheme. See section VI and Figs. 6.12 - 6.18 for additional details.

Bifurcation Diagrams of ODE Solvers for Model (4.3): Again, all of the studied 11 explicit and implicit methods generate spurious asymptotes. Also, some of the explicit methods produce spurious limit cycles. For certain ranges of the Δt, the trapezoidal method turns the saddle points (exact fixed points of (4.3)) into unstable fixed points of different types. Moreover, for certain ranges of the Δt the implicit Euler method turns the saddle points (exact fixed points of (4.3)) into stable or unstable fixed points of different type. The numerical results coincide with analytical analysis by examining the eigenvalues of the Jacobian of the resulting discrete map. Transcritical bifurcations introduced by the R-K 4 method resulted in the production of spurious steady states below (and very near) the linearized stability limit of the scheme. See section VI and Figs. 6.19 - 6.26 for additional details.

More than one spurious fixed point below the linearized stability of the scheme was introduced by the modified Euler method (see Fig. 5.4). From the form of the Modified Euler scheme it is easily seen that as well as the exact fixed points U_E of the ODEs, any other value U_S satisfying

$$U_S + \frac{r}{2} S(U_S) = U_E \tag{5.14}$$

will also be a fixed point of the scheme. As mentioned earlier, we refer to these additional fixed points as spurious fixed points. Note that the U_E on the right-hand side of (5.14) encompasses both stable and unstable fixed points of the ODE and so, for the predator-prey equations (since S contains cubic terms in U), there are up to twelve (real) spurious steady states, three for each exact fixed point U_E. In fact there are six such spurious steady states which lie in the $v = 0$ plane. All of them occur below the linearized stability limits of the exact fixed points, although not all are stable there. Four (stable ones) of the six are shown in the bifurcation diagram of Fig. 5.4. numbered 1,3,4,6 of the bifurcation branch. The other two are unstable. See Sweby and Yee [16] for additional analysis. Note also that the branch numbered 6 is in fact not stable but represents the stable eigen-direction (separatrix) in the $v = 0$ plane of a saddle point.

Bifurcation Diagrams of ODE Solvers for Model (4.4): For $\epsilon = 0$, the ODE (4.4) is nondissipative. Thus when Δt is below the linearized stability limit of the respective 11 schemes, slow convergence was experienced. For Δt beyond the linearized limit with $\epsilon = 0$, all of the explicit methods produce spurious limit cycles.

For $\epsilon > 0$ (and not too large) all of the studied 11 explicit and implicit methods produce spurious asymptotes. Also, all of the explicit methods produce spurious limit cycles. For $\epsilon = 0.1$, the Kutta and Heun methods introduce spurious asymptotes (higher than period one) that are below the linearized stability limit of the scheme. The linearized stability limits of the two implicit methods are similar to their explicit counterpart. The trapezoidal method turns the fixed point $(u, v) = (1/3, 1/3)$ (the exact stable fixed point of the ODE (4.4)) into a spurious

period 2 solution (see Fig. 6.34). See section VI and Figs. 6.27 - 6.34 for additional details.

Summary of the Bifurcation Study of ODE Solvers for Models (4.1) - (4.4): Some of these figures show an interesting consequence of the technique for locating fixed points. For example, since the stable manifold of the saddle at (3,0) for the predator-prey equation (see Figs. 5.4 and 5.7) lies in the $v = 0$ plane, it has been detected and represented on the bifurcation diagram.

In most of the cases when the spiral becomes unstable the eigenvalues are complex and Hopf bifurcation occurs giving rise to a limit cycle. These numerical results indicate that bifurcation to a period two solution is readily detectable in numerical calculations. However, bifurcation to a limit cycle will not be so obvious (without a phase portrait representation), especially in the vicinity of the bifurcation point and in higher dimensional problems. Indeed the phenomenon of an artificial time iteration to steady state of a large system formed by spatial discretization, which nears convergence before the residuals "plateau out", could actually be the result of a stable spurious limit cycle near the Hopf bifurcation point. Also, the above phenomenon of bifurcation of spirals to limit cycles might account in part for the phenomenon of near (but lack of) convergence in large systems. In addition, depending on the dissipation parameter of the system and also the dissipative nature of the scheme, if these dissipation parameters are small (stiff), extremely slow convergence can occur as we encountered in the cases for $\epsilon << 1$ for systems (4.1), (4.2) and (4.4) for all of the explicit and implicit methods. The implicit Euler method exhibits a faster convergence than the trapezoidal formula and explicit methods.

Note that although no spurious fixed points are generated by the Euler scheme (figures not shown), spurious higher order periodic solutions, stable or unstable, are possible (e.g., the predator-prey equation and damped pendulum equation, figures not shown). See Sweby and Yee [16] for analysis. See also Fig. 6.15. As can be seen in section VI, such spurious solutions can have a drastic effect on the basins of attraction of the true fixed points. By looking at the bifurcation diagram, one will not be able to get the full picture of the dynamics of numerics. In particular methods like the pseudo arclength continuation method would not even be able to provide the full bifurcation diagram since this method needs no referencing of the strong dependence of asymptotes on initial data.

For explicit methods, it appears that unstable fixed points of the ODEs in general will not become stable fixed points of the scheme, but the type of the fixed point may change. The situation is different for implicit LMM methods. Although all of the explicit methods behave somewhat differently, they have very similar bifurcation patterns. However, the implicit methods have a very different bifurcation pattern than their explicit counterparts. The next section provides additional global asymptotic numerical solution behavior (or the corresponding basins of attraction) of the 11 ODE solvers for models (4.1) - (4.4). Section VI illustrates that bifurcation diagrams alone do not tell the whole story; i.e., which initial data lead to which asymptotic states.

It should always be kept in mind that in our illustrations, due to their relatively simple nature and the manner of presentation of results (i.e., full representation of parameter space), the spurious dynamics have been readily detected. This will not always be the case in practical computations, especially where higher order systems are involved.

VI. BASINS OF ATTRACTION AND BIFURCATION DIAGRAMS

This section illustrates how basins of attraction can complement the bifurcation diagrams in gaining the global asymptotic numerical solution behavior for nonlinear DEs. Before discussing numerical results for each of the model ODEs, the next subsection gives some preliminaries on how to interpret the basins of attraction diagrams.

6.1. Introduction

Analytical representations (except in isolated cases) for numerical basins of attraction rarely exist for nonlinear DEs. Methods such as generalized cell mapping [56,70-73] can provide an efficient approach to locating these basins, but might not be exact. Here our aim is to numerically compute the basins of attraction as accurately as possible and in the most straightforward way in order to illustrate the key points. Bear in mind that we are not advocating this approach of obtaining basins of attraction for all computations since it is very CPU intensive and thus impractical for frequent use or for higher–dimensional complicated systems of nonlinear ODEs.

As stated in section 5.3, the numerical experiments for this study are most suited for a highly parallel computer such as the CM2. A detailed picture of the numerical basins of attraction can be obtained rather quickly on the CM2 which would be almost impossible (within a reasonable time frame) using scalar or vector computers. Here we use the term "exact" and "numerical" basins of attraction to distinguish "basins of attraction of the DEs" and "basins of attraction of the underlying discretized counterparts".

As a preliminary, and before discussing our major results, we discuss the numerical basins of attraction associated with modified Euler, improved Euler, Kutta and R-K 4 methods for the two scalar first-order autonomous nonlinear ODEs studied in part I of our companion paper [5].

The two scalar ODEs are:

$$\frac{du}{dt} = \alpha u(1-u) \tag{6.1}$$

and

$$\frac{du}{dt} = \alpha u(1-u)(0.5-u). \tag{6.2}$$

The fixed points for (6.1) with $\alpha > 0$ are $u = 0$ (unstable) and $u = 1$ (stable), and no additional higher order periodic fixed points or asymptotes exist. The basin of attraction for the stable fixed point $u = 1$ is the entire positive plane for all values of $\alpha > 0$.

The fixed points for (6.2) with $\alpha > 0$ are $u = 0$ (unstable), $u = 1$ (unstable) and $u = 0.5$ (stable) and no additional higher-order periodic solutions or asymptotes exist. The basin of attraction for the stable fixed point $u = 0.5$ is $0 < u < 1$ for all $\alpha > 0$. Figures 6.1 and 6.2 show the bifurcation diagrams for four of the R-K methods for (6.1) and (6.2). As described in

section 5.3, the bifurcation diagrams are computed using the CM2 machine with 512 equally spaced initial data points and Δt of the domains in question. For more details of the dynamics of numerics for systems (6.1) and (6.2), see Yee et al. [5]. From the fixed point analysis, aside from the difference in topography of the bifurcation curves, all of these diagrams share a common feature; they all exhibit stable and unstable spurious fixed points, as well as fixed points of period higher than one. In particular, for the modified Euler, Kutta and R-K 4 methods, spurious fixed points occurred below the linearized stability of the scheme.

Intuitively, in the presence of spurious asymptotes the basins of the true stable steady states can be separated by the basins of attraction of the stable spurious asymptotes and interwoven by unstable asymptotes, whether due to the physics (i.e., present in both the DEs and the discretized counterparts) or spurious in nature (i.e., introduced by the numerical methods). In other words, associated with the same (common) steady-state solution, the basin of attraction of the DE might be very different from the discretized counterparts. This is due entirely to the different dependence on and sensitivity to initial and boundary conditions (numerical or analytical, if any) for the individual system. Take, for example, the ODE (6.1) where the entire domain u is divided into two basins of attraction for the ODE independent of any real α. Now if one numerically integrates the ODE by the modified Euler method, extra stable and unstable fixed points can be introduced by the scheme, depending on the value of r. That is, for certain ranges of the r values the domain u is divided into four basins of attraction. But, of course higher period spurious fixed points exist for other ranges of r, and more basins of attraction are created within the same u domain.

From the bifurcation diagrams 6.1 and 6.2 it is difficult to distinguish the types of bifurcation and the periodicity of the spurious fixed points of any order. Figures 6.3 and 6.4 show the numerical basins of attraction with their respective bifurcation diagrams (white curves and white dense dots) superimposed. Note "a" in Figs. 6.1 - 6.4 is "α" in equations (6.1) and (6.2). The selected ranges of domains and Δt are divided into 512 equal increments. For each initial data inside the domain and Δt ranges, we iterate the discretized equations typically 10,000 times (more or less depending on the problem and scheme) and keep track of where each initial data asymptotically approaches and color code them according to the individual asymptotes. The basins of attraction for the various methods were computed and color coded according to this procedure. Unless noted, the black regions represent divergent solutions. Note that basins with the same color do not mean they have the same period, but rather for each r value within the preselected domain of initial data, the number of distinct basins are color coded. Details of the techniques used for detection of the orbits and basins of attraction are given in the Appendix of Sweby and Yee [16]. Note that in all of the plots, if color printing is not available, the different shades of grey represent the diffferent colors.

Figures 6.3 and 6.4 show not only which initial data asymptote to which stable asymptotes, but also indicate the types of bifurcation behavior (full bifurcation diagram). The white curves and white dense dots represent the full bifurcation diagrams. Any initial data residing in the green region in Fig. 6.3 for the modified Euler method belong to the numerical basin of attraction of the spurious (stable) branch emanating from $u = 3$ and $r = 1$. Thus, if the initial data is inside the green region, the solution can never converge to the exact steady state using even

a small fixed but finite Δt (all below the linearized stability limit of the scheme). Note that the green region extends upward as r decreases below 1.

A similar situation exists for the R-K 4 method (Fig. 6.3), except now the numerical basins of attraction of the spurious fixed points occurred very near the linearized stability limit of the scheme, with a small portion occurring below the linearized stability limit. In contrast to the improved Euler method (Fig. 6.3), the green region represents the numerical basins of one of the spurious stable transcritical bifurcation branches of the fixed point. The bifurcation curve directly below it with the corresponding red portion is the basin of the other spurious branch. See [5] or [3] for a discussion of the different types of bifurcations. The black regions represent divergent or nonconvergent solutions (after the preselected number of iterations has been reached). With this way of color coding the basins of attraction, one can readily know (from the plots) that for ODE (6.2), the improved Euler experiences two consecutive steady bifurcations before period doubling bifurcation occurs (Fig. (6.4)). Using the PC3 method to solve (6.2) (figure not shown; see [5]), four consecutive steady bifurcations occur before period doubling bifurcations. The modified Euler and R-K 4 methods, however, experience only one steady bifurcation before period doubling bifurcations occur.

The next section presents similar diagrams for the 2×2 systems of model nonlinear ODEs (4.1) - (4.4). In this case, only basins of attraction with bifurcation diagrams superimposed on $v =$ constant planes are shown (to enhance viewing and decrease CPU computations). Basins of attraction with the asymptotic phase trajectories superimposed on the phase plane with selected values of Δt are also shown. These selected values of Δt are obtained by looking at the combined basins of attraction and bifurcation diagrams on the various $v =$ constant plane. The latter basins of attraction diagrams exhibit a clearer and more complete picture of the basins of attraction than the former type of diagrams. However, one needs the former diagrams to guide the selection of the Δt values. One can see the added complication when going from scalar ODEs to 2×2 system of ODEs. Unlike the exact basins of attraction and asymptotic phase trajectories shown in Figs. 4.1 - 4.4, *only the stable asymptotes* are plotted.

In all of Figs. 6.5 - 6.34, $a = 1$ unless indicated, and black regions represent divergent solutions (after the preselected number of iterations has been reached). White dots and white curves on the basins of attraction with bifurcation diagrams superimposed represent the bifurcation curves. White dots and white closed curves on the basins of attraction with the phase trajectories superimposed represent the stable fixed points, stable periodic solutions or stable limit cycles. Also bear in mind that for the basins of attraction with bifurcation diagrams superimposed, the different colors represent the different numerical basins of attraction for each r value. Due to the high cost of logic in keeping track of the color coding procedure, it is not possible to keep the same color for the numerical basins of attraction of a particular asymptote as Δt is varied. These types of plots might appear to be confusing at first and require some familiarization before their meaning becomes transparent. On the other hand, the basins of attraction with asymptotic phase trajectories superimposed are easier to read.

6.2. Numerical Results for the Dissipative Complex Equation

Recall that the exact basin of attraction for the model (4.1) is the entire phase plane (see Fig. 4.1) for all real $\epsilon < 0$ for the stable spiral (0,0). For $\epsilon > 0$, the entire phase plane except the unstable fixed point (0,0) is the exact basin of attraction for the stable limit cycle with radius $\sqrt{\epsilon}$ centered at the unstable fixed point (0,0). Figures 6.5 - 6.11 show the two types of numerical basins of attraction diagrams and phase portrait diagrams for $\epsilon = 1$ for some of the ODE solvers. The basins of attraction are color coded and computed in the same manner as discussed in the previous section.

Comparing Figs. 6.5, 6.6 and 6.7 with Fig. 5.5, one can appreciate the added information that the basin of attraction diagrams can provide. The key result is that as Δt moves closer to the linearized stability limit of the limit cycle, the size (red) of the numerical basins of attraction decreases rapidly. This is due to the existence of spurious unstable asymptotes below as well as above the linearized stability limit. The green region, shown in Fig. 6.7 using the implicit Euler method, is the numerical basin of attraction for the attracting fixed point (0,0). Note how the implicit Euler method turns an unstable fixed point of the ODE system into a stable one for $r \geq 1$.

Figures 6.8 and 6.9 show the phase trajectories for four different Δt by the R-K 4 and implicit Euler methods, respectively. Note how little information these figures can provide as compared to Figs. 6.10 and 6.11. Note also how rapidly the size of the basin (red) decreases as r increases for the R-K 4 method. This phenomenon can relate to practical computations where only a fraction of the allowable linearized stability limit of Δt is safe to use if the initial data is not known. For $\Delta t = 1.75$ and 2, spurious limit cycles of higher order period exist.

Figure 6.11 illustrates the situation where unconditionally stable LMM schemes can converge to a wrong solution if one picks the initial data inside the green region (which is expected to be a physical initial data for the ODE) instead of the red region. Thus even though LMM preserved the same number of fixed points as the underlying ODE, these fixed points can change types and stability. This phenomenon can relate to the "non-robustness" of linearized implicit methods sometimes experienced in CFD computations, where if the initial data are not known, the highest possibility of avoiding spurious asymptotes is to use a fraction of the allowable linearized stability limit of Δt.

Figures 6.8 and 6.9 are obtained by dividing the (u, v) domain into 512×512 points of initial datum. With each initial datum and Δt, we preiterate the respective discretized equation 5,000 steps and plot the next 6,000 steps. Figures 6.10 and 6.11 is obtained by dividing the (u, v) domain in the same manner but with the basins of attraction superimposed. The remaining Figs. 6.15 - 6.17, 6.22 - 6.26, 6.30, and 6.32 - 6.34 are computed in the same way.

6.3. Numerical Results for the Damped Pendulum Equation

The exact basins of attraction for model (4.2) are shown in Fig. 4.2 with different shades of grey color. The two types of numerical basin of attraction diagrams for all of the studied ODE

solvers for $\epsilon = 1$ and $\epsilon = 1.5$ are shown in Figs. 6.12 - 6.18. Here, for each Δt value the different colors represent different numerical basins of attraction of the respective asymptotes. Observe the striking difference in behavior between the explicit and implicit methods. From the different colors of the basins in Fig. 6.15 one can readily identify that spurious higher than period one and spurious limit cycles exist for the different Δt values. For $\Delta t = 1.4$, the scheme produces spurious period two fixed points. Figure 6.16 shows the existence of spurious fixed points below the linearized stability limit by the modified Euler method and spurious fixed points of period 4 (the four white dots on each basins) above the linearized stability limit by the R-K 4 method. Figures 6.17 and 6.18 show the evolution (birth and death) of spurious fixed points of higher-order period for the implicit Euler and trapezoidal methods. These figures illustrate yet another situation where unconditionally stable schemes can converge to a wrong solution even though these schemes preserved the same number and type of fixed points as the underlying ODE. In this case it is the birth of spurious stable and unstable asymptotes or even numerical chaos that contribute to the size reduction of the true basins of attraction of the ODE.

6.4. Numerical Results for the Predator-Prey Equation

The exact basins of attraction for model (4.3) is shown in Fig. 4.3 with a lighter shade of grey for the stable spiral (2.1,1.98) and a darker shade of grey for the stable node (0,0). The two types of numerical basins of attraction diagrams for all of the studied ODE solvers (except explicit Euler) are shown in Figs. 6.19 - 6.26. Comparing Figs. 6.19, 6.22 and 6.24 with Figs. 5.4 and 5.7, one can again appreciate the added information that the basin of attraction diagrams can provide. Here for all of Figs. 6.22 - 6.26 (except Fig. 6.22 for the last four Δt values and Fig. 6.23 for $\Delta t = 0.37$ and $\Delta t = 0.46$), the green regions represent the numerical basins of attraction for the stable spiral (2.1,1.98) and red regions represent the numerical basins of attraction for the stable node (0,0). We present more basins of attraction in the (u, v) plane for the predator-prey equation than the other three because this is one of the most interesting models (next to the perturbed Hamiltonian model) among the four. Besides, we want to present a general representative dynamical behavior of the studied ODE solvers.

In summary, all explicit methods have a distinct but similar trend in bifurcation diagrams and basin of attraction diagrams. See how the schemes redistribute and recreate spurious basins of attraction (numerical basins of attraction other than the ones belonging to the exact fixed points of the ODEs). Note how the numerical basins of attraction bear no resemblance to the exact basins of attraction for r values that are not sufficiently small. In addition, observe how the dynamics of numerics of the two implicit methods differ from each other and how they differ from the explicit method.

Take, for example, one of the most interesting cases, the modified Euler method. Figure 6.22 shows how spurious stable fixed points can alter the numerical basins of attraction of the stable node and spiral. For $\Delta t = 0.8$, the stable node bifurcates into a spurious fixed point. Without performing the bifurcation analysis one would not be able to detect this particular spurious fixed point, since the value of the spurious one is so close to the exact fixed point $U_E = (0, 0)$. For $\Delta t = 0.9524$, there is the birth of a spurious limit cycle (the white close curve). For $\Delta t = 1.2$,

spurious higher-order periodic solutions exist. Note that for the first four Δt values in Fig. 6.22, the fixed points and asymptotic values are colored black instead of white due to the existence of "spurious" numerical basins of attraction that are colored white.

As discussed in section 5.3, the implicit method can turn saddles into stable and unstable fixed points of a different kind. Thus, without the basins of attraction, it would be more difficult to avoid spurious dynamics (when using a fixed time step that is larger than the explicit counterpart). Note that standard variable time step control might alleviate the problem, but it is not foolproof. With a clear picture of the basins of attraction, spurious dynamics can be avoided. The size of the numerical basins of attraction by the implicit Euler method settle down after $\Delta t \geq 3$. The two fixed points (2.1,1.98) and (0,0) are unconditionally stable and the newly "created" (i.e., fixed points that change type with no additional fixed points created beyond the exact ones) stable fixed points (1,0) and (3,0) (saddles for the original ODE) are almost unconditionally stable except for small Δt. This is the most interesting case in the sense that the numerical basins of attraction for U_E of the model (4.3) by the implicit Euler method were permanently altered for Δt near or larger than 3 (similar to most of the linearized stability limits for R-K methods). No newly created stable fixed points were generated by the trapezoidal method. The evolution of the numerical basin of attraction as Δt changes is very traumatic. The scheme becomes effectively unstable for Δt near 10,000. The size of the numerical basins of attraction for the stable exact fixed points U_E is reduced to almost nonexistence. The basins are so fragmented and small and they are beyond the accuracy of the single precision of the CM2. Due to the high cost of double precision computations on the CM2, no further attempt was made for Δt near 10,000. A better approach in computing these types of basins is the use of interval arithmetic or the enclosure type method [74]. These are yet two more illustrations where in practice linearized implicit methods have a higher success rate of leading to a physically correct solution if one uses a Δt far below what the linearized stability limit predicts (in this case equivalent to typical explicit methods).

6.5. Numerical Results for the Perturbed Hamiltonian Equation

The exact basins of attraction for model (4.4) are shown in Fig. 4.4. The shaded regions represent the exact basin of attraction for the stable spiral (1/3,1/3) or center. The two types of numerical basins of attraction of the various ODE solvers are shown in Figs. 6.27 - 6.34. Our investigation indicates that all of the studied Runge-Kutta methods exhibit spurious limit cycles and other spurious periodic solutions. For the Kutta and Heun methods, stable spurious asymptotes can occur below the linearized stability of the scheme. In addition, all of the studied explicit and implicit methods exhibit spurious asymptotes. In particular, unstable spurious asymptotes were produced below the linearized stability limit by all of the studied schemes. Although this example consists of an artificially small number of grid points, it can shed some light on the interplay between initial data, spurious stable and unstable asymptotes, basins of attraction and the time-dependent approach to the asymptotic numerical solutions. A solid understanding of this concept at the fundamental level can help to determine the reliability of the time-dependent approach to obtaining steady-state numerical solutions.

In all of Figs. 6.32 - 6.34, red regions represent the numerical basins of attraction for the stable spiral (1/3,1/3) when Δt is below the linearized stability of the scheme. When Δt is above the linearized stability, some of the red regions represent the numerical basin of attraction of the stable spurious asymptotes. The discussion is restricted to the second-order improved Euler, the Kutta, the implicit Euler and the trapezoidal methods.

Improved Euler Method: To give an example of the existence of spurious limit cycles and its effect on the numerical basins of attraction for the exact steady state for $\epsilon > 0$ (stable spiral fixed point at (1/3, 1/3)), Fig. 6.30 shows the basins of attraction of the improved Euler method for 4 different $\Delta t = 0.1,\ 1,\ 2.25,\ 2.35$ with $\beta = .1$. By a bifurcation computation shown in Fig. 6.27, we found that the first two time steps are below the linearized stability limit around the exact stable steady state (1/3, 1/3), and the last two time steps are above the limit. Through this numerical study, the following phenomena were observed:

(a) Below the linearized stability limit of the scheme, no spurious stable steady states were observed (see Figs. 6.27 and 6.30). However, this does not preclude the existence of unstable spurious asymptotes that can influence the numerical basins of attraction of the true steady states. As a matter of fact, this is precisely the case. The red regions are the numerical basins of attraction for (1/3, 1/3) for $\Delta t = 0.1$ and 1 respectively. The black region is the numerical basin of divergent solutions. Increasing the time step to $\Delta t = 1$ (below the linearized stability limit) resulted in an enlargement of the numerical basin of attraction for (1/3, 1/3). In other words, what was expected to be nonphysical initial data can now actually be in the numerical basin for (1/3, 1/3).

(b) Above the linearized stability limit spurious limit cycles and higher dimensional periodic solutions were observed (see Figs. 6.27 and 6.30). Further increasing Δt resulted in numerical chaos type phenomena and eventually divergence (with additional increase in Δt). What is expected to be physical initial data now can either converge to a spurious limit cycle or other periodic solution or diverge. Now the red or multicolors are the basins of the spurious limit cycle (the irregular white closed curve shown on Fig. 6.30) and the spurious periodic solution (white dots for Fig. 6.30). For these latter two time steps the numerical basins for the exact steady state (1/3, 1/3) by the improved Euler method disappeared. However, if the initial data are in the red or multicolor region, one gets nonconvergence of the numerical steady state instead of what the linearized stability predicts. The phenomena observed above might well be an explanation of the nonrobustness or nonconvergence of numerical methods encountered in practice.

(c) Although no spurious steady-state numerical solutions exist for this case, the existence of unstable asymptotes below the linearized stability limit and/or the existence of stable and unstable asymptotes above the linearized stability limit is just as detrimental to the numerical basins of attraction for the true steady state as if a spurious steady state occurred below the linearized stability limit. In the latter case, however, a spurious steady-state can be mistaken for the true steady state in practical computations.

Kutta Method: To give an example of the existence of spurious asymptotes below the linearized

stability limit of the scheme, as well as the existence of spurious limit cyles above the linearized stability limit, Fig. 6.32 shows the basins of attraction of the Kutta method for 6 different fixed time steps $\Delta t = 0.1,\ 1,\ 1.826,\ 1.85,\ 2.75$ and 2.785 (the first four below the linearized stability of the scheme) with $\epsilon = 0.1$. The red regions are the numerical basins of attraction of the asymptotic state (1/3,1/3) for the first four Δt. The same domain, and same number of initial data and iterations as the improved Euler case were used. All of the phenomena observed for the improved Euler method hold true for the current case. In addition, new phenomena arise that complicate the numerical basin of attraction tremendously. This occurs in the form of stable and unstable spurious asymptotes below the linearized stablility of the scheme (see Fig. 6.31). The numerical basin for (1/3, 1/3) has become fractal like with the birth of fragmented, isolated new basins of attraction due to the presence of spurious periodic solutions (the three white complicated closed curves with the associated purple, green and blue basins shown in Fig. 6.32). For the case of the existence of unstable spurious asymptotes, the numerical basins for (1/3, 1/3) is fractal like. Figure 6.32 also shows the basins for the spurious limit cycles above the linearized stability limit. In general, these basins have similar structure and features as the improved Euler method except that no higher order periodic solution exists. Note also that with the same time step $\Delta t = 1$, both ODE solvers behave approximately in a similar manner (i.e, enlargement of the numerical basin of attraction for (1/3,1/3).

Implicit Euler Method: This is yet another interesting illustration of the use of an unconditionally stable implicit method where in practical computations, when the initial data are not know, the scheme has a higher chance of obtaining a physically correct solution if one uses a Δt restriction slightly higher than an explicit method. Figures 6.29 and 6.33 show the two types of numerical basins of attraction using the implicit Euler method. Figure 6.33 shows the generation of stable spurious asymptotes for $\Delta t \geq 1$. Note that the numerical basin of attraction (red) for (1/3, 1/3) is larger than the corresponding exact basin of attraction for $\Delta t < 1$. As Δt increases further, the size of the same numerical basin decreases and becomes fractal like, and new numerical basins are generated. The behavior is similar to the predator-prey model (4.3) in a sense that the numerical basin of attraction for (1/3,1/3) was permanently altered for Δt near or larger than 10.

Trapezoidal Method: Figures 6.29 and 6.34 show the two types of numerical basins of attraction using the trapezoidal method. As in the implicit Euler case, this scheme has a higher chance of obtaining a physically correct solution if one uses a Δt similar to that of an explict method. The numerical basins of attraction for (1/3, 1/3) are much larger than the corresponding exact basin of attraction for $\Delta t \leq 2$. Their sizes are bigger than the ones generated by the implicit Euler method with the same Δt values. Observe the interesting phenomena for $\Delta t = 500$ where spurious stable periodic solutions occur (white dots near the three saddle (numerical) regions away from (1/3,1/3) with the scattered small basins of divergent solutions. As Δt increases further, the size of the same numerical basin decreases. For Δt near 10,000, the scheme becomes effectively unstable due to the fragmentation of the numerical basins of attraction. Again due to the high cost of double precision computations, no further attempts were made for Δt near 10,000. The computation of these basins requires an interval arithmetic or the enclosure [74] type of mathematical operation before a more precise behavior can be revealed.

Newton Method:

Figure 6.35 shows the basin of attraction using Newton method compared with the implicit Euler at $\Delta t = 1$. One can see that Newton method has a smaller attracting basin for the stable spiral (1/3,1/3) than the implicit Euler method for $\Delta t < 100,000$. In fact its basin (independent of Δt) is the same as the implicit Euler using $\Delta t = 1,000,000$. Figure 6.35 illustrates the situation where quadratic convergence by Newton method can be achieved only if the initial data are in the red regions. Figure 6.35 also illustrates the fact that using very large Δt by the (linearized) implicit Euler method has the same chance of obtaining the correct steady state as the Newton method if the initial data are not known. Comparison of Newton method with other iteration procedures for the implicit Euler and trapezoidal methods will be reported in a future paper.

From the above study of the dynamics of numerics of ODEs and ODE solver combinations, one can conclude that depending on the initial data, for a given Δt below the linearized stability limit, the numerical solution can (a) converge to an exact steady state, (b) converge to a spurious periodic solution, (c) yield spurious asymptotes other than (a) and (b), or (d) diverge, even though the initial data are physically relevant. In general, for different nonlinear DE and numerical method combinations, the numerical solution can have all the phenomena discussed in Table 1.1 in addition to the above phenomena. To get a feel for numerical basins of attraction for a combination of a variety of time discretizations and commonly used upwind and central spatial discretizations, similar but less extensive studies were performed for a model reaction-convection PDE. They are reported in our companion papers [8,18].

VII. Concluding Remarks

The symbiotic relationship between the strong dependence on initial data and the permissibility of spurious stable and unstable asymptotic numerical solutions for commonly used time discretizations in CFD are illustrated for four different nonlinear model ODEs with known analytic solutions. Although in actual computations variable time steps or local time-stepping are used, our study is restricted to the case where the time step and grid spacing are fixed in order to gain an understanding of the global asymptotic behavior of ODE solvers from a fundamental level for highly nonlinear and stiff DEs.

The implications we reached in [5,7,8] on asymptotic numerical solution behavior of finite discretizations for strongly nonlinear CFD computations are reconfirmed here with additional insights and analysis for 11 different commonly used explicit and implicit time discretizations in CFD. The numerical basins of attraction for the explicit Euler method, five different multistage Runge-Kutta methods (modified Euler, improved Euler, Heun, Kutta and 4th-order methods), two and three-step predictor-corrector methods, Adams-Bashforth method, and implicit Euler and trapezoidal method with linearization are compared for different model nonlinear ODEs. With the aid of the CM2, the complex behavior and sometimes fractal like structure of the associated numerical basins of attraction of these time discretizations are compared and revealed for the first time. Due to the fact that there is no limit cycle or higher dimensional tori counterparts

for the scalar first-order autonomous ODEs, spurious limit cycles and higher dimensional tori can only be introduced by the numerics when solving nonlinear ODEs other than scalar first-order autonomous ODEs (if two time-level schemes are used) and/or by using a scheme with higher than two time levels for the scalar first-order autonomous ODEs. Our numerical results indicate that with sufficiently small Δt and initial data close to the steady state (usually not known for the time-marching method), one can have the highest chance of convergence to the correct asymptote. Our numerical results also indicate that bifurcation to a period two or lower order periods solution is readily detectable in numerical calculations. However, bifurcation to a limit cycle will not be so obvious (without a phase portrait representation), especially in the vicinity of the bifurcation point and in higher dimensional problems. Indeed the phenomenon of an artificial time iteration to steady-state of a large system formed by spatial discretization, which nears convergence before the residuals "plateau out", could actually be the result of a stable spurious limit cycle around the Hopf bifurcation point. In addition, the bifurcation of spirals to limit cycles might account in part for the phenomenon of near (but lack of) convergence in large systems.

One important finding is that for a given nonlinear DE and a choosen ODE solver, the size of the numerical basins of attraction changes (decreases normally) as the time step increases even though the time step is within the linearized stability limit. Our numerical study shows that the numerical basins of attraction for all of the 11 ODE solvers might contract in one direction, expand in another direction, contract or expand in more than one direction, expand in all directions, or be very different from the exact basins of attraction of the original DE, depending on the numerical method and the time step (regardless whether or not the time discretizations are LMMs). In other words, for a given initial data and two finite different but not sufficiently small Δt's that are below the linearized stability limit, their numerical solutions might converge to two different solutions even if no spurious stable steady-state numerical solution is introduced by the scheme and the initial data are physically relevant. The source of the behavior is due to the existence of unstable spurious asymptotes or stable asymptotes other than steady states which have the same detrimental (in terms of robustness) effect. However, in the case of the occurrence of stable spurious steady states, they can be mistaken for the true steady states in practical computations.

Another important finding is that unlike the scalar first-order autonomous ODE discussed in part I, the fixed points can change types as the time step is varied even for two-time level LMMs for 2×2 systems of first-order autonomous ODEs. An unstable fixed point can become a stable fixed point and can e.g., change from a saddle to a stable or unstable node. One consequence of this behavior is that the flow pattern can change type as the discretized parameter is varied even though the flow type of the DE remains unchanged. Also all of the studied explicit and noniterative linearized implicit methods can introduce spurious fixed points of higher order period below and above the linearized stability limit of the scheme. Thus even though LMMs preserve the same number (but not the same types) of fixed points as the underlying DEs, the numerical basins of attraction of LMMs (explicit or implicit) do not always coincide with the exact basins of attraction of the DEs. The present results can explain the root of why we cannot achieve the theoretical linearized stability limit of the typical implicit Euler and trapezoidal time discretizations in practice when solving strongly nonlinear DEs e.g., in CFD. The results

can also shed some light in bridging some of the gaps between theoretical convergence criterion ($\Delta t \to 0$, as $n \to \infty$) and practical scientific computation (finite Δt as $n \to \infty$).

We emphasize here that in order to isolate the different causes and cures of slow convergence and nonconvergence of time-marching methods, our study concerns nonlinearity and stiffness that are introduced by DEs containing smooth solutions. Nonlinearity and stiffness that are introduced by the scheme, by the coupling effect in the presence of source term (terms) in a coupled system of PDEs, by highly stretched nonuniform structured and unstructured grids, by discontinuities in grid interfaces and/or discontinuities inherent in the solutions, and by external flows that need special boundary condition treatment with a truncated finite computation domain are added factors and require additional treatment or different analysis. For some of the causes and cures of these issues, the readers is referred to the various excellent work appearing in the Proceedings of the ICFD Conference in Numerical Methods for Fluid Dynamics [75]. The use of the dynamics of numerics as an alternate to address these issues is a subject of continuous research.

Acknowledgement

The authors wish to thank Andrew Stuart and David Griffiths for their valuable discussions during the course of this research and for suggesting the model equations (4.1) and (4.4). Special thanks to Andre Lafon, M. Vinokur and T. Coakley for their critical review of the manuscript and Chris Gong for helping with the workstation graphics layout. Financial support from T. Lasinski for the second author as a visiting scientist at NASA Ames is greatfully acknowledged.

References

[1] J. Guckenheimer and P. Holmes, *Nonlinear Oscillations, Dynamical Systems, and Bifurcations of Vector Fields*, Springer-Verlag, New York, 1983.

[2] J. Hale and H. Kocak, *Dynamics and Bifurcations*, Springer-Verlag, New York, 1991.

[3] R. Seydel, *From Equilibrium to Chaos*, Elsevier, New York, 1988.

[4] M. Kubicek and M. Marek, *Computational Methods in Bifurcation Theory and Dissipative Structures*, Springer-Verlag, New York, 1983.

[5] H.C. Yee, P.K. Sweby and D.F. Griffiths, "Dynamical Approach Study of Spurious Steady-State Numerical Solutions for Nonlinear Differential Equations, Part I: The Dynamics of Time Discretizations and Its Implications for Algorithm Development in Computational Fluid Dynamics," NASA TM-102820, April 1990, also J. Comput. Phys., Vol. 97, 1991, pp. 249-310.

[6] H.C. Yee, "A Nonlinear Dynamical Approach to Algorithm Development in Hypersonic CFD," Proceedings of the 4th International Symposium on Computational Fluid Dynamics, Davis, Calif., Sept. 9-12, 1991.

[7] A. Lafon and H.C. Yee, "Dynamical Approach Study of Spurious Steady-State Numerical Solutions for Nonlinear Differential Equations, Part III: The Effects of Nonlinear Source

Terms and Boundary Conditions in Reaction-Convection Equations," NASA TM-103877, July 1991.

[8] A. Lafon and H.C. Yee, "Dynamical Approach Study of Spurious Steady-State Numerical Solutions of Nonlinear Differential Equations, Part IV: Stability vs. Numerical Treatment of Nonlinear Source Terms," ONERA-CERT Technical Report DERAT 45/5005.38, Feb. 1992.

[9] A. Iserles, "Nonlinear Stability and Asymptotics of O.D.E. Solvers," International Conference on Numerical Mathematics, Singapore, R.P. Agarwal, ed., Birkhauser, Basel, 1989.

[10] P.K. Sweby, H.C. Yee and D.F. Griffiths, "On Spurious Steady-State Solutions of Explicit Runge-Kutta Schemes," University of Reading, Department of Mathematics, Numerical Analysis Report 3/90, also NASA TM 102819, April 1990.

[11] D.F. Griffiths, P.K. Sweby, and H.C. Yee, "On Spurious Asymptotes Numerical Solutions of Explicit Runge-Kutta Schemes," to appear IMA J. Numer. Anal., 1992.

[12] A. Iserles and J.M. Sanz-Serna, "Equilibria of Runge-Kutta Methods," Numerical Analysis Reports, DAMTP 1989/NA4, May 1989, Univeristy of Cambridge, England.

[13] A. Iserles, A.T. Peplow and A.M. Stuart, "A Unified Approach to Spurious Solutions Introduced by Time Discretisation, Part I: Basic Theory," DAMTP 1990/NA4, Numerical Analysis Reports, University of Cambridge, March 1990.

[14] E. Hairer, A. Iserles and J.M. Sanz-Serna, "Equilibria of Runge-Kutta Methods," 1989, to appear in Numer. Math.

[15] A.R. Humphries, "Spurious Solutions of Numerical Methods for Initial Value Problems," submitted to IMA J. Num. Anal. June, 1991.

[16] P.K. Sweby and H.C. Yee, "On Spurious Asymptotic Numerical Solutions of 2×2 Systems of ODEs," Numerical analysis Report 7/91, October, 1991, University of Reading, England.

[17] H.C. Yee and P.K. Sweby, "On Reliability of the Time-Dependent Approach to Obtaining Steady-State Numerical Solutions," Proceedings of the 9th GAMM Conference on Numerical Methods in Fluid Mechanics, Lausanne, Switzerland, Sept. 25-27, 1991.

[18] A. Lafon and H.C. Yee, "On the Numerical Treatment of Nonlinear Source Terms in Reaction-Convection Equations," AIAA 92-0419, 30th AIAA Aerospace Sciences Meeting, Jan. 6-9, 1992, Reno, Nevada.

[19] H.C. Yee, G.H. Klopfer and J.-L. Montagne, "High-Resolution Shock-Capturing Schemes for Inviscid and Viscous Hypersonic Flows," J. Comput. Phys., Vol. 88, No. 1, May 1990.

[20] G. Klopfer and H.C. Yee, "Viscous Hypersonics Shock on Shock Interaction on Blunt Cowl Lips," AIAA-88-0233, AIAA 26th Aerospace Science Meeting, Jan. 11-14, 1988, Reno, Nevada.

[21] G. Klopfer, H.C. Yee and P. Kutler, "Numerical Study of Unsteady Viscous Hypersonic Blunt," Body Flows with an Impinging Shock," Proceedings of the 11th International Conference on Numerical Methods in Fluid Dynamics, June 27 - July 1, 1988, Williams-

burg, Virgina, also NASA TM-100096, April 1988.

[22] R.M. Beam and H.E. Bailey, "Direct Solver for Navier-Stokes Equations," Proceedings of International Conference on Computational Engineering Science, April 10-14, 1988, Atlanta, GA.

[23] A. Jameson, "Airfoils Admitting Nonunique Solutions to the Euler Equations," AIAA-91-1625, June, 1991.

[24] A.E. Perry, "A Study of Degenerate and Nondegenerate Critical Points in Three-Dimensional Flow Fields, DFVLR-FB 84-36, Oct. 1984.

[25] U. Dallmann and G. Schewe, "On Topological Changes of Separating Flow Structures at Transition Reynolds Numbers," AIAA-87-1266, AIAA 19th Fluid Dynamics, Plasma Dynamics and Lasers Conference, June 8-10, 1987, Honolulu, Hawaii.

[26] U. Dallmann, "Three-Dimensional Vortex Structures and Vorticity Topology," Fluid Dynamics Research, Vol. 3, 1988, pp. 183-189.

[27] U. Dallmann and B. Schulte-Werning, "Topological Changes of Axisymmetric and Non-Axisymmetric Vortex Flows," IUTAM Symposium on Topological Fluid Mechanics, Cambridge, UK, Aug. 13-18, 1989.

[28] J. Helman and L. Hesselink, "Surface Representations of Two- and Three-Dimensional Fluid Flow Topology," Proc. Visualization '90, San Francisco, IEEE Computer Society Press, 1990.

[29] M.S. Chong, A.E. Perry and B.J. Cantwell, "A General Classification of Three-Dimensional Flow Fields," Phys. Fluid A, Vol. 2, No. 5, May 1990, pp. 765-777.

[30] U. Dallmann and B. Schulte-Werning, "On the Three-Dimensionality and Unsteadiness of Separated Flows," Third International Congress of Fluid Mechanics, Cairo, Egypt, Jan. 2-4, 1990.

[31] A. Globus, C. Levit and T. Lasinski, "A Tool for Visualizing the Topology of Three-Dimensional Vector Fields," NAS Applied Research Branch Report RNR-91-017, April 1991, NASA Ames Research Center.

[32] C.M. Hung, C.H. Sung and C.L. Chen, "Computation of Saddle Point of Attachment," AIAA-91-1713, AIAA 22nd Fluid Dynamics, Plasma Dynamics and Lasers Conference, June 24-26, 1991, Honolulu, Hawaii.

[33] A. Lafon and H.C. Yee, "Nonlinear Reaction-Convection BVPs vs. Their Finite Difference Approximations: Spurious Steady-State Numerical Solutions," Proceedings of the 4th International Symposium on Computational Fluid Dynamics, Davis, Calif., Sept. 9-12, 1991.

[34] G. Strang, "On the Construction and Comparison of Difference Schemes," SIAM J. Num. Anal. Vol. 5, 1968, pp. 506-517.

[35] R.D. Richtmyer and K.W. Morton, *Difference Methods for Initial-Value Problems*, Interscience-Wiley, New York, 1967.

[36] C. Foias, G. Sell and R. Temam, "Varietes Inertielles des Equations Differentielles Dissipatives," C.R. Acad. Sci. Paris, Ser. I Math., Vol. 301, 1985, pp. 139-141.

[37] C. Foias, G. Sell and R. Temam, "Inertial Manifolds for Nonlinear Evolutionary Equations," J. Diff. Eqns, Vol. 73, 1988, pp. 309-353.

[38] R. Temam, "Inertial Manifolds and Multigrid Methods," SIAM J. Math. Anal. Vol. 21, No. 1, pp. 154-178, Jan. 1990, pp. 154-178.

[39] M. Marion and R. Temam, "Nonlinear Galerkin Methods: The Finite Elements Case," Numer. Math., Vol. 57, 1990, pp. 205-226.

[40] R. Temam, "Attractors for the Navier-Stokes Equations: Localization and Approximation," J. Facu. Sci., U. Tokyo, Sec. IA, Vol. 36, No. 3, Dec. 1989, pp. 629-647.

[41] R. Temam, "Do Inertial Manifolds Apply to Turbulence?," Physica D, Vol. 37, 1989, pp. 146-152.

[42] P. Constantin, C. Foias, B. Nicolaenko, and R. Temam, "Spectral Barriers and Inertial Manifolds for Dissipative Partial Differential Equations," J. Dynamics and Diff. Eqns., Vol. 1, No. 1, 1989, pp. 45-73.

[43] M. Kwak, "Finite Dimensional Inertial Forms for the 2D Navier-Stokes Equations," IMA preprint Series # 828, June 1991.

[44] A. Eden, C. Foias, B. Nicolaenko, and R. Temam, "Inertial Sets for Dissipative Evolution Equations, Part I: Construction and Applications," IMA Preprint Series # 812, May 1991.

[45] C. Foias, G. Sell and E.S. Titi, "Exponential Tracking and Approximation of Inertial Manifolds for Dissipative Nonlinear Equations,"J. Dyn. Diff. Eqns., Vol. 1, 1989, pp. 199-244.

[46] M.W. Smiley, "Global Attractors and Approximate Inertial Manifolds for Nonautonomous Dissipative Equations," submitted to J. Diff. Eqns., 1990.

[47] G.I. Barenblatt, G. Iooss and D.D. Joseph, editors, *Nonlinear Dynamics and Turbulence*, Pitman Advance Publishing Program, Boston, 1983.

[48] P.H. Coullet and E.A. Spiegel, "Amplitude Equations for Systems with Competing Instabilities," SIAM J. Appl. Math., Vol. 43, No. 4, 1983, pp. 776-821.

[49] S. Schecter and M. Shearer, "Undercompressive Shocks for Nonstrictly Hyperbolic Conservation Laws," IMA Preprint Series # 619, Feb. 1990.

[50] M. Shearer, D.G. Schaeffer, D. Marchesin and P. Paes-Leme, "Solution of the Riemann Problem for a Prototype 2×2 System of Non-Strictly Hyperbolic Conservation Laws," Arch. Rat. Mech. anal. 97, 1987, pp. 299-320.

[51] H.B. Keller, "Numerical Solution of Bifurcation and Nonlinear Eigenvalue Problems", in *Applications of Bifurcation Theory*, P.H. Rabinowitz, ed., Academic Press, 1977, pp. 359-384.

[52] E. Doedel, "AUTO: Software for Continuation and Bifurcation Problems in Ordinary Differential Equations," Cal. Tech. Report, Pasadena, Calif., May, 1986.

[53] H.C. Yee, " A Class of High-Resolution Explicit and Implciit Shock-Capturing Methods," VKI Lecture Notes, March 6-10, 1989, also NASA TM-101088, Feb., 1989.

[54] A.M. Panov, "Behavior of the Trajectories of a System of Finite Difference Equations in

the Neighbourhood of a Singular Point," Uch. Zap. Ural. Gos. Univ. vyp, Vol. 19, 1956, pp. 89-99.

[55] O. Perron, "Uber Stabilitat und Asymtotisches Uberhalten de Losungen eines Systems endlicher Differenzengleichungen," J. Reine Angew. Math. Vol. 161, 1929, pp. 41-64.

[56] C.S. Hsu, *Cell-to-Cell Mapping*, Springer-Verlag, New York, 1987.

[57] H.C. Yee, "A Study of Two-Dimensional Nonlinear Difference Systems and Their Applications," Ph.D. Dissertation, University of Calif, Berkeley, Calif., USA, 1975.

[58] C.S. Hsu, "On Nonlinear Parameteric Excitation Problems," *Advances in Applied Mechanics*, Vol. 17, 1977, pp. 245-301, Academic Press, New York.

[59] W.F. Langford and G. Iooss, "Interactions of Hopf and Pitchfork Bifurcations," ISNM 54, *Bifurcation Problems and Their Numerical Solution*, Workshop on Bifurcation Problems and Their Numerical Solution, Dortmund, Jan. 15-17, 1980, Edited by H.D. Mittelmann and H. Weber, Birkhauser Verlag, Basel, 1980, pp. 103-134.

[60] B. Werner, "Turning Points of Branches of Positive Solutions," ISNM 54, *Bifurcation Problems and Their Numerical Solution*, Workshop on Bifurcation Problems and Their Numerical Solution, Dortmund, Jan. 15-17, 1980, Edited by H.D. Mittelmann and H. Weber, Birkhauser Verlag, Basel, 1980, pp. 211-226.

[61] J.D. Lambert, *Computational Methods in Ordinary Differential Equations,* John Wiley, New York, 1973.

[62] C.W. Gear, *Numerical Initial Value Problems in Ordinary Differential Equations* (Prentice-Hall, 1971).

[63] J.C. Butcher, *The Numerical Analysis of Ordinary Differential Equations,* John Wiley, New York, 1987.

[64] R.M. Beam and R.F. Warming, "Implicit Numerical Methods for the Compressible Navier-Stokes and Euler Equations," Lecture Notes for Computational Fluid Dynamics, von Karman Institute for Fluid Dynamics, March 29 - April 2, 1982, Rohde-Saint-Genese, Belgium.

[65] R.M. Beam and R. F. Warming, "An Implicit Finite-Difference Algorithm for Hyperbolic Systems in Conservation Law Form," J. Comp. Phys., Vol. 22, pp. 87-110, 1976.

[66] DERIVE, "Algebraic Manipulation package for IBM PC Compatibles," Uniware, Austria.

[67] MAPLE, "Algebraic Manipulation package," University of Waterloo, Canada, 1988.

[68] S. Wolfram, "Mathematica, a System Doing Mathematics by Computer," Addison Wesley, California, 1988.

[69] J.M. Sanz-Serna, "Numerical Ordinary Differential Equations vs. Dynamical Systems," Applied Math. Comput. Report 1990/3, Universidad de Valladolid, June 1990.

[70] C.S. Hsu and R.S. Guttalu, "An Unravelling Algorithm for Global Analysis of Dynamical Systems: An Application of Cell-to-Cell Mappings," J. App. Mech., Vol. 47, 1980, pp. 941-948.

[71] C.S.Hsu, R.S. Guttalu and W.H. Zhu, "A Method of Analyzing Generalized Cell Mappings," J. App. Mech., Vol. 49, 1982, pp. 885-894.

[72] J. Xu, R.S. Guttalu and C.S. Hsu, "Domains of Attraction for Multiple Limit Cycles of Coupled Van der Pol Equations by Simple Cell Mapping," Int. J. Non-Linear Mechanics, Vol. 20, 1985, pp. 507-517.

[73] H. Flashner and R.S. Guttalu, "A Computational Approach for Studying Domains of Attraction for Non-Linear Systems," Int. J. Non-Linear Mechanics, Vol. 23, No. 4, 1988, pp. 279-295.

[74] E. Adams, "Periodic Solutions: Enclosure, Verification, and Applications," in *Computer Arithmetic and Self-Validating Numerical Methods*, Academic Press, 1990, pp. 199-245.

[75] Proccedings of the ICFD Conference in Numerical Methods for Fluid Dynamics, April 7-10, 1992, University of Reading, England.

Possible Stable Asymptotic Solution Behavior for DEs and Their Discretized Counterparts

Solution Type	ODEs or PDEs	Discretized Counterparts
Steady-State Solutions	Single	Single
		Multiple
	Multiple	Same # of Multiple
		Additional # of Multiple
Periodic Solutions	No	Yes
	Yes	Yes (+ Extra)
Chaos	No	Yes
	Yes	Yes (+ Extra)

Table 1.1

Genuinely Nonlinear Behavior of Asymptotic Numerical Solutions of Nonlinear PDEs vs. Time Steps

BELOW **CFL or Linearized Stability Limit**	**ABOVE** **CFL or Linearized Stability Limit**
Can converge to **(a) correct exact steady state** **(b) incorrect exact asymptotes** **(c) spurious asymptotes** **(d) divergent solution**	Same as **BELOW** **Except** (a)

Table 1.2

Stability Guidelines for Time Step Constraints for Time-Dependent Approach to Steady-State Numerical Solutions

Type	CFL Limit (von Neumann analysis)	Linearized Stability I	Linearized Stability II	Nonlinear Stability
Assumption & Usage	perturbed around u^n	perturbed around exact SS		
	ignore the source term if exists		include the source term if exists	
	inside the stability interval ⇒ converges to the correct SS outside the stability interval ⇒ diverges			spurious asymptotes exist
	local behavior weakly nonlinear			global behavior strongly nonlinear
Stability Region	consists of a single continuous interval		can consist of disjoint intervals	
Initial Data (IC)	no concept of strong dependence on IC			strong dependence on IC
Applicability	insufficient for strongly nonlinear ODEs & PDEs		closer to nonlinear analysis	for strongly nonlinear ODEs & PDEs

(ss: steady state)

Table 1.3

Types of Time-Dependent PDEs

Reaction-Convection-Diffusion PDEs	**Convection and/or Diffusion**	
Homogeneous PDEs	Linear	Nonlinear
Nonhomogeneous PDEs (**Linear** Source Terms)		
Nonhomogeneous PDEs (**Nonlinear** Source Terms)		

Table 2.1

Existence of Spurious Asymptotic Numerical Solutions for Homogeneous 1-D Hyperbolic and Parabolic PDEs

PDE Type	Homogeneous PDEs (Linear)		Homogeneous PDEs (Nonlinear)	
Discretizations / Possible Spurious Asymptotes	Time	Spatial	Time	Spatial
SSS	No	No	Yes	No
S. Limit Cycles				
S. Tori				
Numerical Chaos				

(SSS: Spurious Steady States; S: Spurious)

Table 2.2

Existence of Spurious Asymptotic Numerical Solutions for Nonhomogeneous 1-D Hyperbolic and Parabolic PDEs

PDE Type	Nonhomogeneous PDEs (Linear Source Terms)				Nonhomogeneous PDEs (Nonlinear Source Terms)			
Convection/Diffusion	Linear		Nonlinear		Linear		Nonlinear	
Discretization / Possible Spurious Asymptotes	Time	Spatial	Time	Spatial	Time	Spatial	Time	Spatial
SSS	No	No	Yes	Yes	Yes	Yes	Yes	Yes
S. Limit Cycles								
S. Tori								
Numerical Chaos								

(SSS: Spurious Steady States; S: Spurious)

Table 2.3

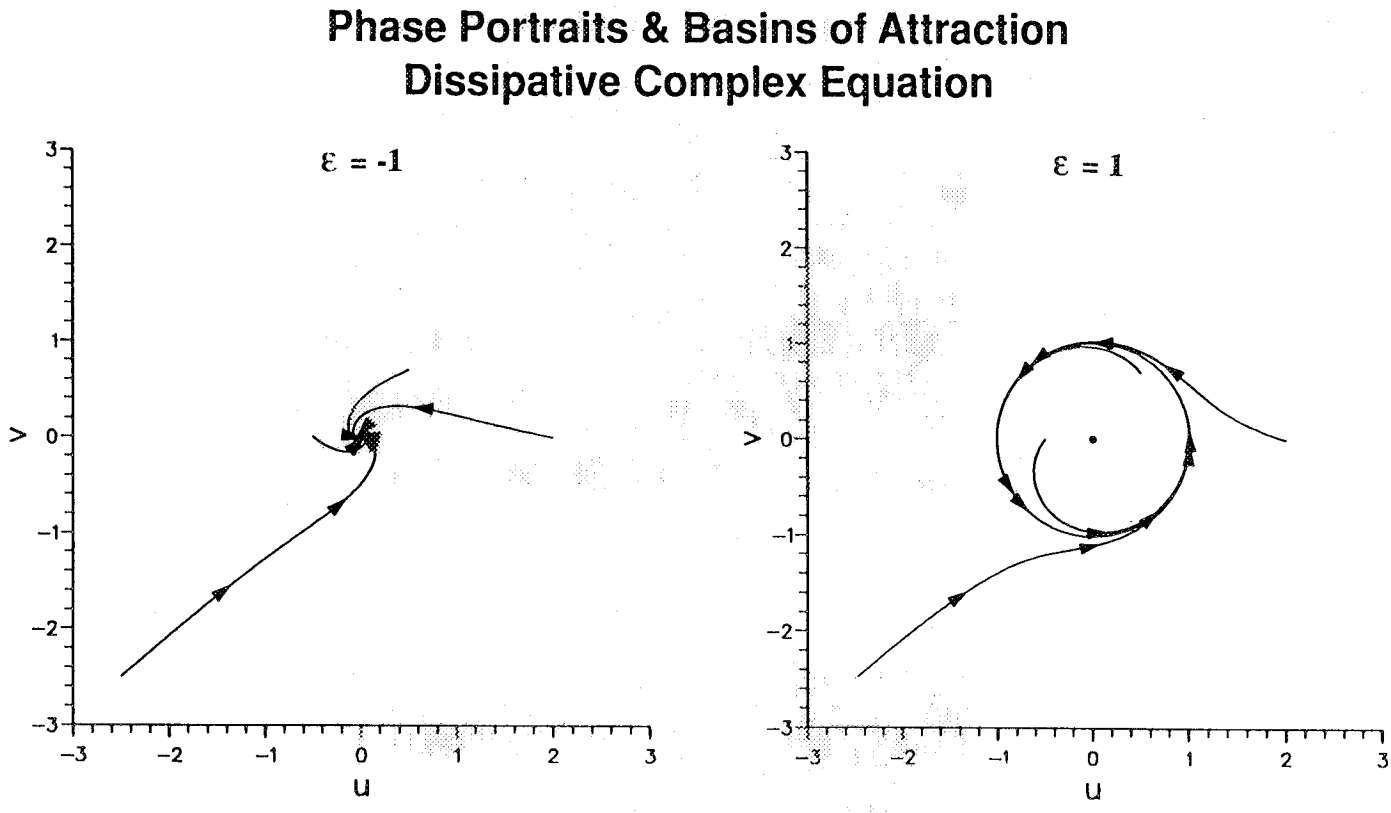
Phase Portraits & Basins of Attraction
Dissipative Complex Equation
ε = -1
ε = 1
v
u
3
2
1
0
−1
−2
−3

Figure 4.1

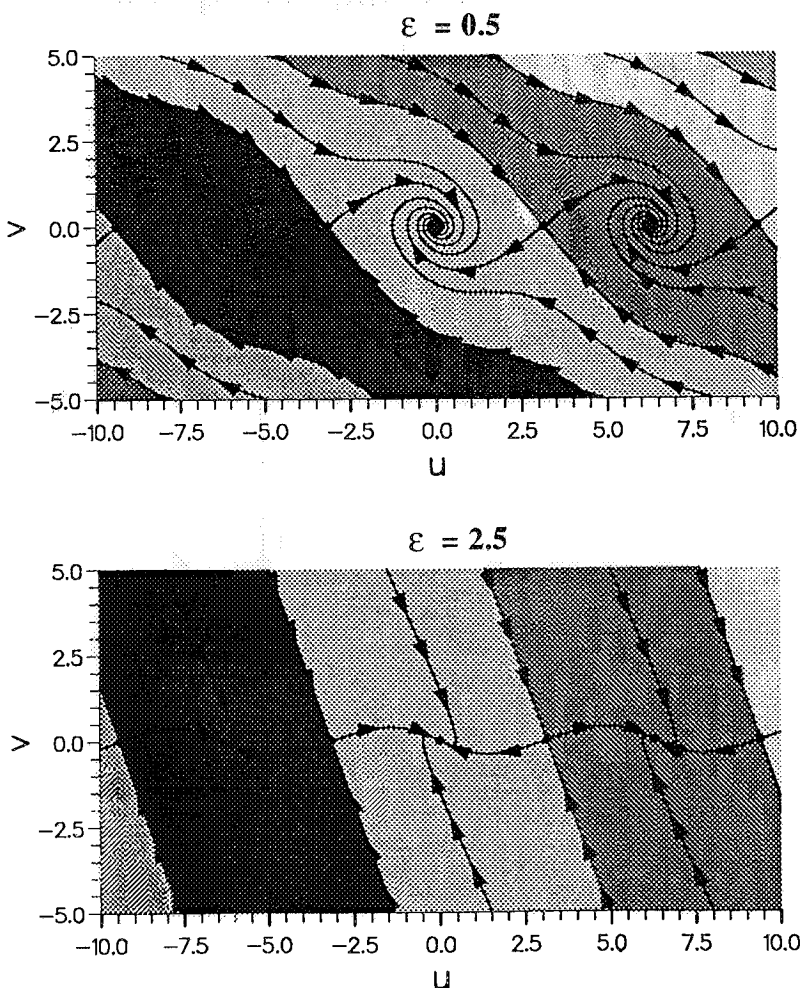
Phase Portraits & Basins of Attraction
Damped Pendulum Equation
ε = 0.5
5.0
2.5
0.0
−2.5
−5.0
v
−10.0
−7.5
−5.0
−2.5
0.0
2.5
5.0
7.5
10.0
u
ε = 2.5
5.0
2.5
0.0
−2.5
−5.0
v
−10.0
−7.5
−5.0
−2.5
0.0
2.5
5.0
7.5
10.0
u

Figure 4.2

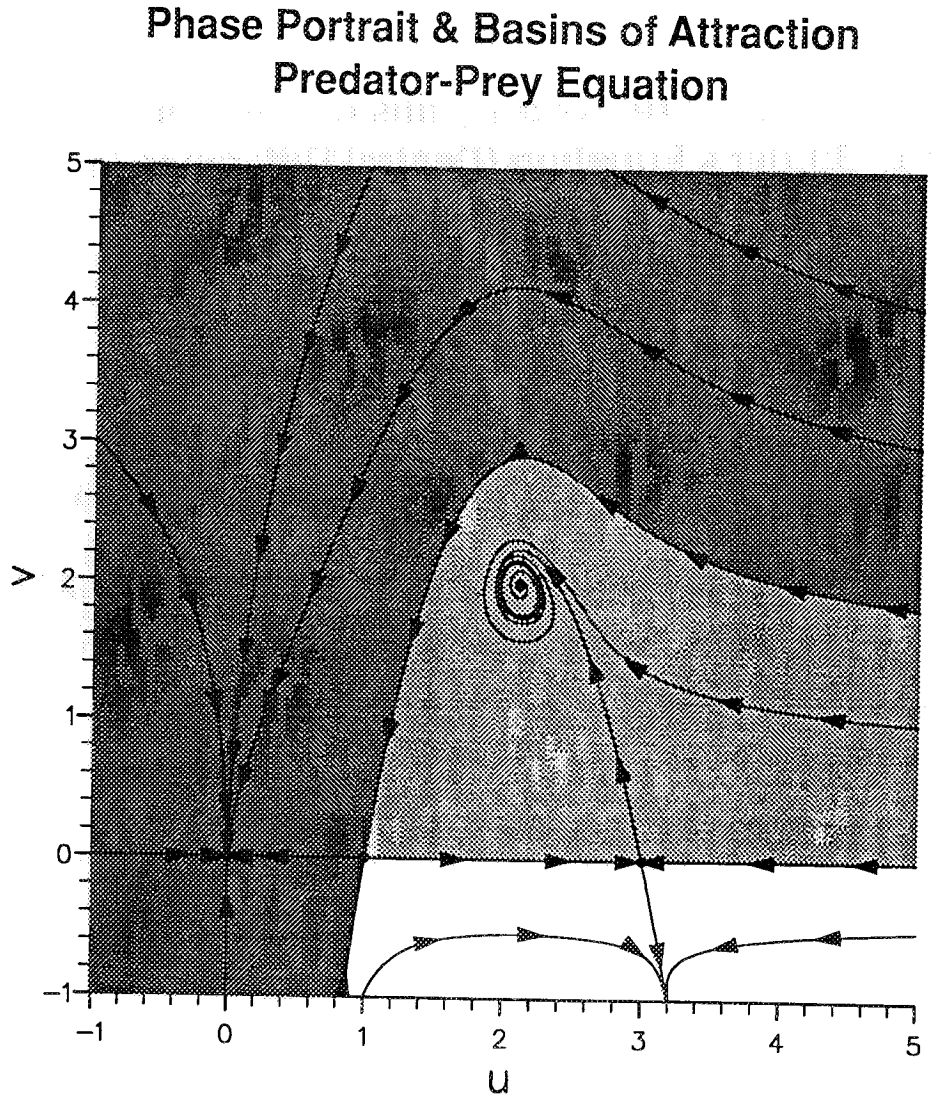
Phase Portrait & Basins of Attraction
Predator-Prey Equation
5
4
3
2
1
0
−1
v
−1
0
1
2
3
4
5
u

Figure 4.3

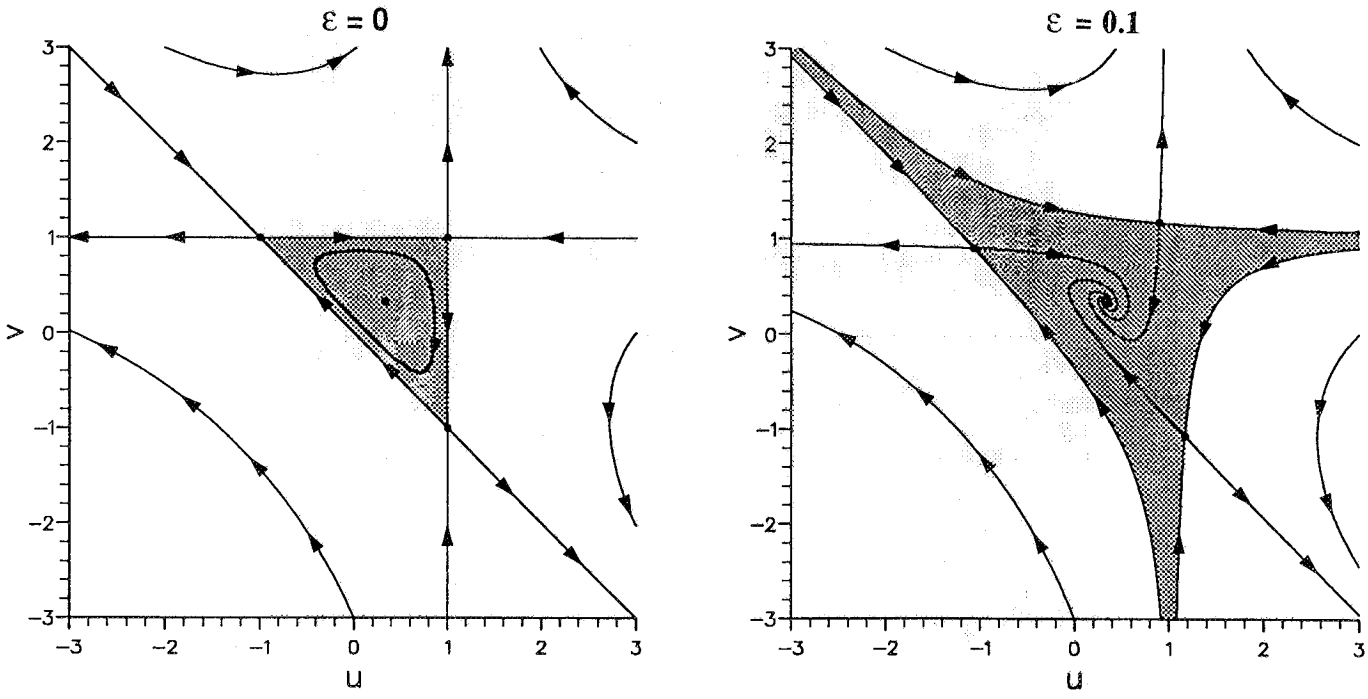
Phase Portraits & Basins of Attraction
Viscous Burger's Equation (Central Difference in Space)
ε = 0
ε = 0.1
v
u
3
2
1
0
−1
−2
−3

Figure 4.4

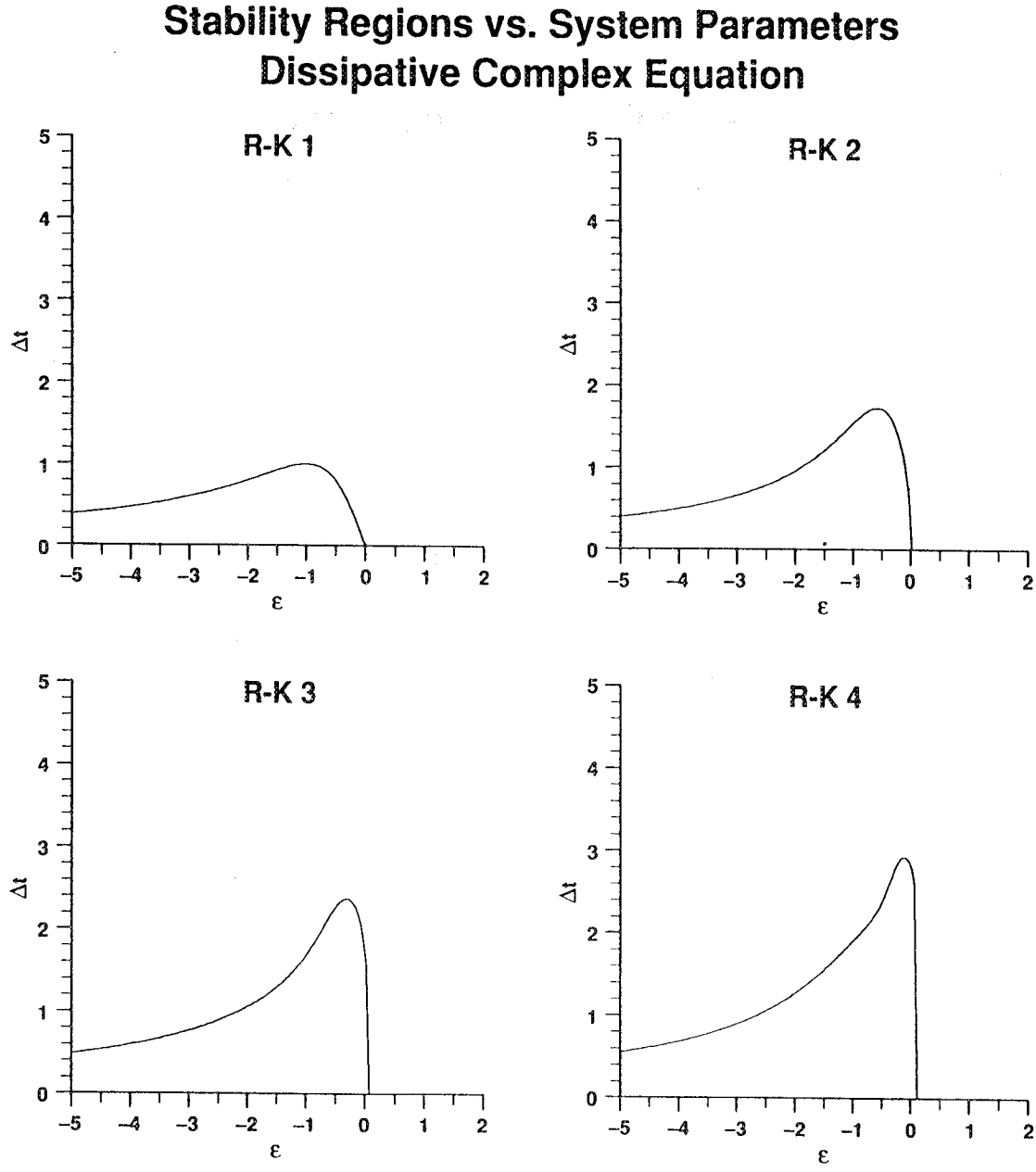
Stability Regions vs. System Parameters
Dissipative Complex Equation
R-K 1
R-K 2
R-K 3
R-K 4
Δt
ε
0
1
2
3
4
5
−5
−4
−3
−2
−1
0
1
2

Figure 5.1

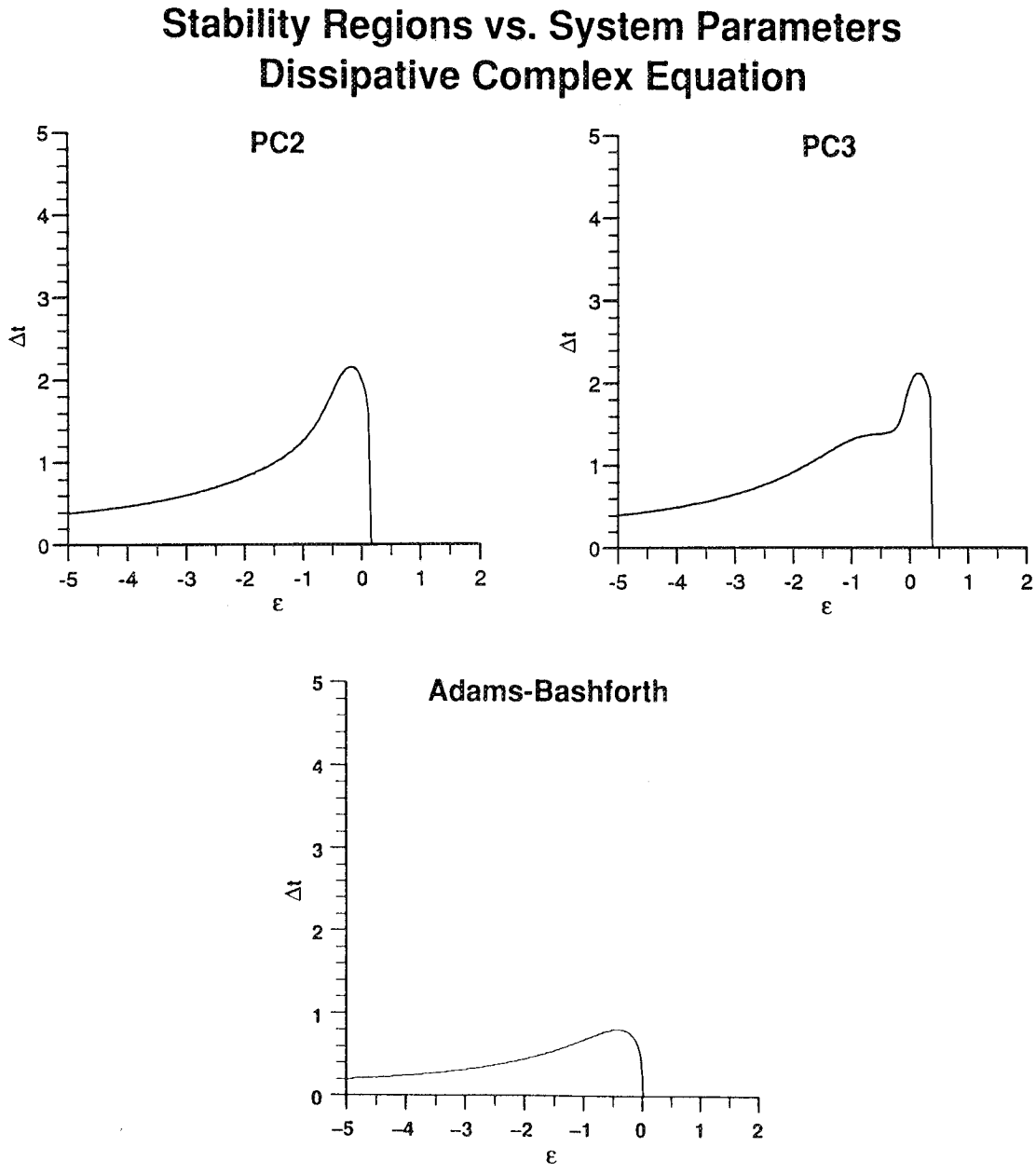

Figure 5.1 (Cont.)

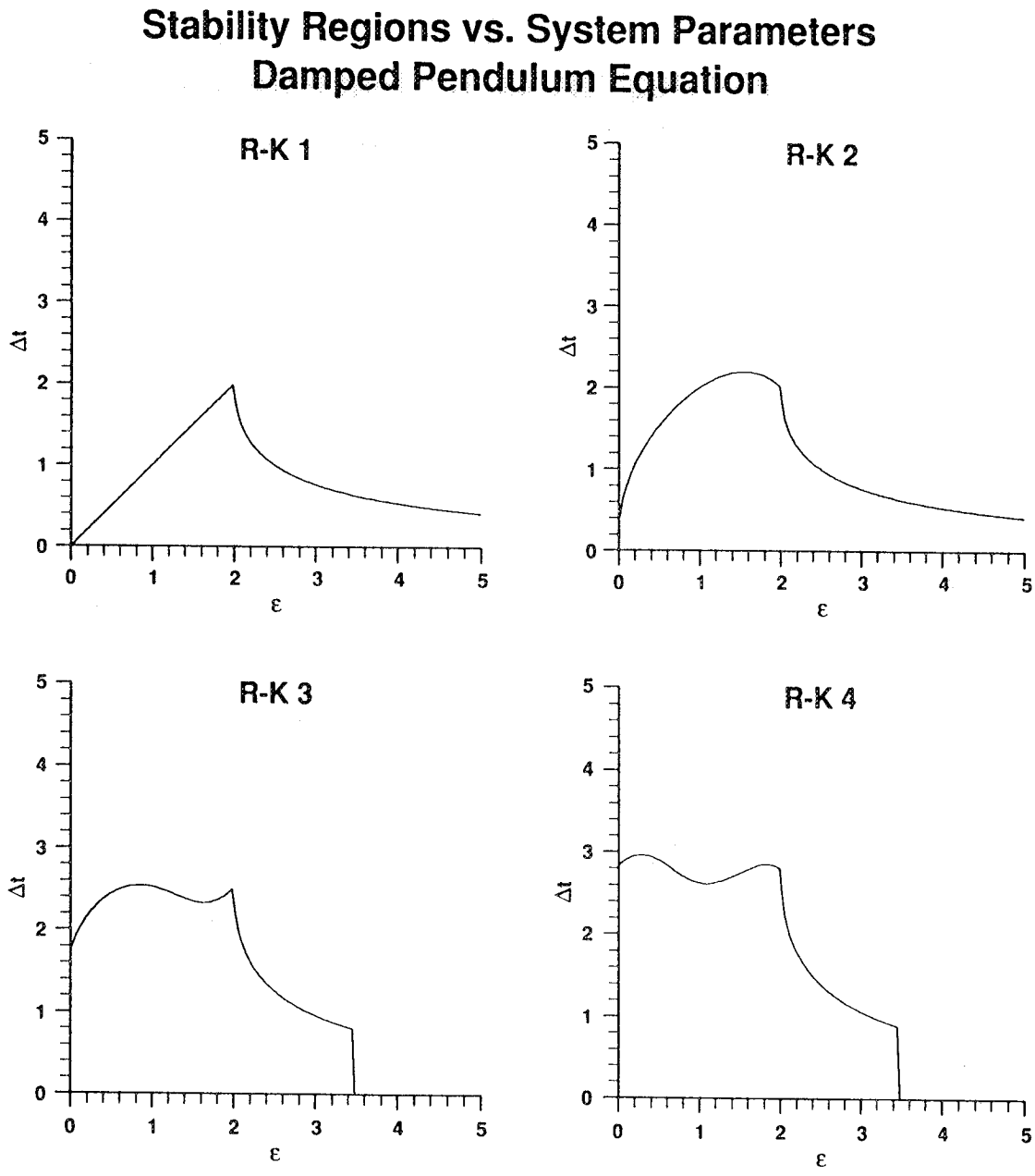
Stability Regions vs. System Parameters
Damped Pendulum Equation
R-K 1
R-K 2
R-K 3
R-K 4
Δt
ε
0
1
2
3
4
5

Figure 5.2

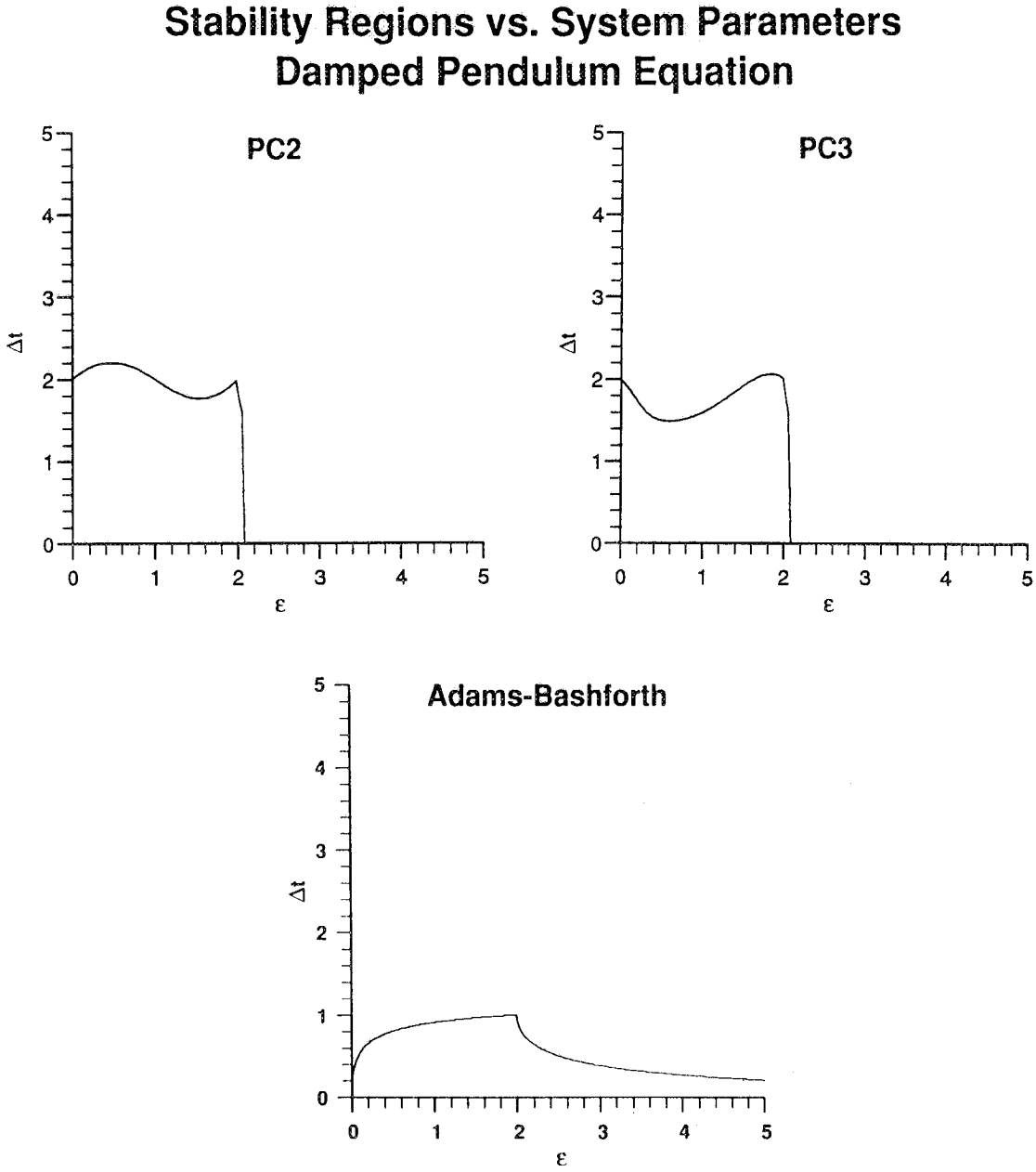

Figure 5.2 (Cont.)

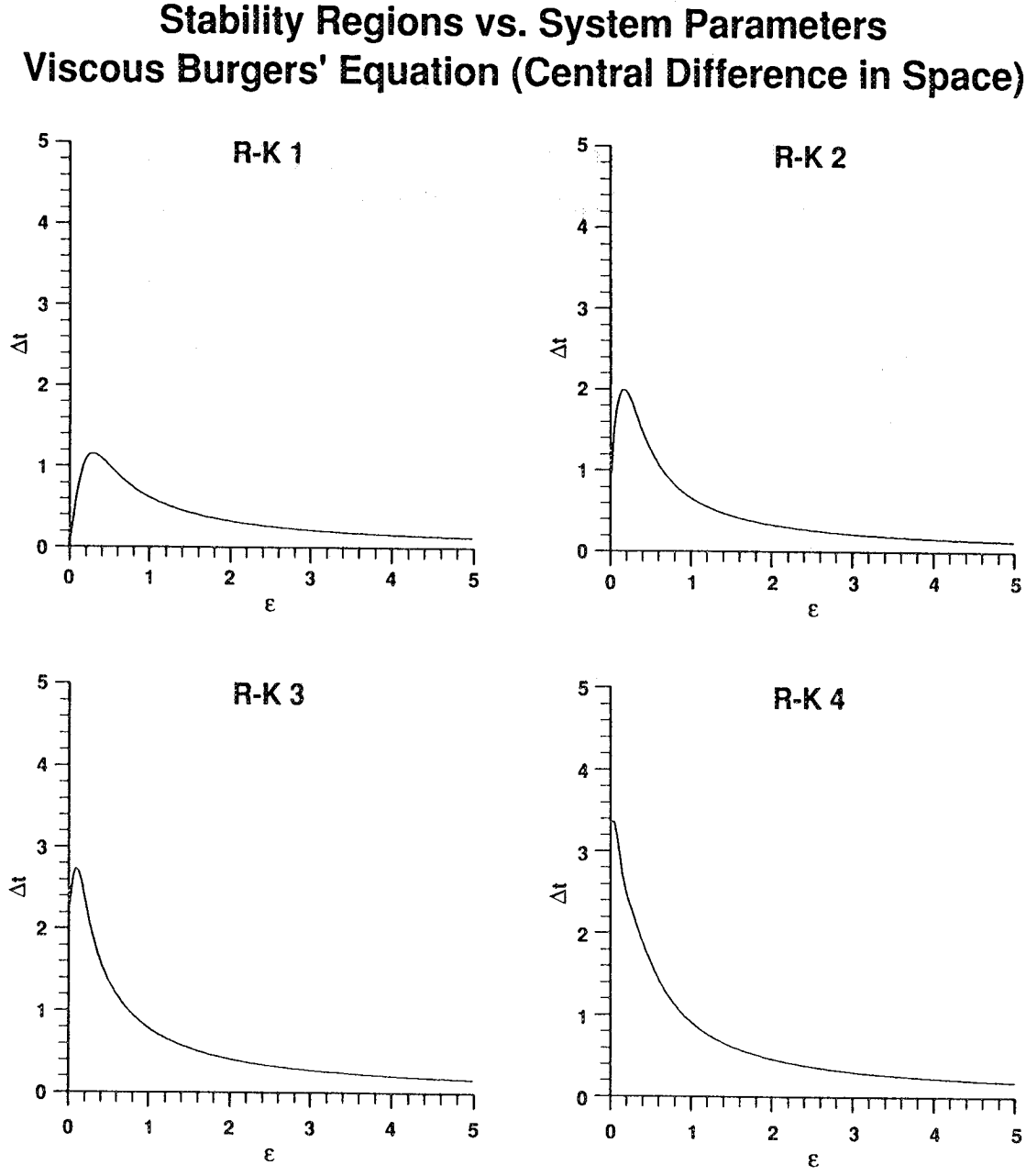
Stability Regions vs. System Parameters
Viscous Burgers' Equation (Central Difference in Space)
R-K 1
R-K 2
R-K 3
R-K 4
Δt
ε
0
1
2
3
4
5

Figure 5.3

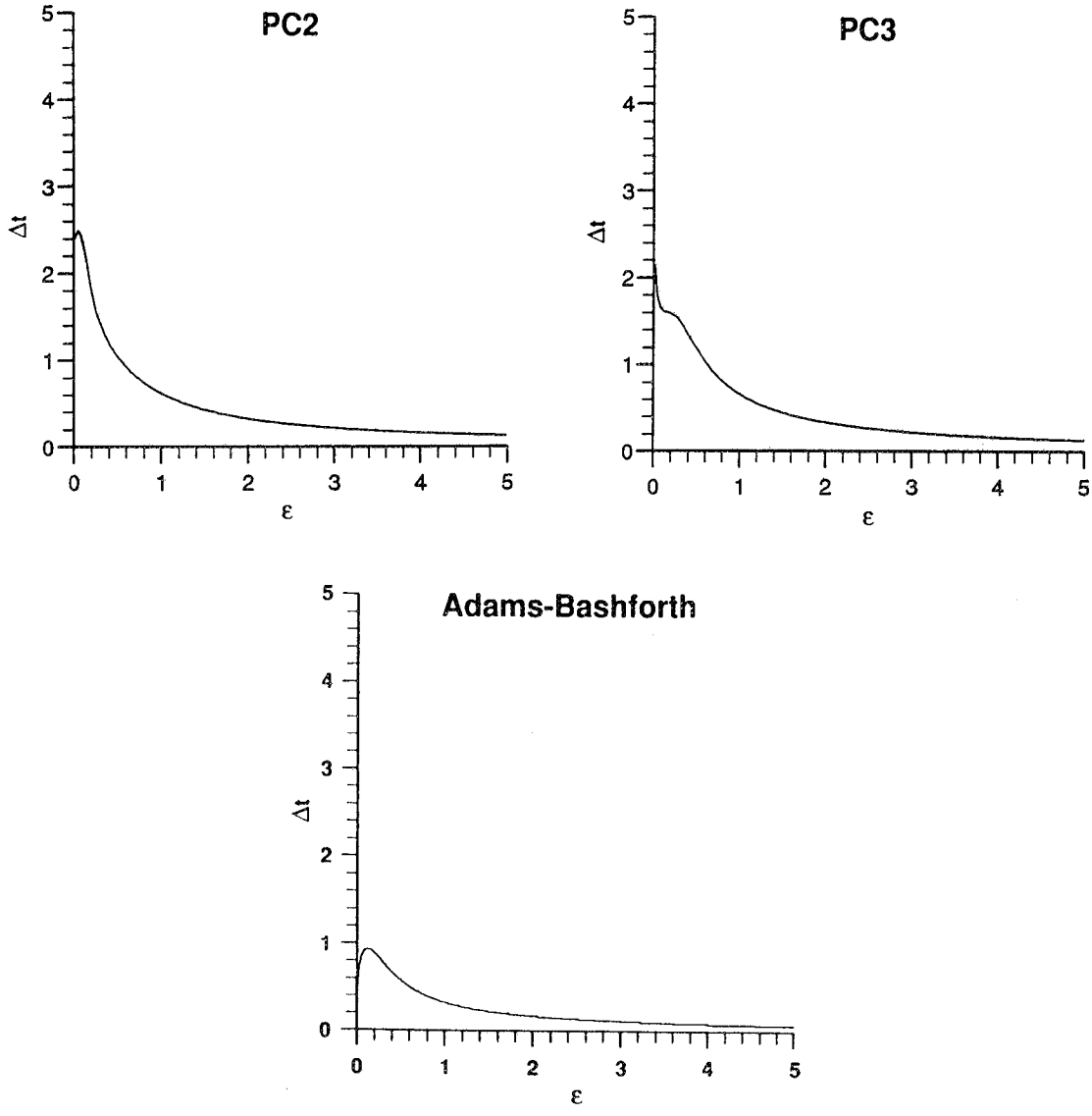

Figure 5.3 (Cont.)

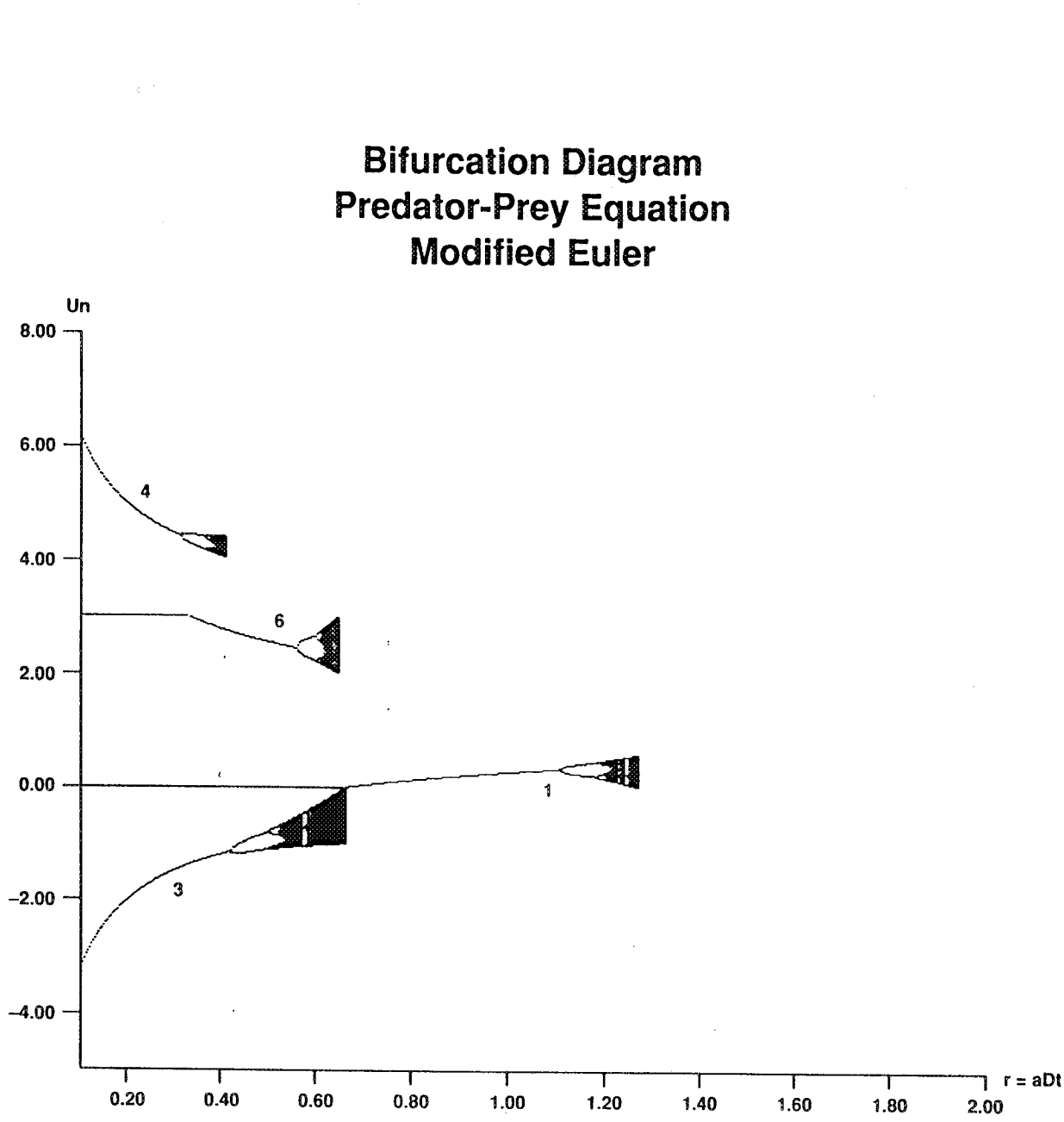
Bifurcation Diagram
Predator-Prey Equation
Modified Euler
Un
8.00
6.00
4.00
2.00
0.00
-2.00
-4.00
4
6
1
3
0.20
0.40
0.60
0.80
1.00
1.20
1.40
1.60
1.80
2.00
r = aDt

Figure 5.4

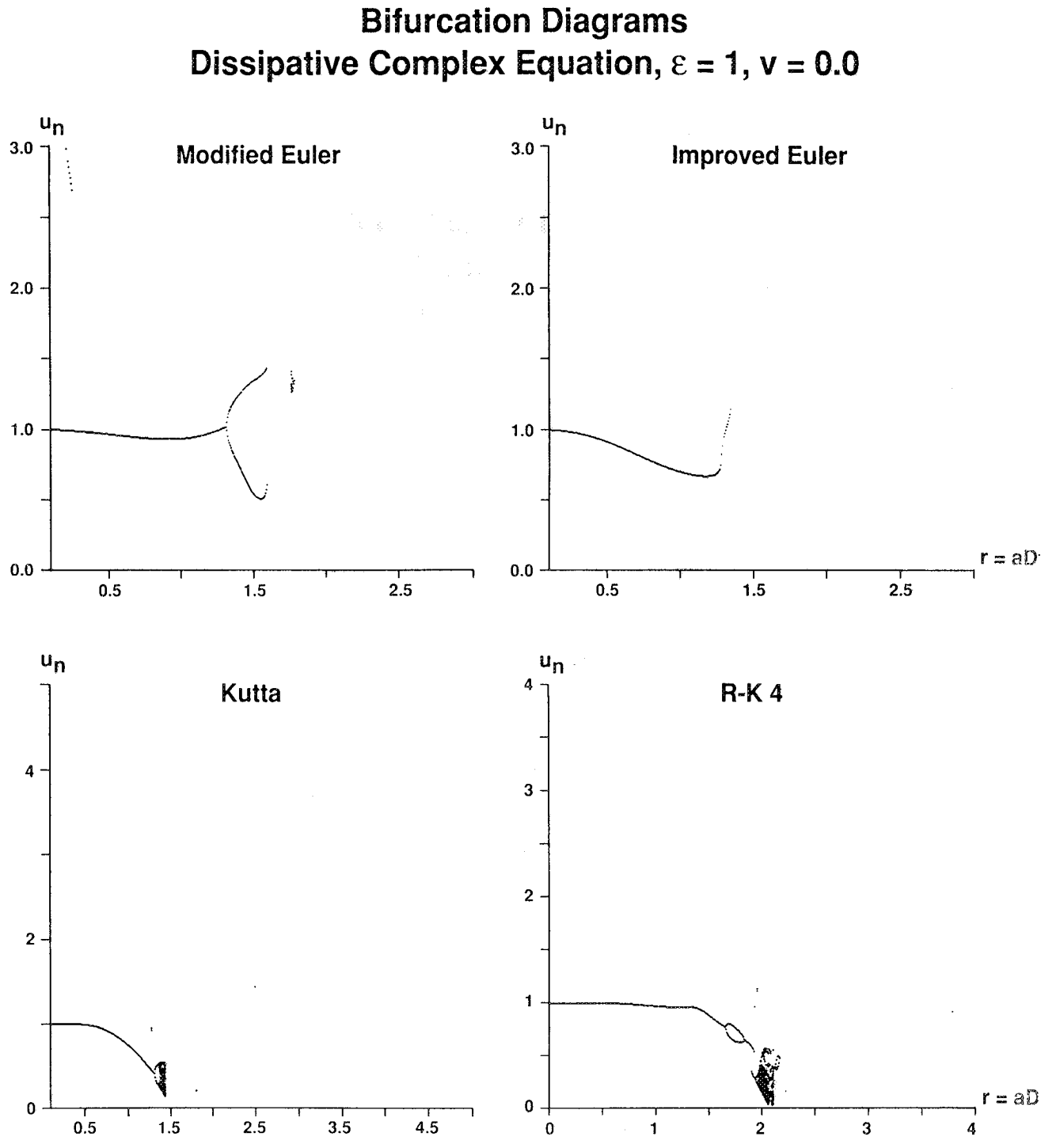
Bifurcation Diagrams
Dissipative Complex Equation, ε = 1, v = 0.0
Modified Euler
Improved Euler
Kutta
R-K 4
u_n
r = aD
3.0
2.0
1.0
0.0
0.5
1.5
2.5
3.5
4.5
4
3
2
1
0
1
2
3
4

Figure 5.5

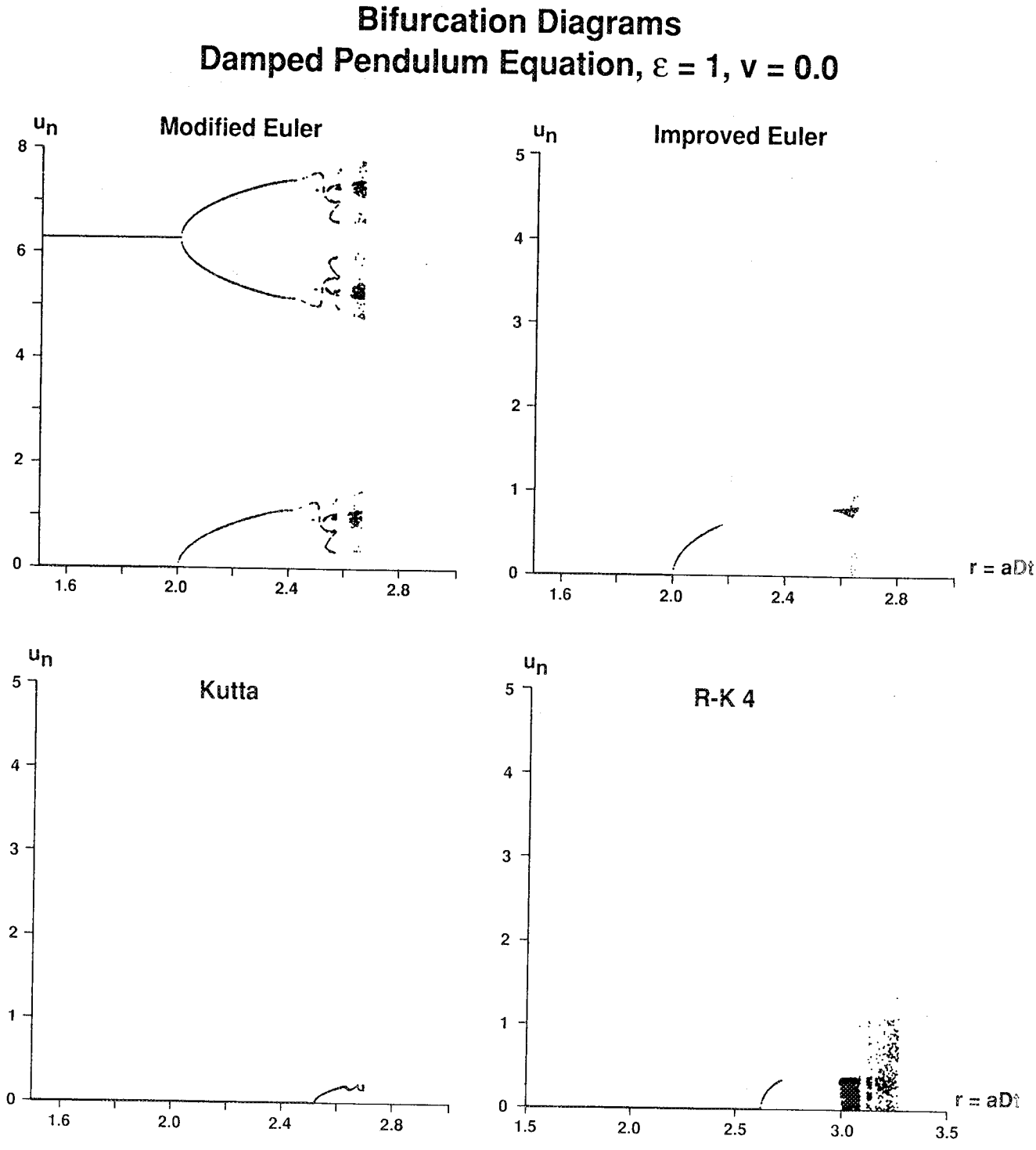
Bifurcation Diagrams
Damped Pendulum Equation, ε = 1, v = 0.0
Modified Euler
Improved Euler
Kutta
R-K 4
u_n
r = aDt

Figure 5.6

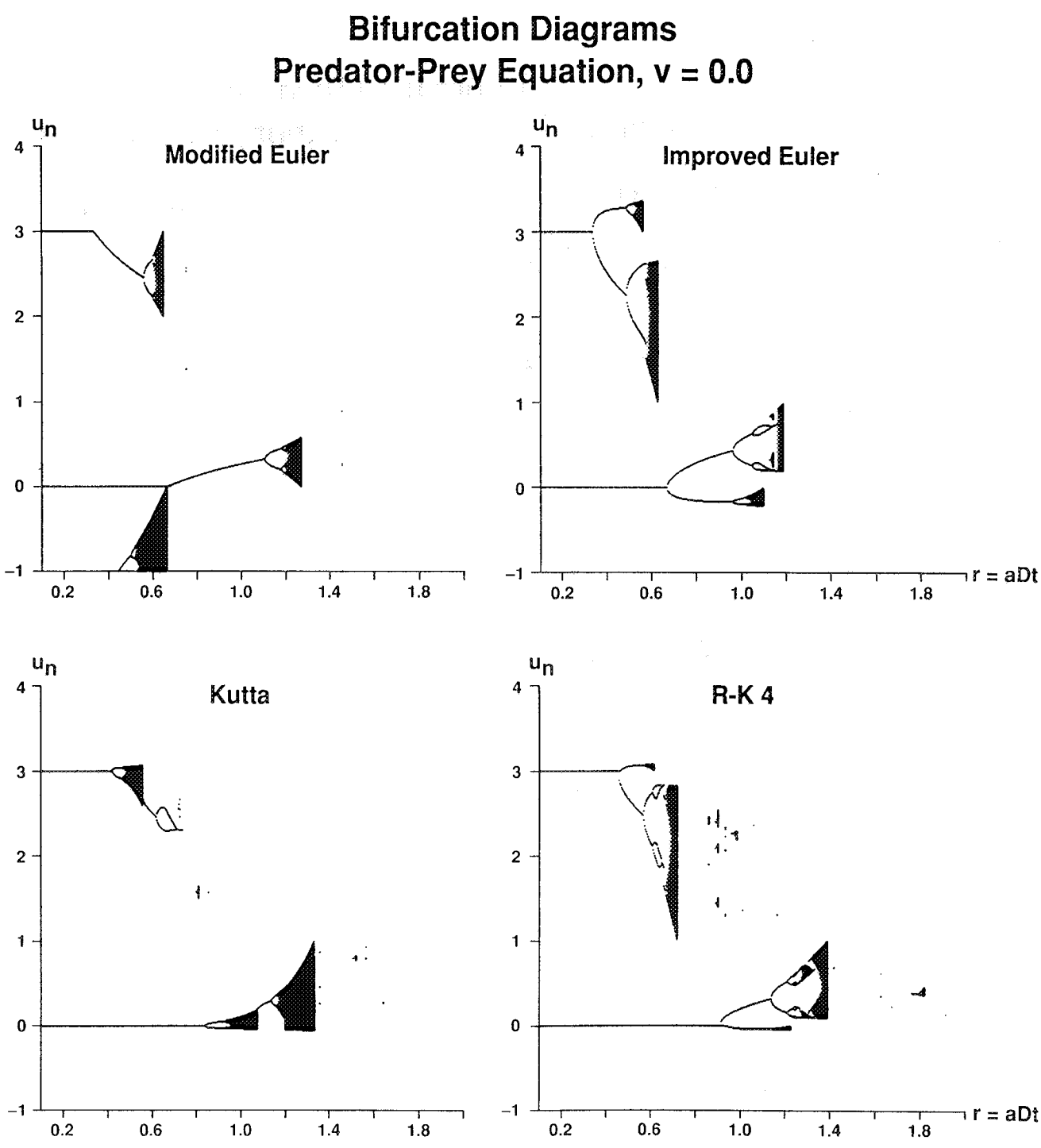
Bifurcation Diagrams
Predator-Prey Equation, v = 0.0
Modified Euler
Improved Euler
Kutta
R-K 4
u_n
r = aDt
4
3
2
1
0
−1
0.2
0.6
1.0
1.4
1.8

Figure 5.7

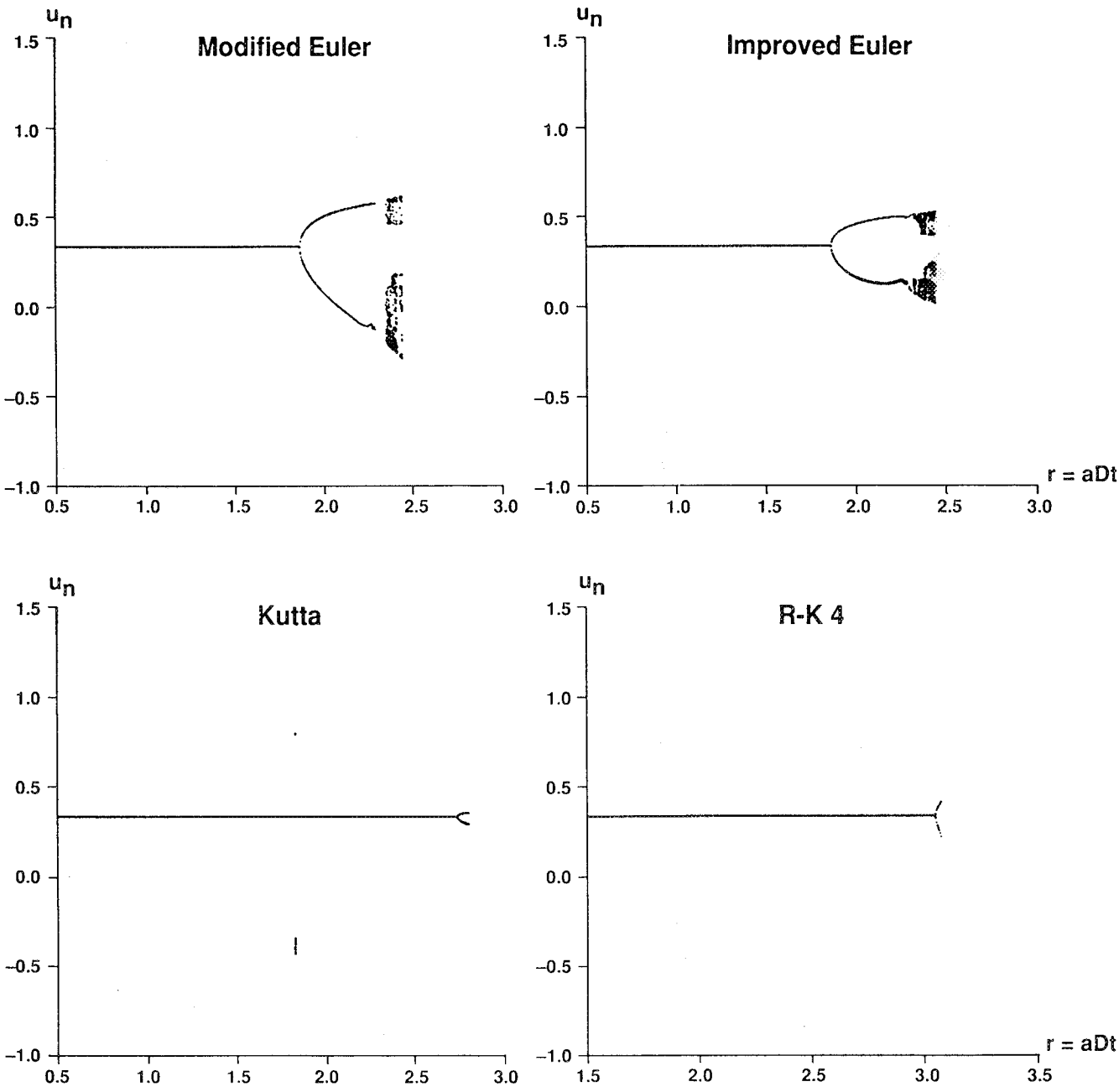
Bifurcation Diagrams
Viscous Burgers' Equation, ε = 0.1, v = 0.333
(Central Difference in Space)
Modified Euler
Improved Euler
Kutta
R-K 4
u_n
r = aDt
1.5
1.0
0.5
0.0
−0.5
−1.0
0.5
1.0
1.5
2.0
2.5
3.0
3.5

Figure 5.8

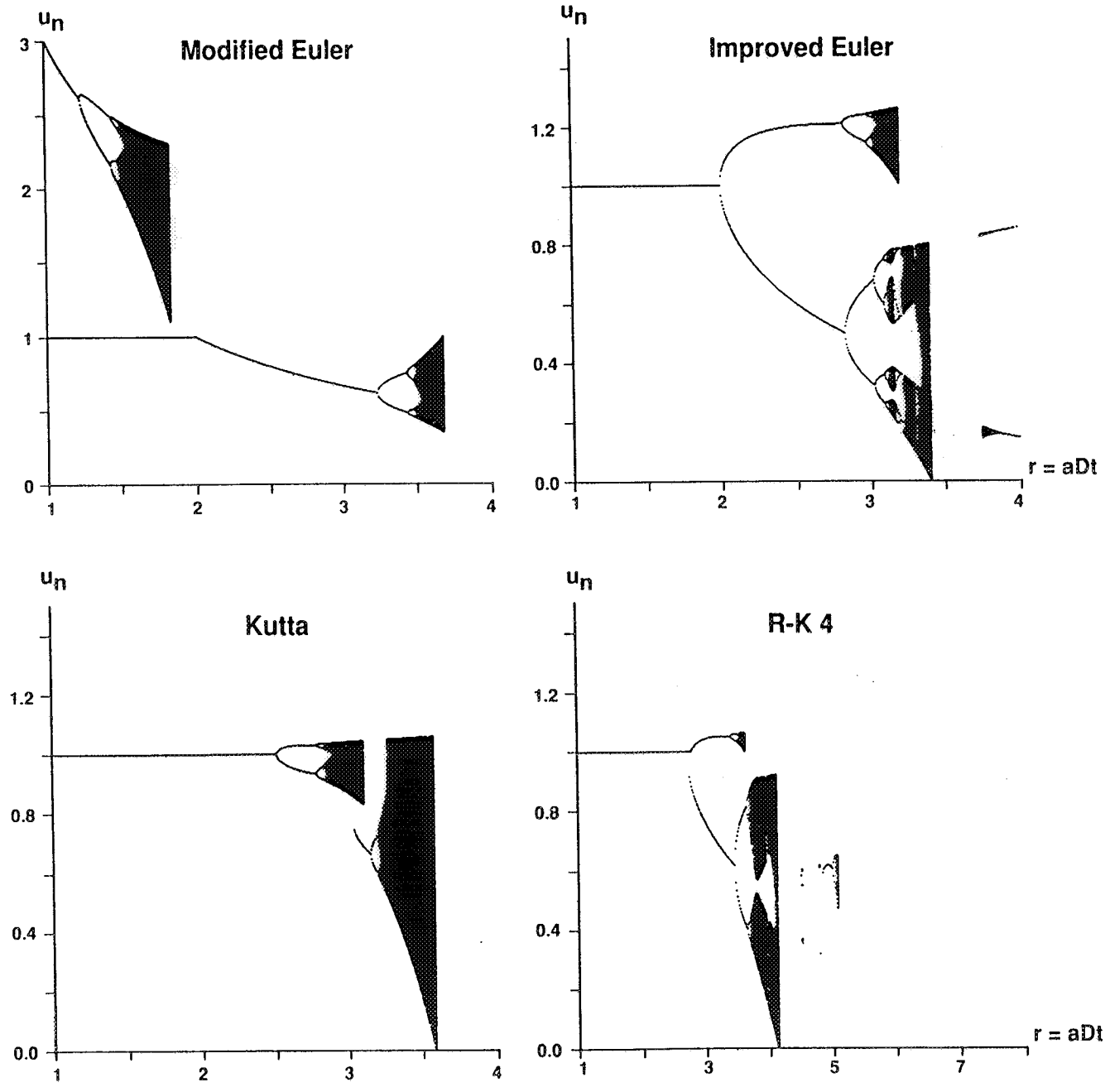
Bifurcation Diagrams
u' = au(1-u)
Modified Euler
Improved Euler
Kutta
R-K 4
u_n
r = aDt

Figure 6.1

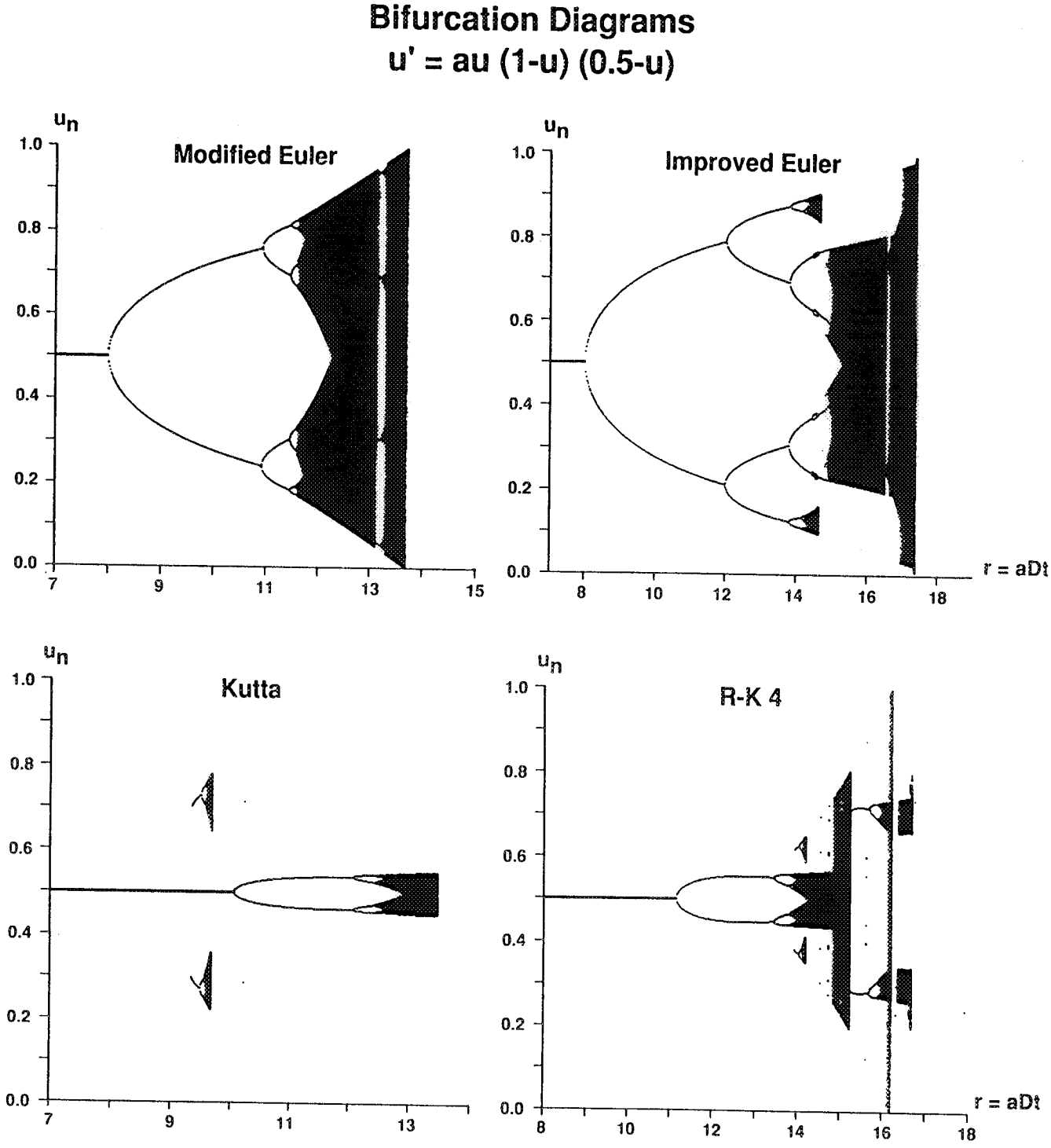
Bifurcation Diagrams
u' = au (1-u) (0.5-u)
Modified Euler
Improved Euler
Kutta
R-K 4
u_n
r = aDt
1.0
0.8
0.6
0.4
0.2
0.0
7
9
11
13
15
8
10
12
14
16
18

Figure 6.2

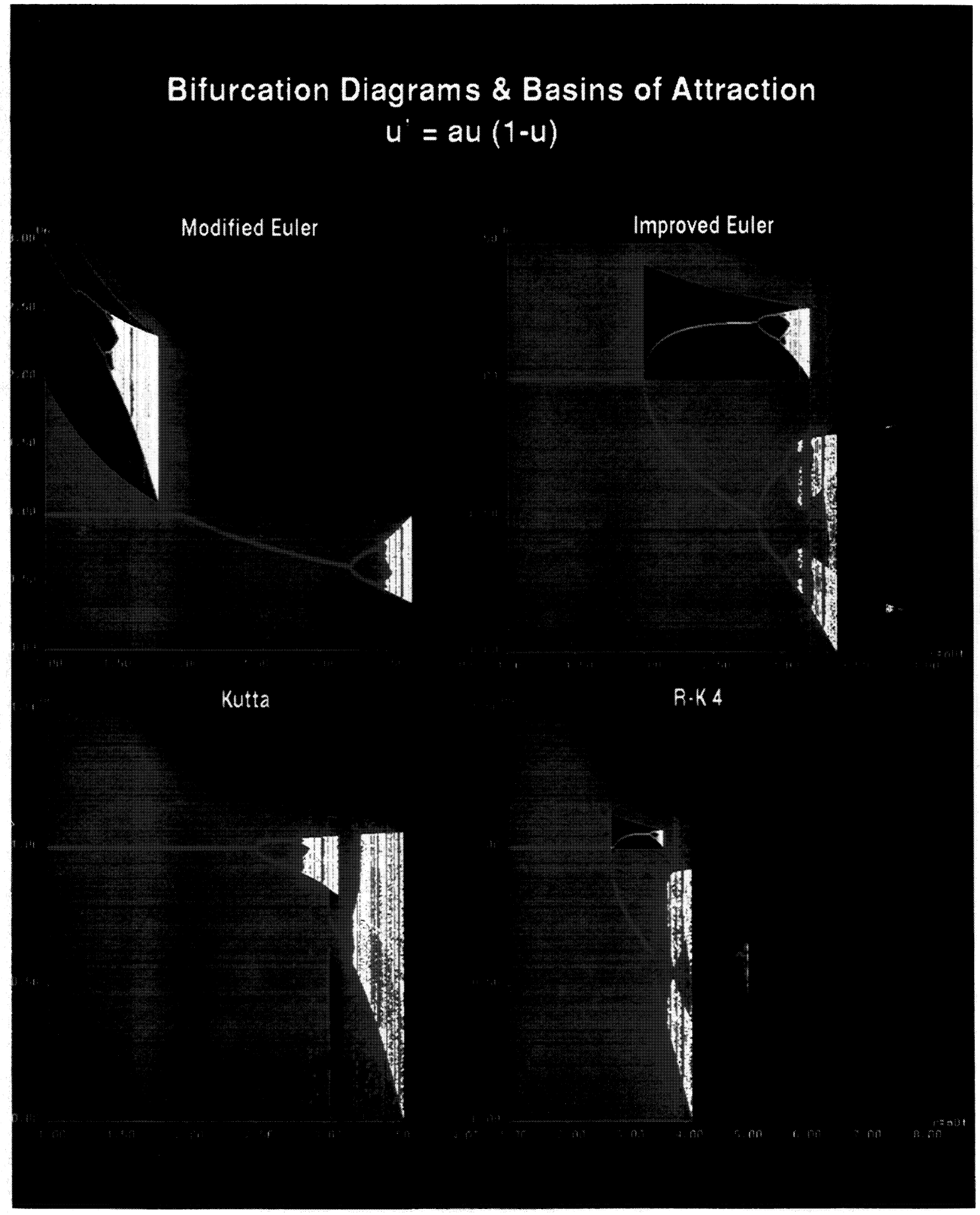
Bifurcation Diagrams & Basins of Attraction
u' = au (1-u)
Modified Euler
Improved Euler
Kutta
R-K 4

Figure 6.3

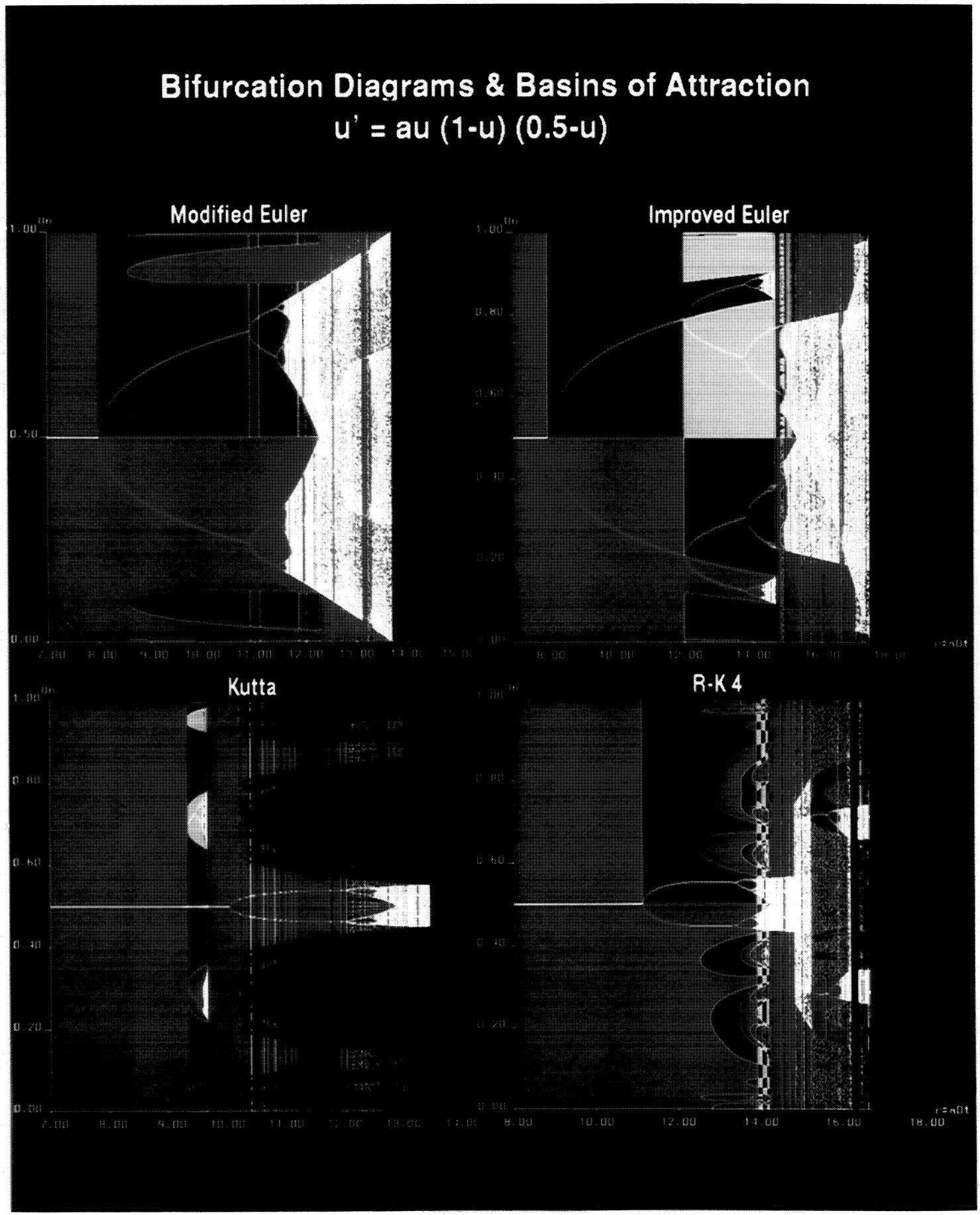
Bifurcation Diagrams & Basins of Attraction
u' = au (1-u) (0.5-u)
Modified Euler
Improved Euler
Kutta
R-K 4

Figure 6.4

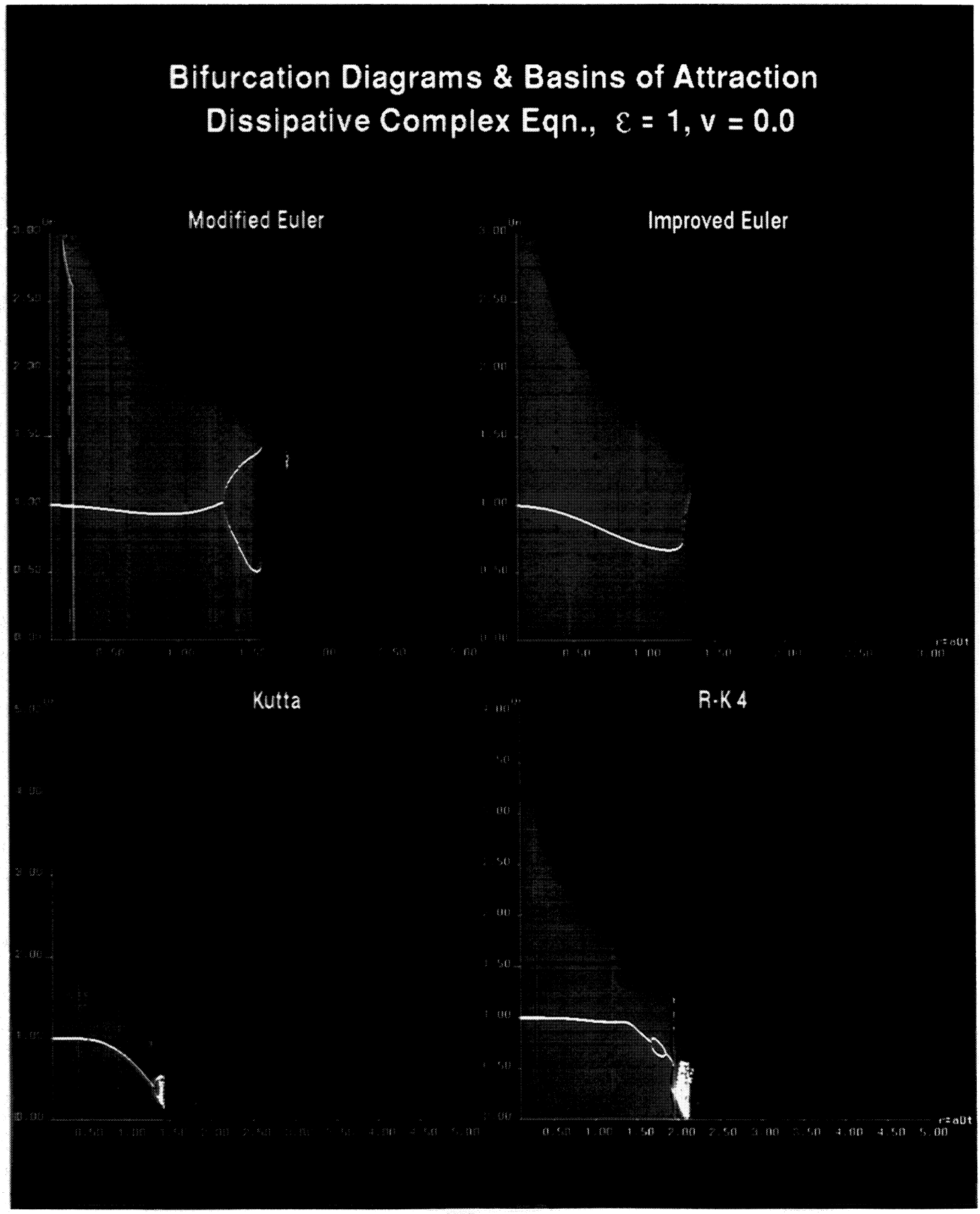
Bifurcation Diagrams & Basins of Attraction
Dissipative Complex Eqn., ε = 1, v = 0.0
Modified Euler
Improved Euler
Kutta
R-K 4

Figure 6.5

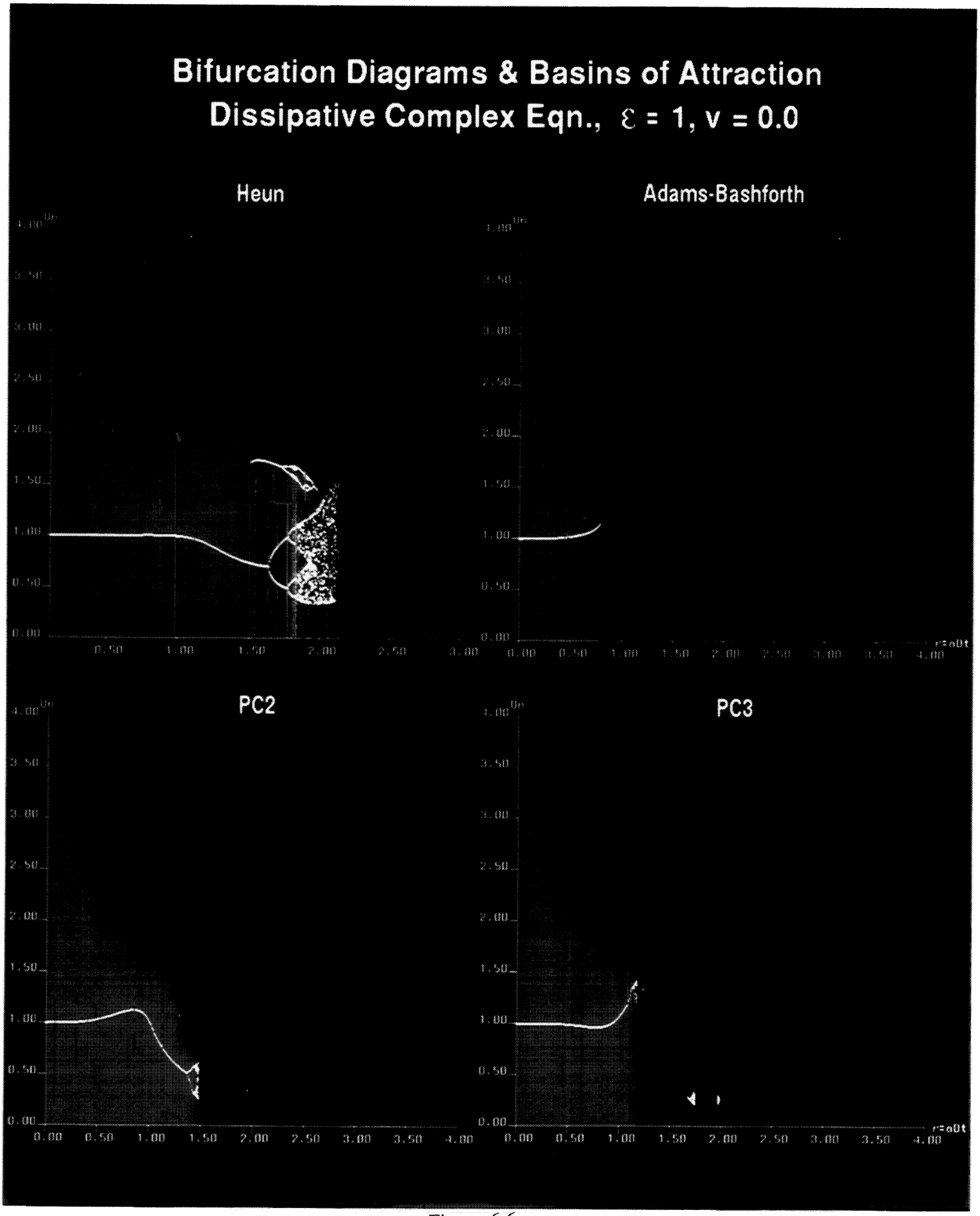
Bifurcation Diagrams & Basins of Attraction
Dissipative Complex Eqn., ε = 1, v = 0.0
Heun
Adams-Bashforth
PC2
PC3
r=aDt

Figure 6.6

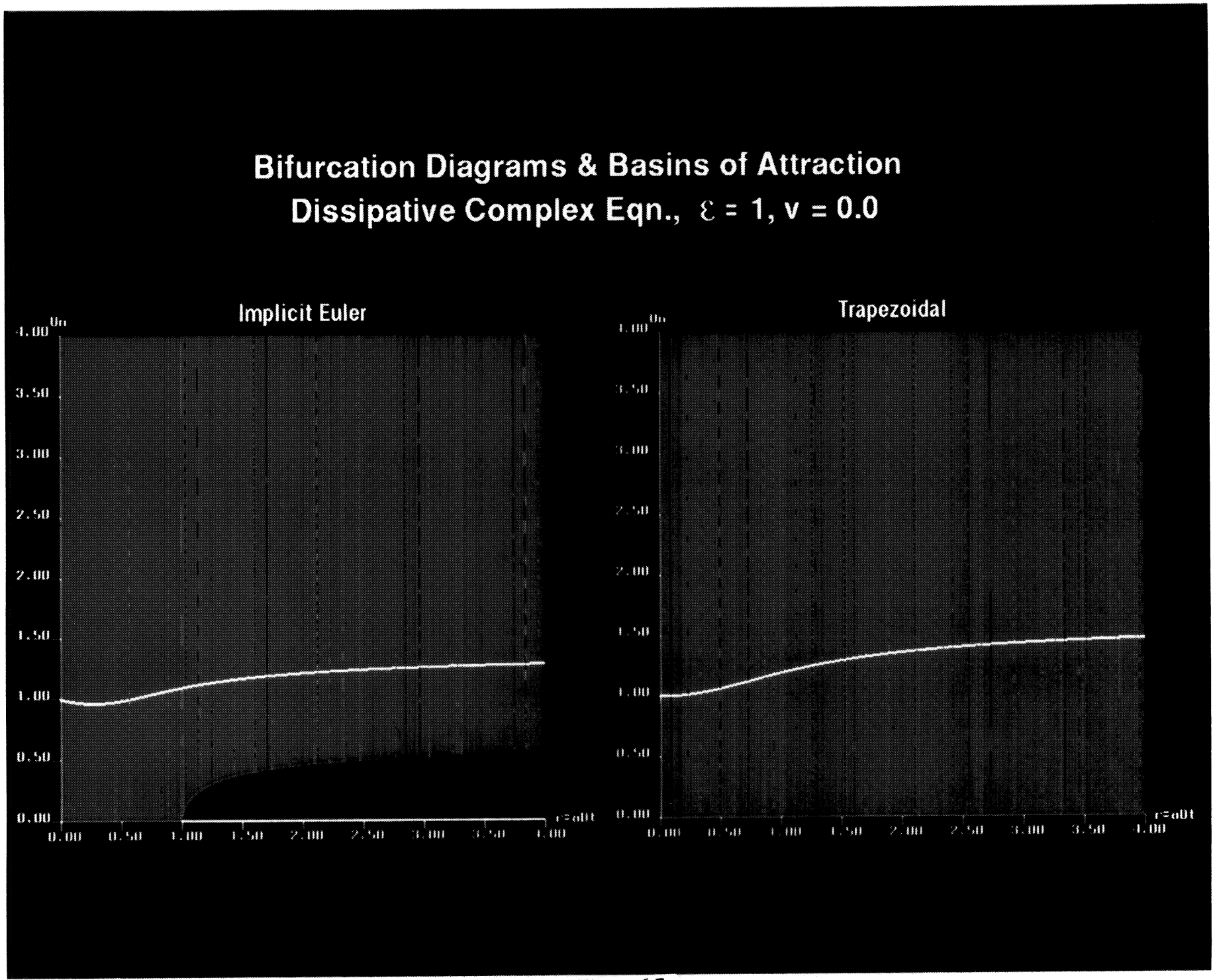
Bifurcation Diagrams & Basins of Attraction
Dissipative Complex Eqn., ε = 1, v = 0.0
Implicit Euler
Trapezoidal
4.00
3.50
3.00
2.50
2.00
1.50
1.00
0.50
0.00
0.00
0.50
1.00
1.50
2.00
2.50
3.00
3.50
4.00

Figure 6.7

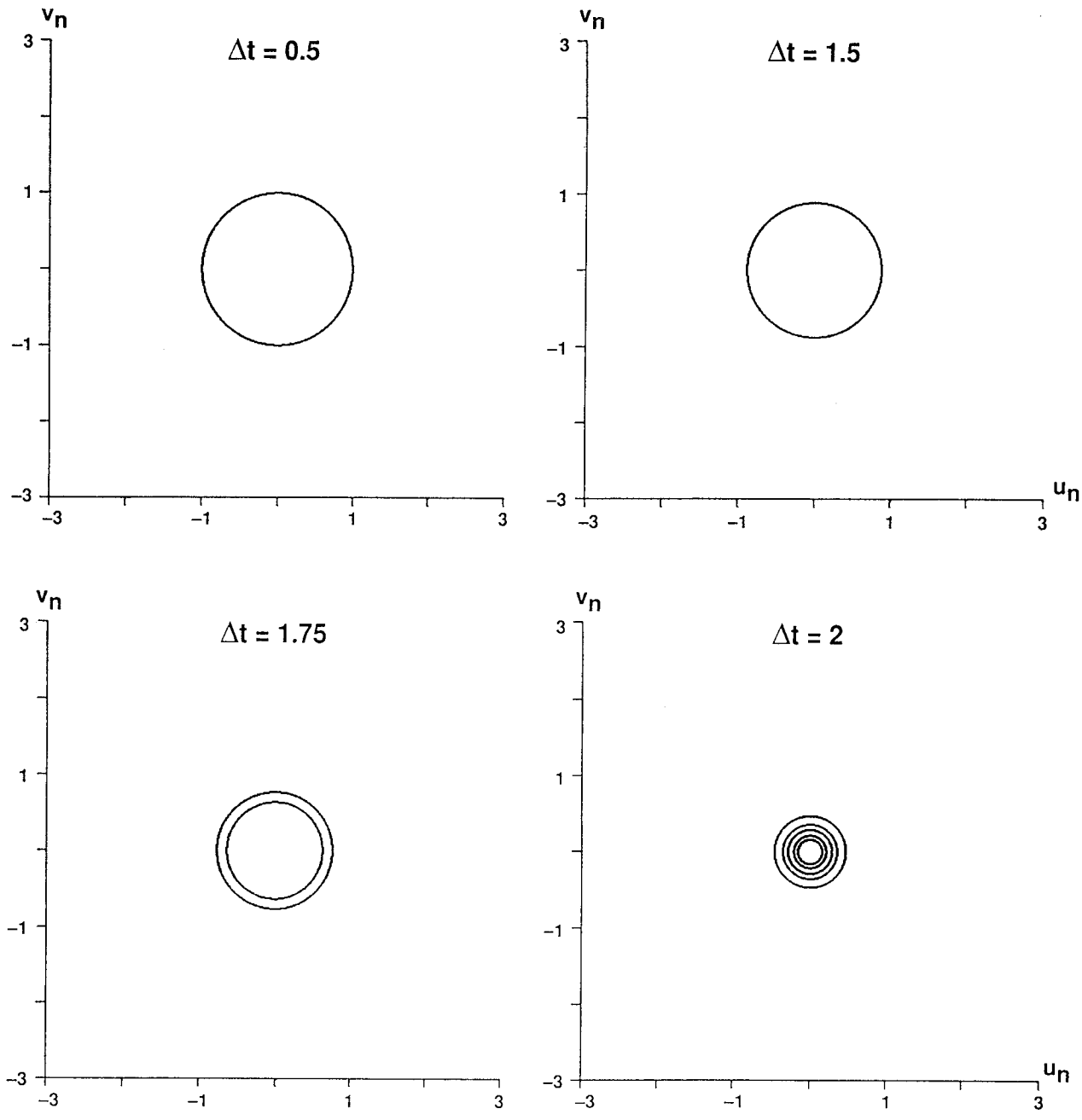
Phase Trajectories
Dissipative Complex Equation, ε = 1
R-K 4
vn
Δt = 0.5
Δt = 1.5
Δt = 1.75
Δt = 2
un
3
1
−1
−3

Figure 6.8

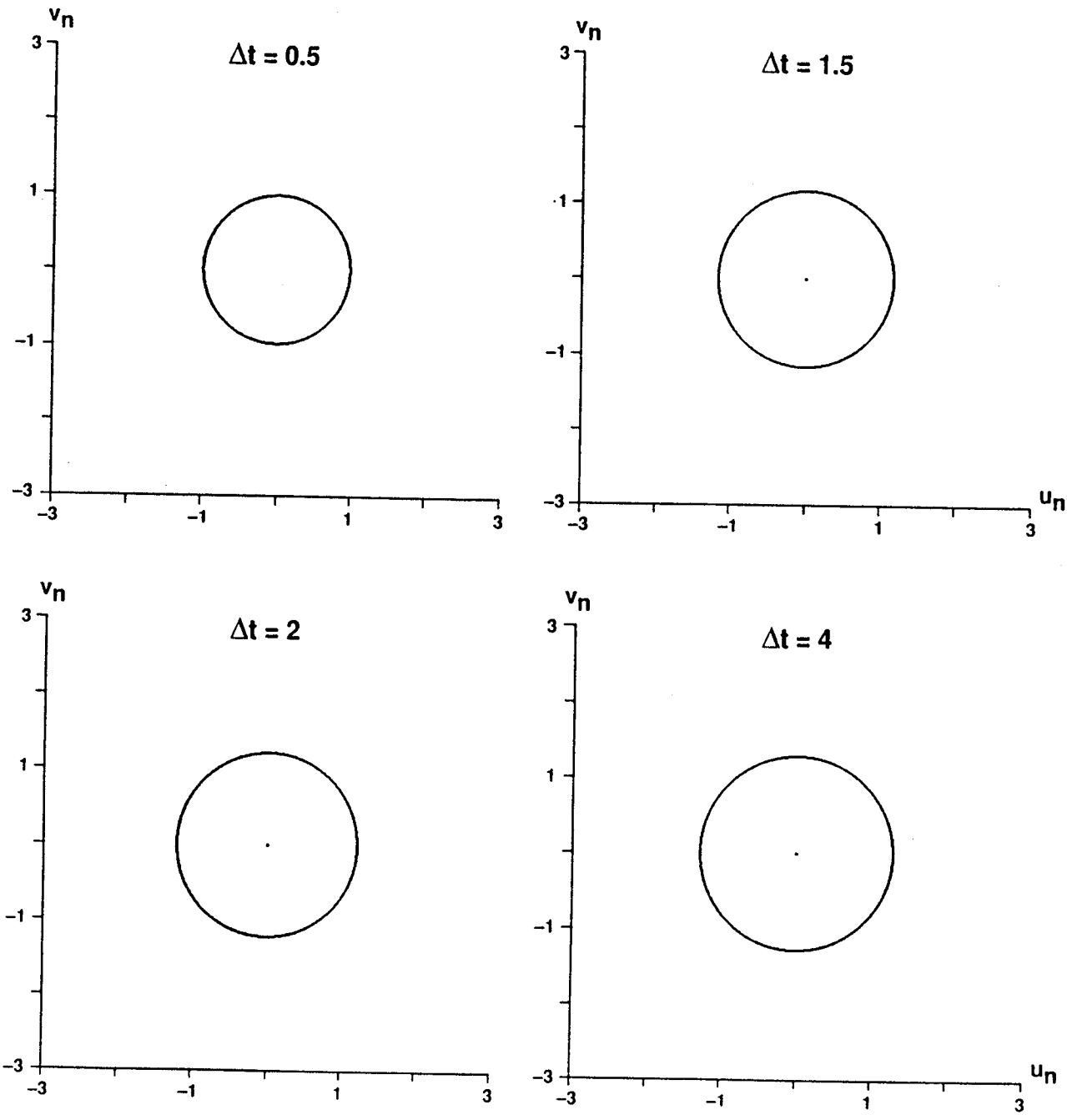
Phase Trajectories
Dissipative Complex Equation, ε = 1
Linearized Implicit Euler
Δt = 0.5
Δt = 1.5
Δt = 2
Δt = 4
vn
un
3
1
-1
-3

Figure 6.9

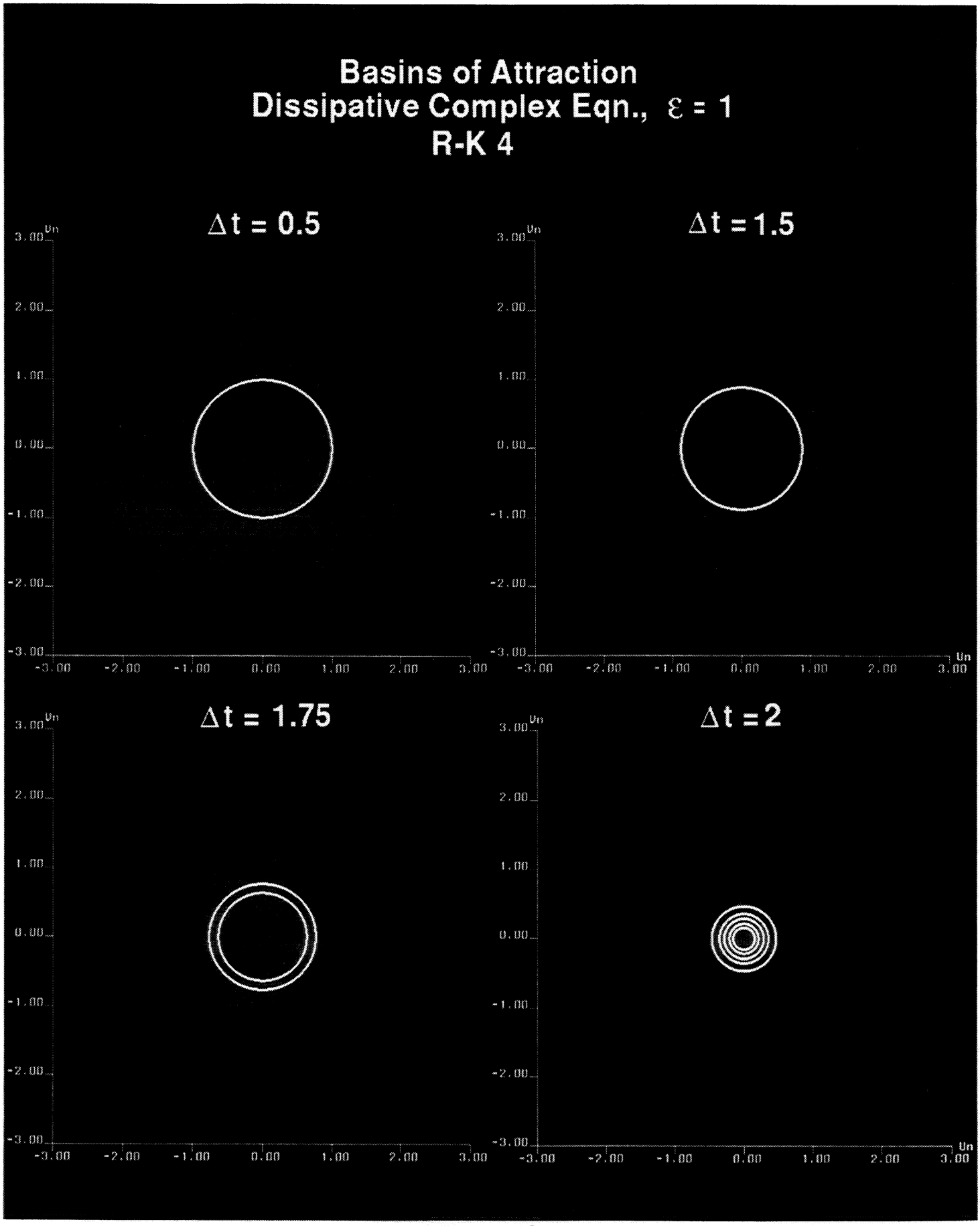
Basins of Attraction
Dissipative Complex Eqn., ε = 1
R-K 4
Δt = 0.5
Δt = 1.5
Δt = 1.75
Δt = 2
Un
3.00
2.00
1.00
0.00
-1.00
-2.00
-3.00

Figure 6.10

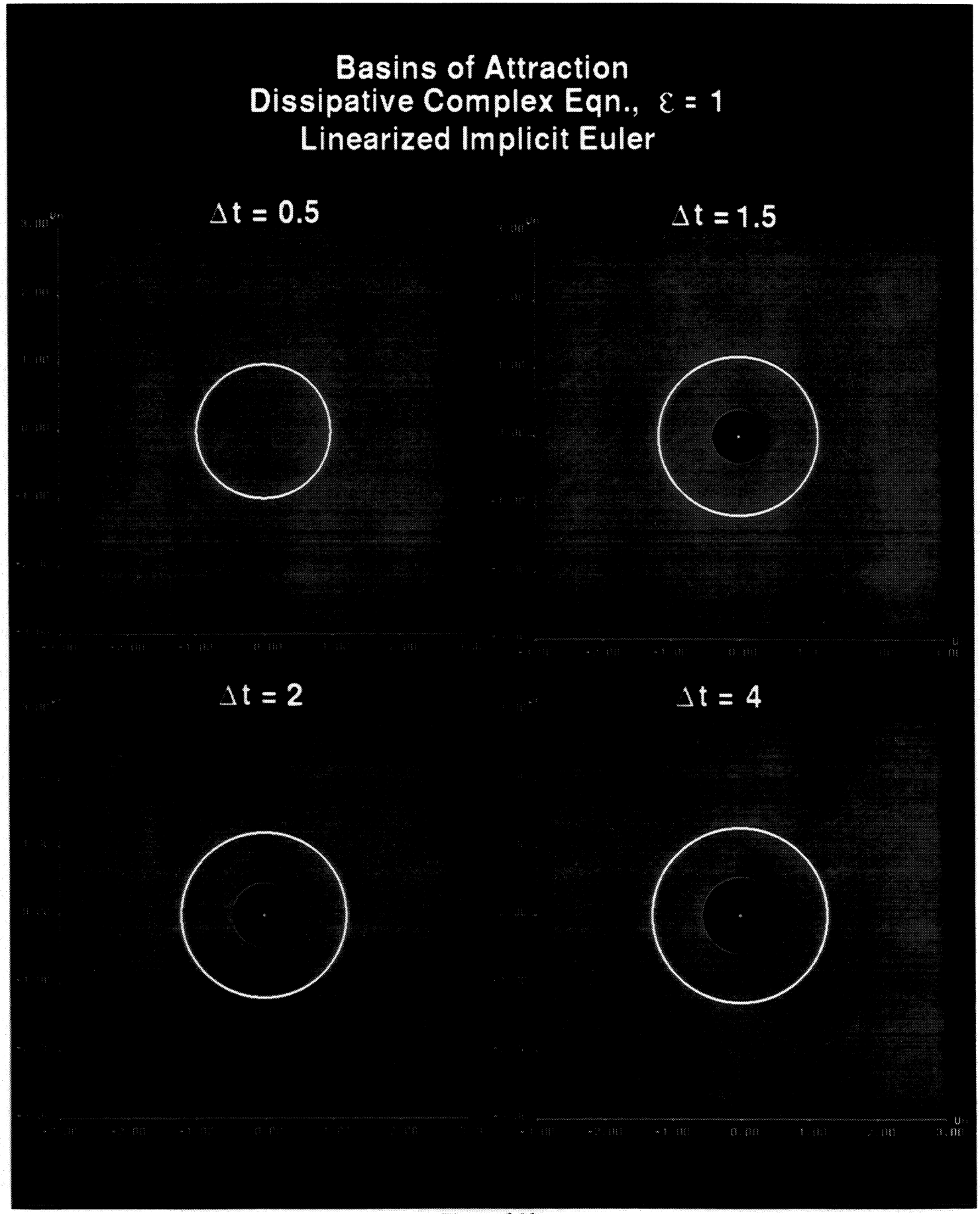
Basins of Attraction
Dissipative Complex Eqn., ε = 1
Linearized Implicit Euler
Δt = 0.5
Δt = 1.5
Δt = 2
Δt = 4

Figure 6.11

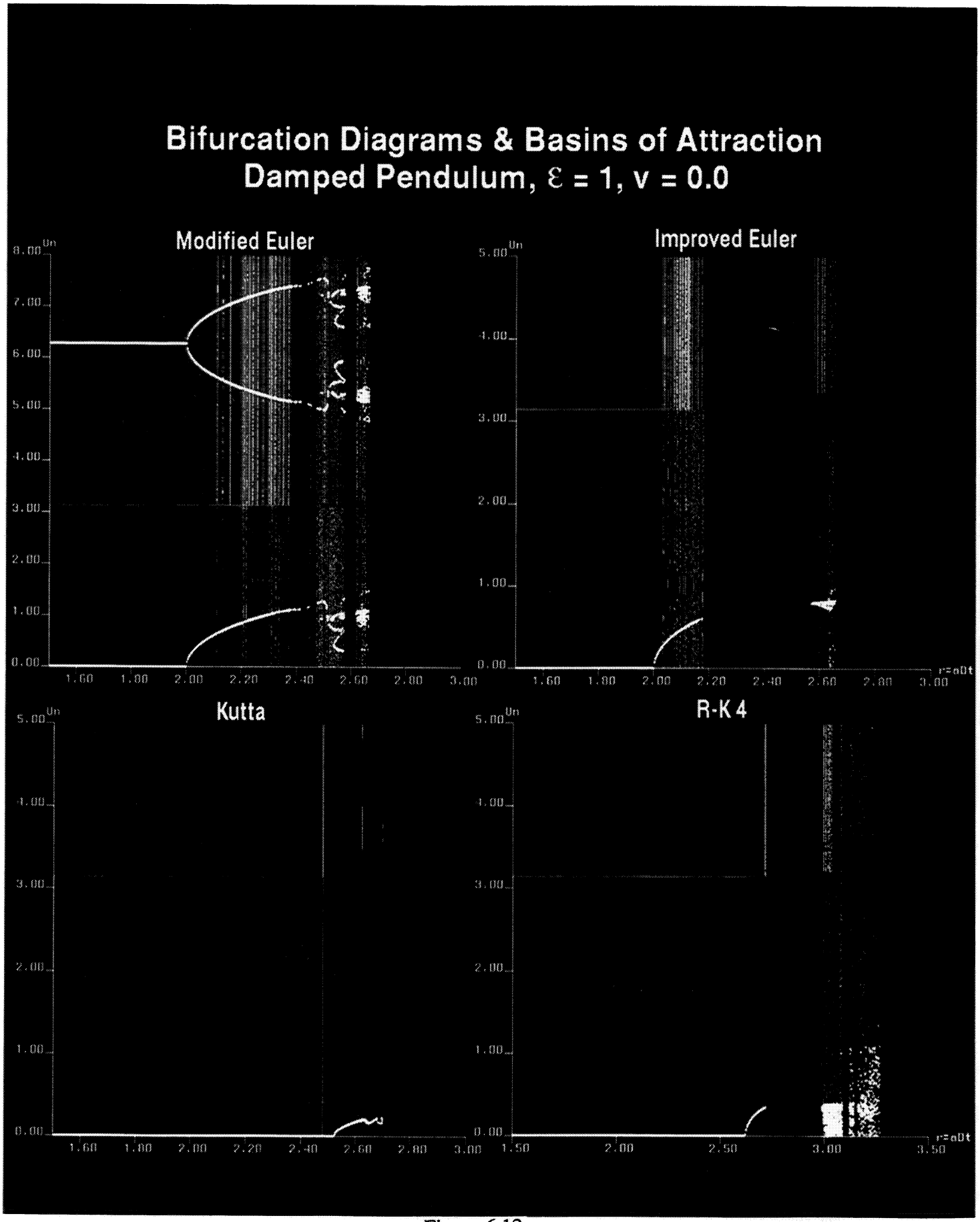
Bifurcation Diagrams & Basins of Attraction
Damped Pendulum, ε = 1, v = 0.0
Modified Euler
Improved Euler
Kutta
R-K 4
Un
r=aDt

Figure 6.12

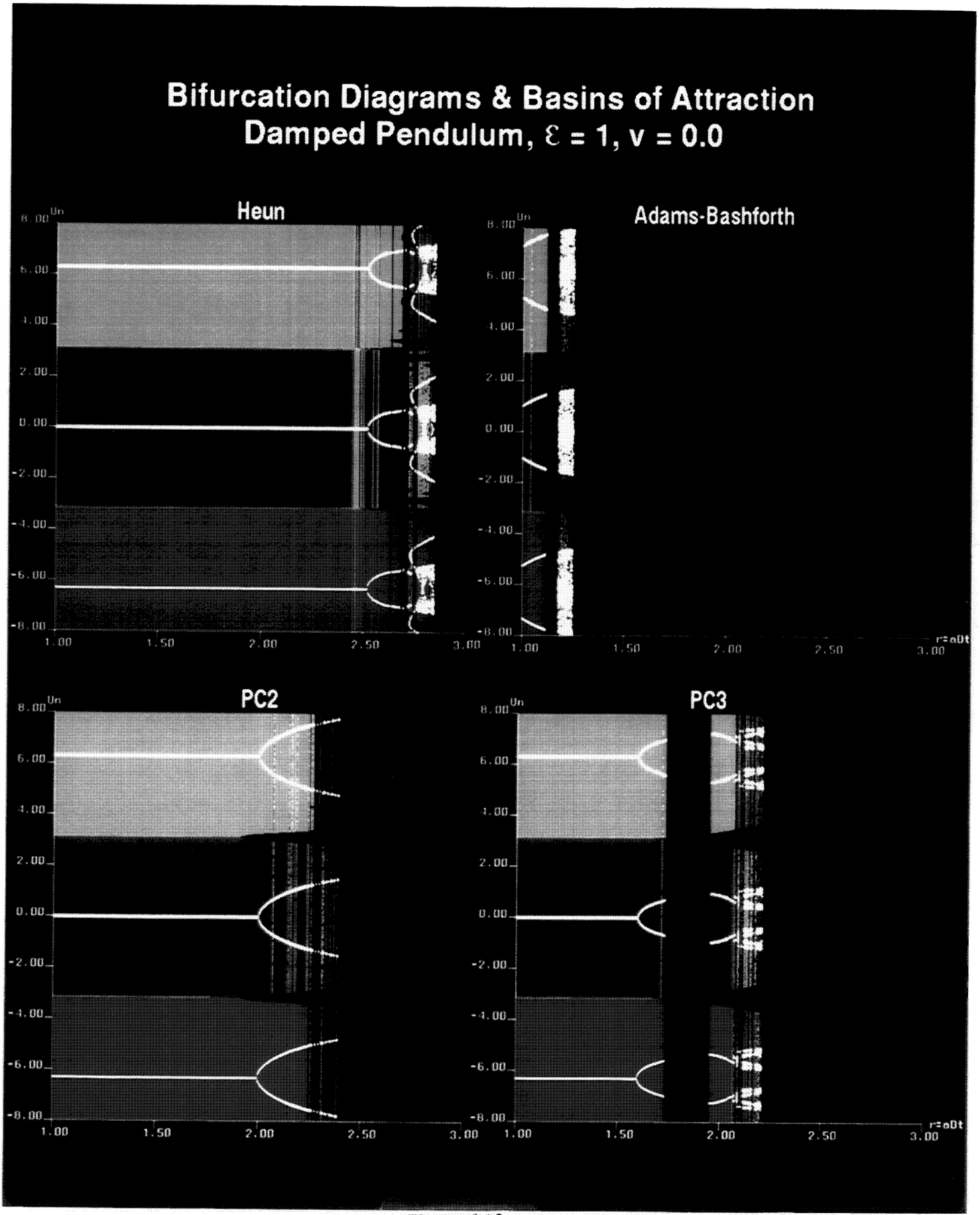
Bifurcation Diagrams & Basins of Attraction
Damped Pendulum, ε = 1, v = 0.0
Heun
Adams-Bashforth
PC2
PC3
Un
r=aDt
8.00
6.00
4.00
2.00
0.00
-2.00
-4.00
-6.00
-8.00
1.00
1.50
2.00
2.50
3.00

Figure 6.13

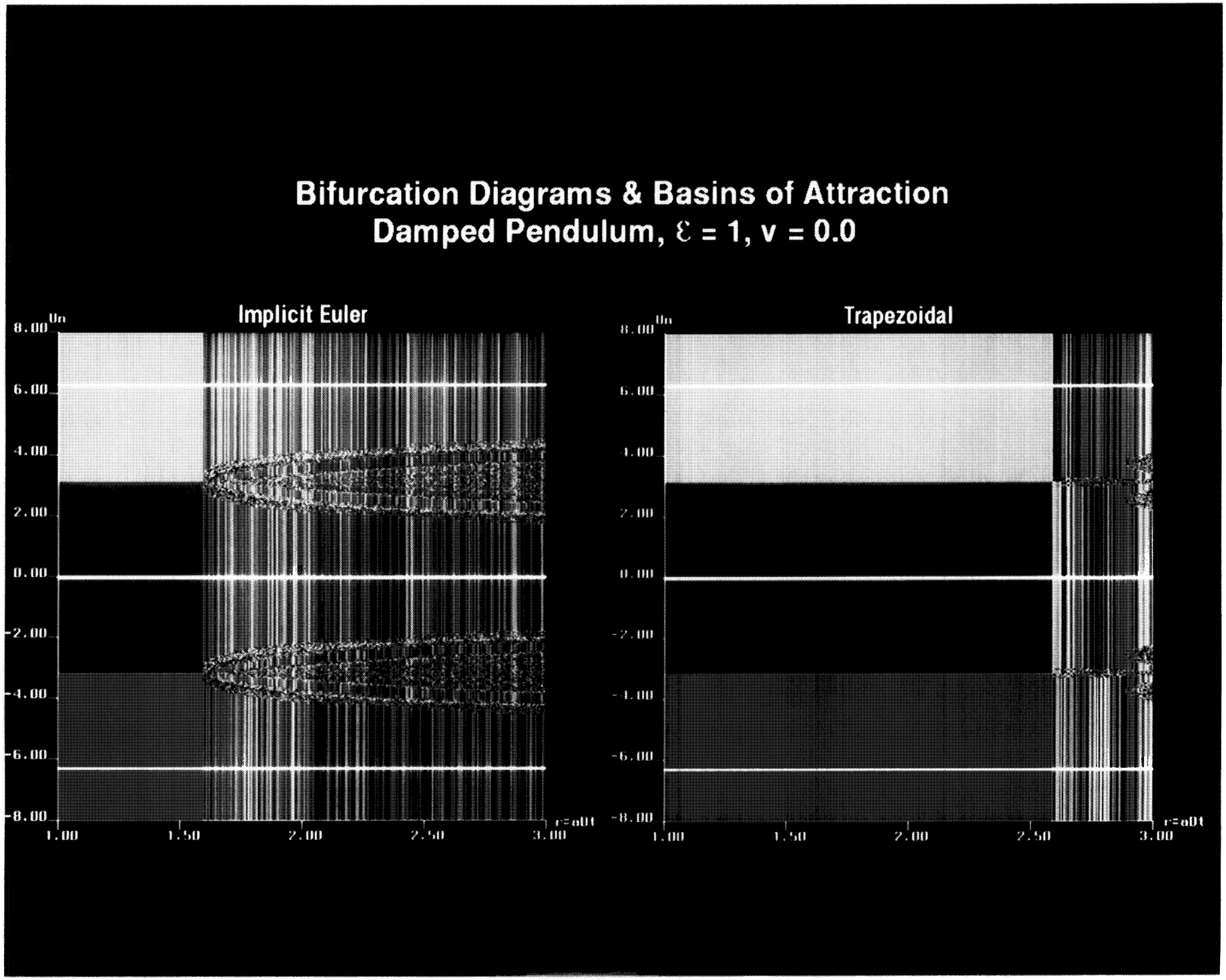
Bifurcation Diagrams & Basins of Attraction
Damped Pendulum, ε = 1, v = 0.0
Implicit Euler
Trapezoidal
θn
8.00
6.00
4.00
2.00
0.00
-2.00
-4.00
-6.00
-8.00
1.00
1.50
2.00
2.50
3.00
r=ωΔt

Figure 6.14

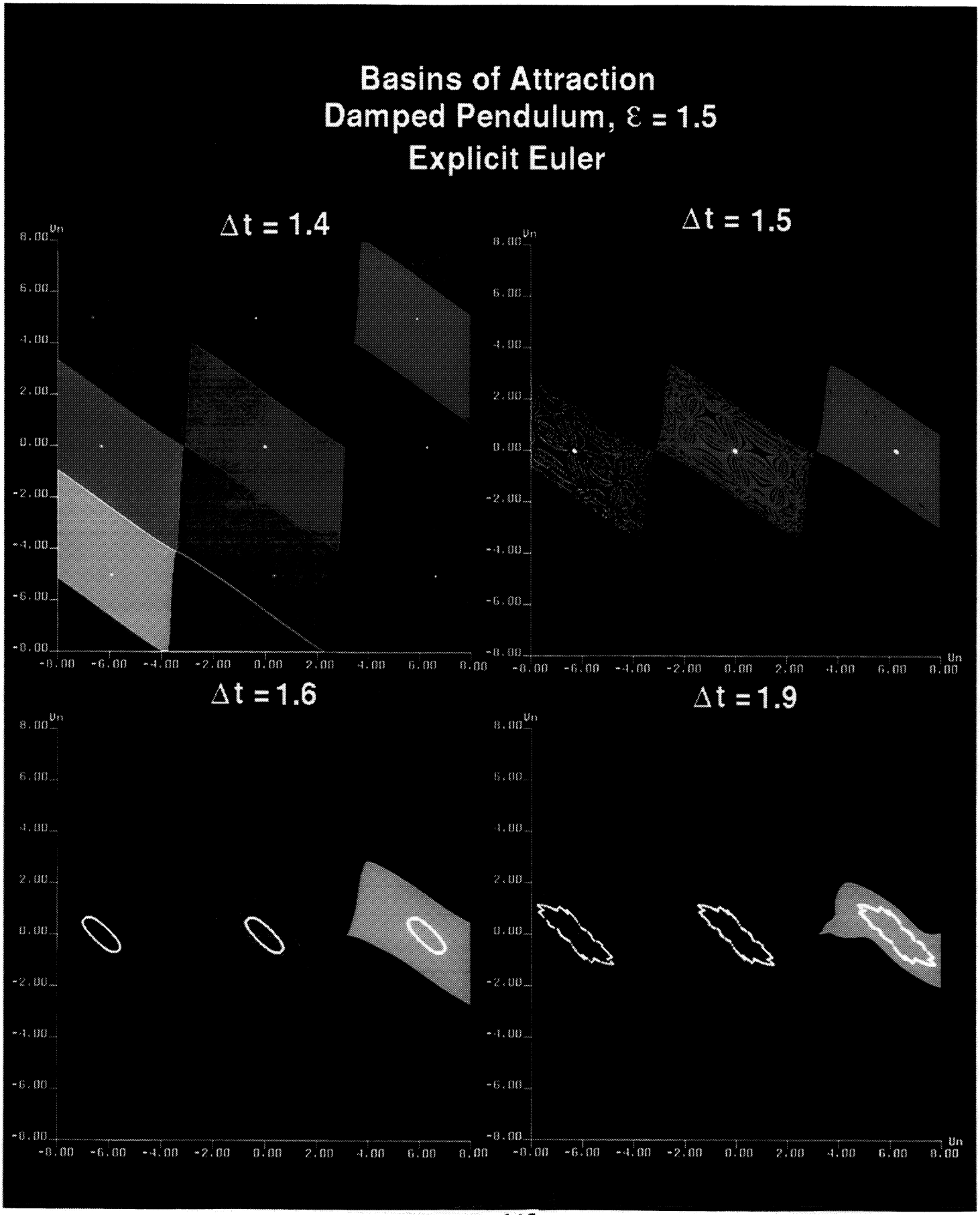
Basins of Attraction
Damped Pendulum, ε = 1.5
Explicit Euler
Δt = 1.4
Δt = 1.5
Δt = 1.6
Δt = 1.9
Un
8.00
6.00
4.00
2.00
0.00
-2.00
-4.00
-6.00
-8.00

Figure 6.15

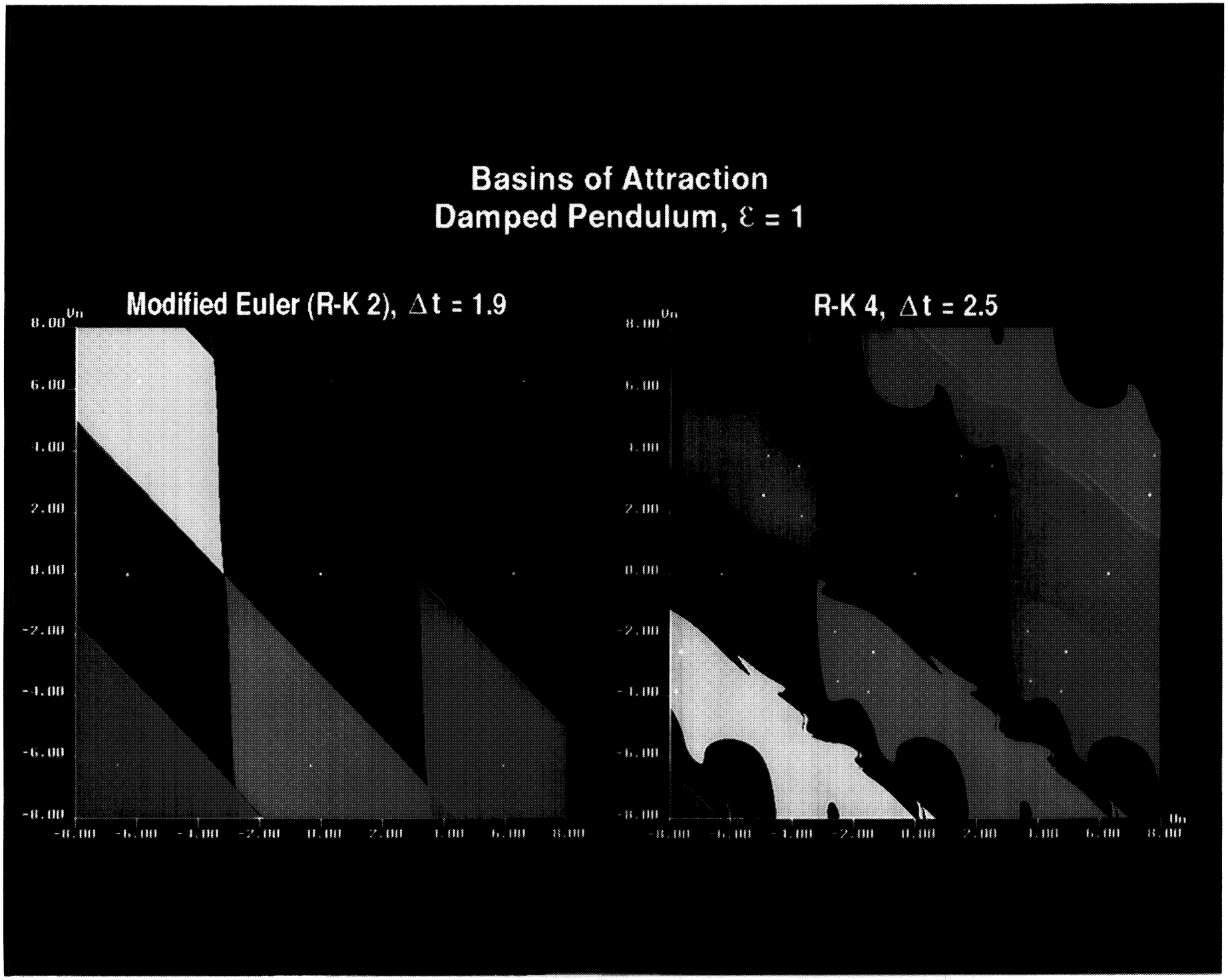
Basins of Attraction
Damped Pendulum, ε = 1
Modified Euler (R-K 2), Δt = 1.9
R-K 4, Δt = 2.5
8.00
6.00
4.00
2.00
0.00
-2.00
-4.00
-6.00
-8.00
-8.00 -6.00 -4.00 -2.00 0.00 2.00 4.00 6.00 8.00

Figure 6.16

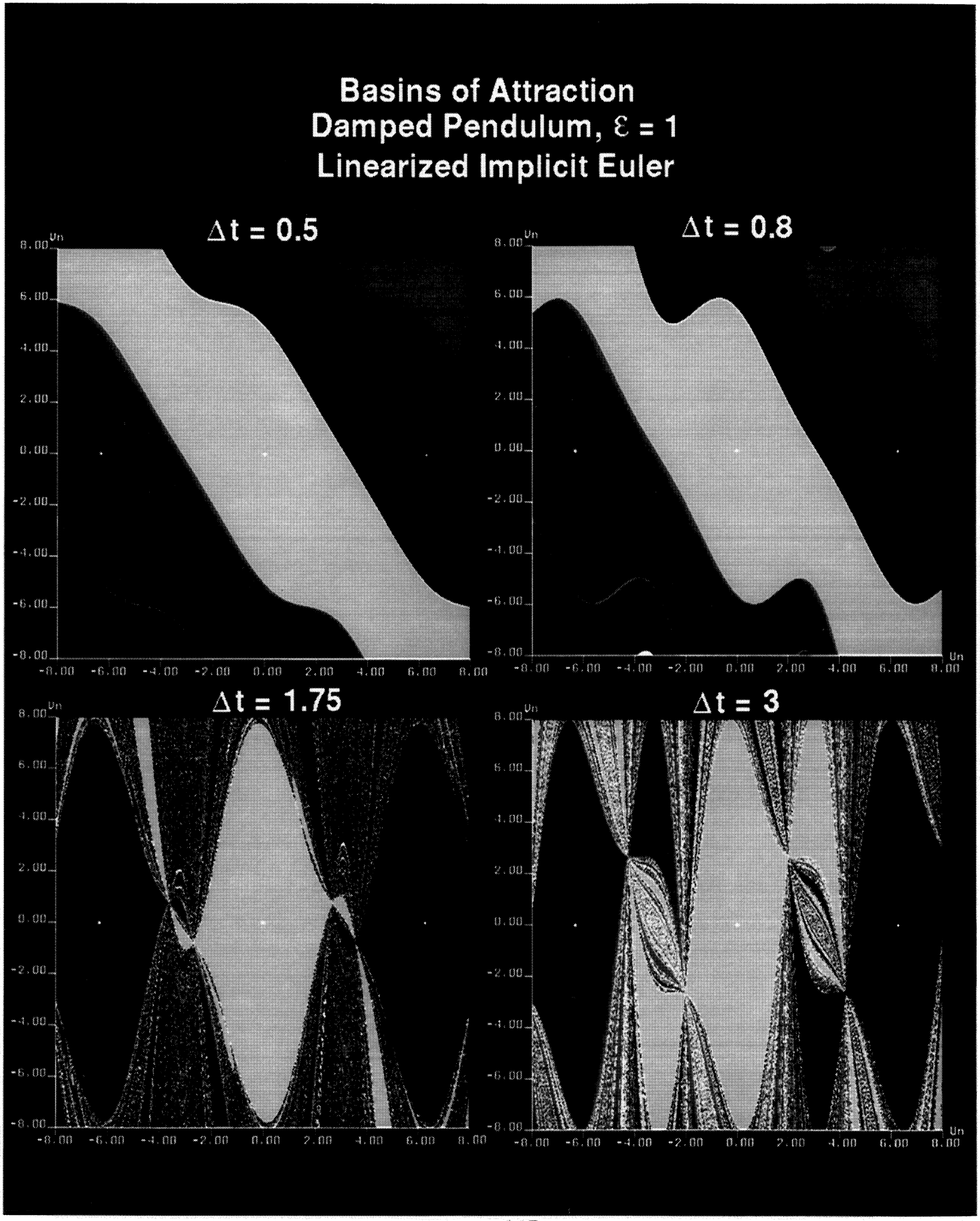
Basins of Attraction
Damped Pendulum, ε = 1
Linearized Implicit Euler
Δt = 0.5
Δt = 0.8
Δt = 1.75
Δt = 3
Vn
Un
8.00
6.00
4.00
2.00
0.00
-2.00
-4.00
-6.00
-8.00

Figure 6.17

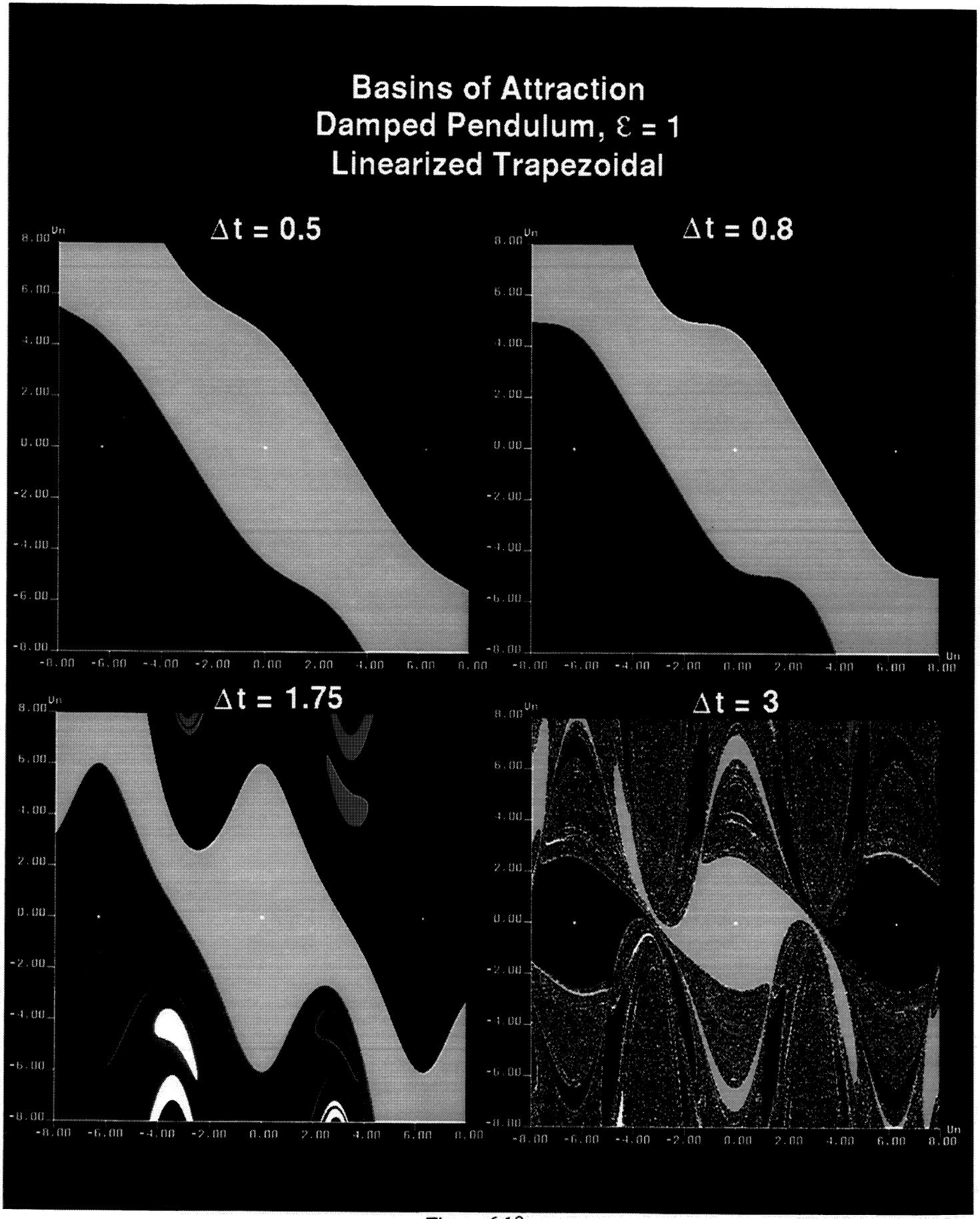
Basins of Attraction
Damped Pendulum, ε = 1
Linearized Trapezoidal
Δt = 0.5
Δt = 0.8
Δt = 1.75
Δt = 3
Vn
8.00
6.00
4.00
2.00
0.00
-2.00
-4.00
-6.00
-8.00
-8.00 -6.00 -4.00 -2.00 0.00 2.00 4.00 6.00 8.00

Figure 6.18

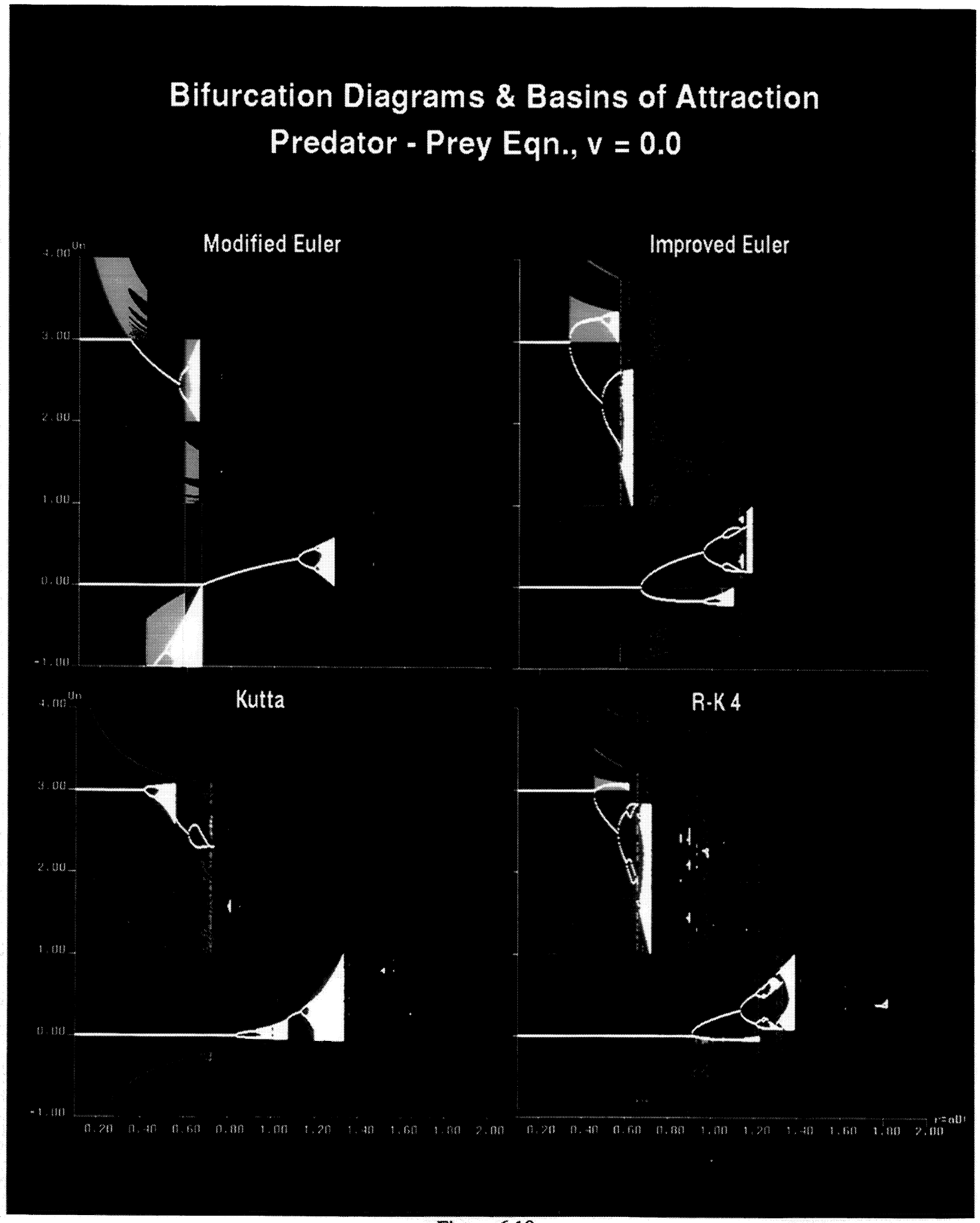
Bifurcation Diagrams & Basins of Attraction
Predator - Prey Eqn., v = 0.0
Modified Euler
Improved Euler
Kutta
R-K 4
4.00
3.00
2.00
1.00
0.00
-1.00
0.20
0.40
0.60
0.80
1.00
1.20
1.40
1.60
1.80
2.00

Figure 6.19

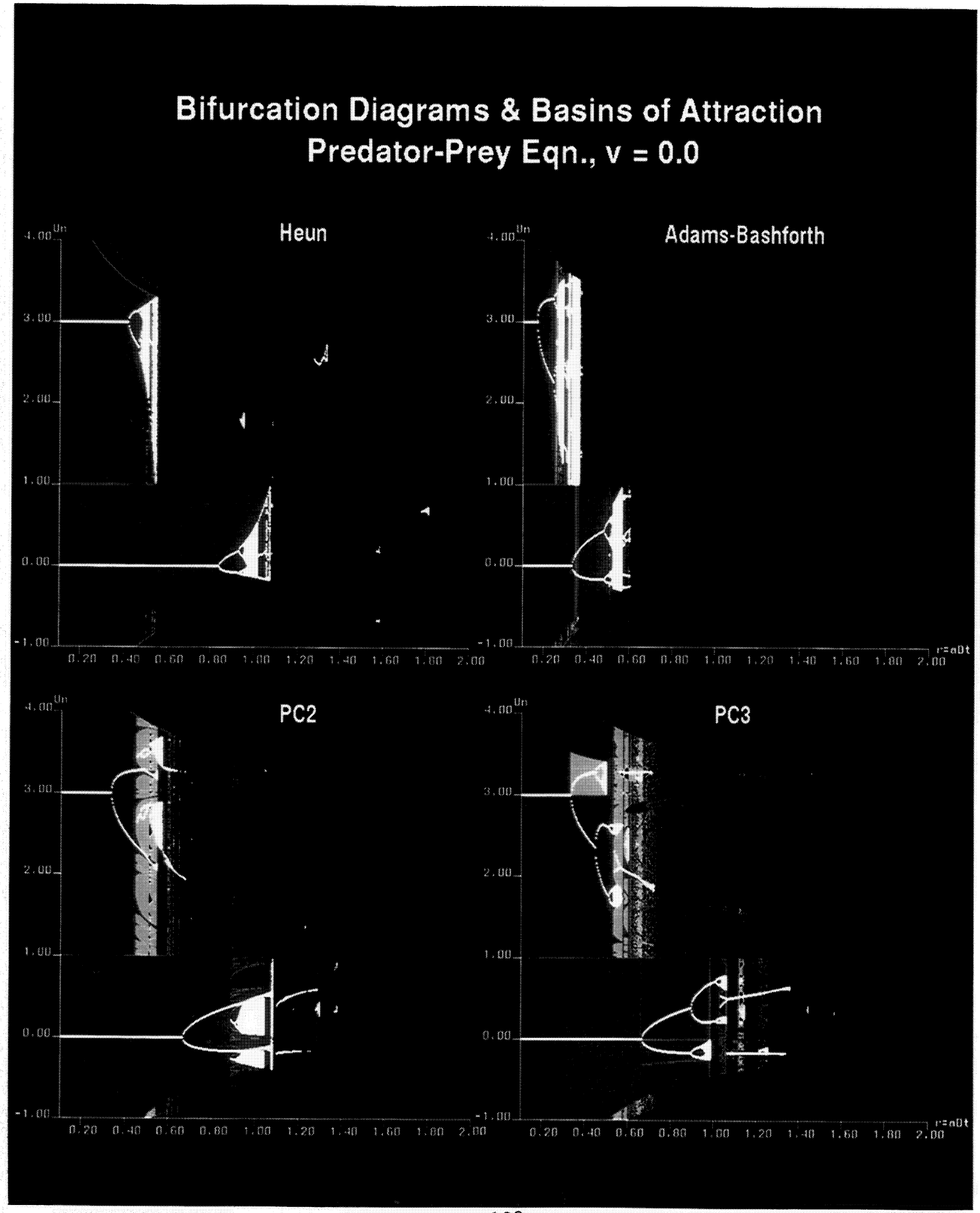
Bifurcation Diagrams & Basins of Attraction
Predator-Prey Eqn., v = 0.0
Heun
Adams-Bashforth
PC2
PC3
Un
r=aDt
4.00
3.00
2.00
1.00
0.00
-1.00
0.20
0.40
0.60
0.80
1.00
1.20
1.40
1.60
1.80
2.00

Figure 6.20

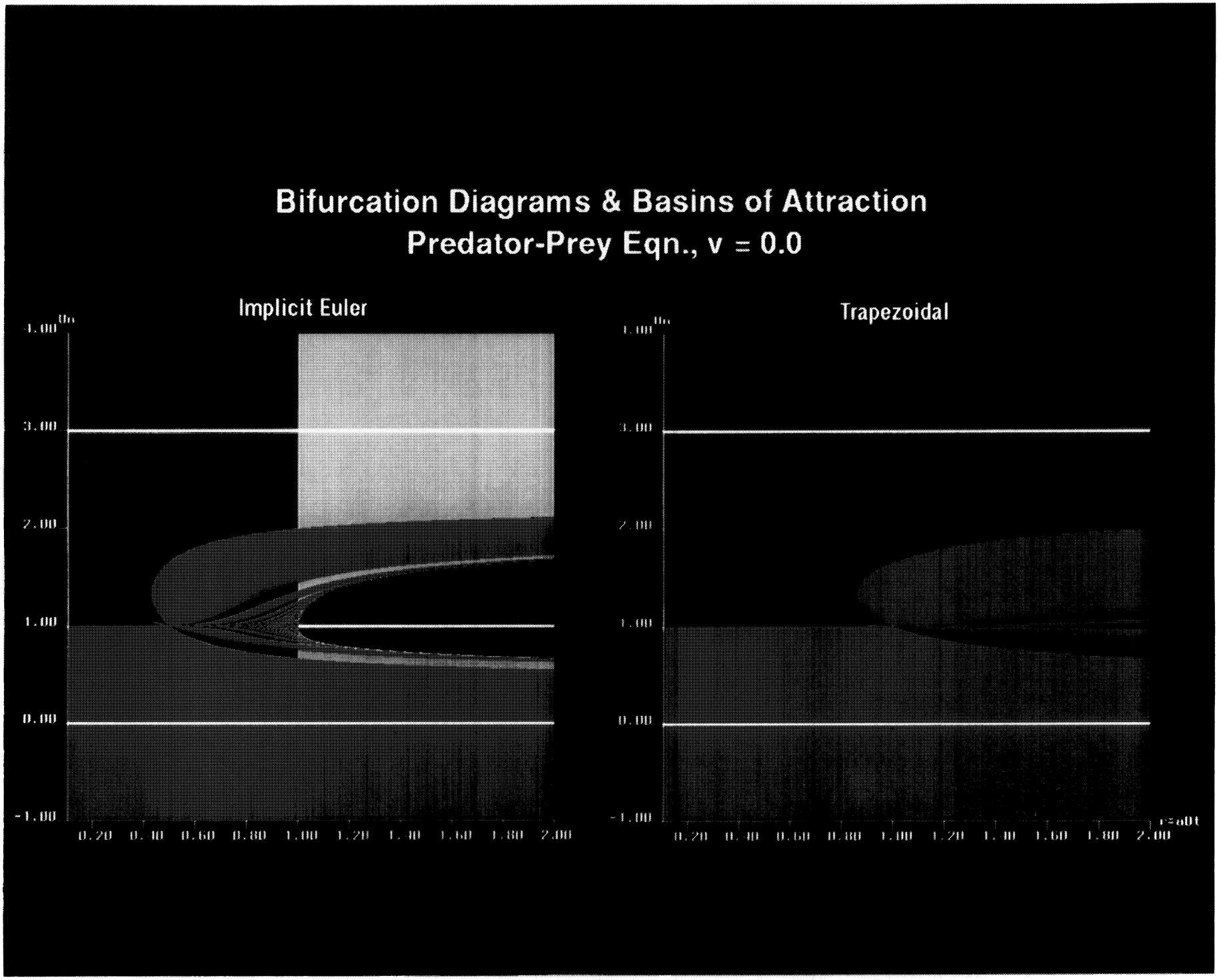
Bifurcation Diagrams & Basins of Attraction
Predator-Prey Eqn., v = 0.0
Implicit Euler
Trapezoidal
4.00
3.00
2.00
1.00
0.00
-1.00
0.20
0.40
0.60
0.80
1.00
1.20
1.40
1.60
1.80
2.00

Figure 6.21

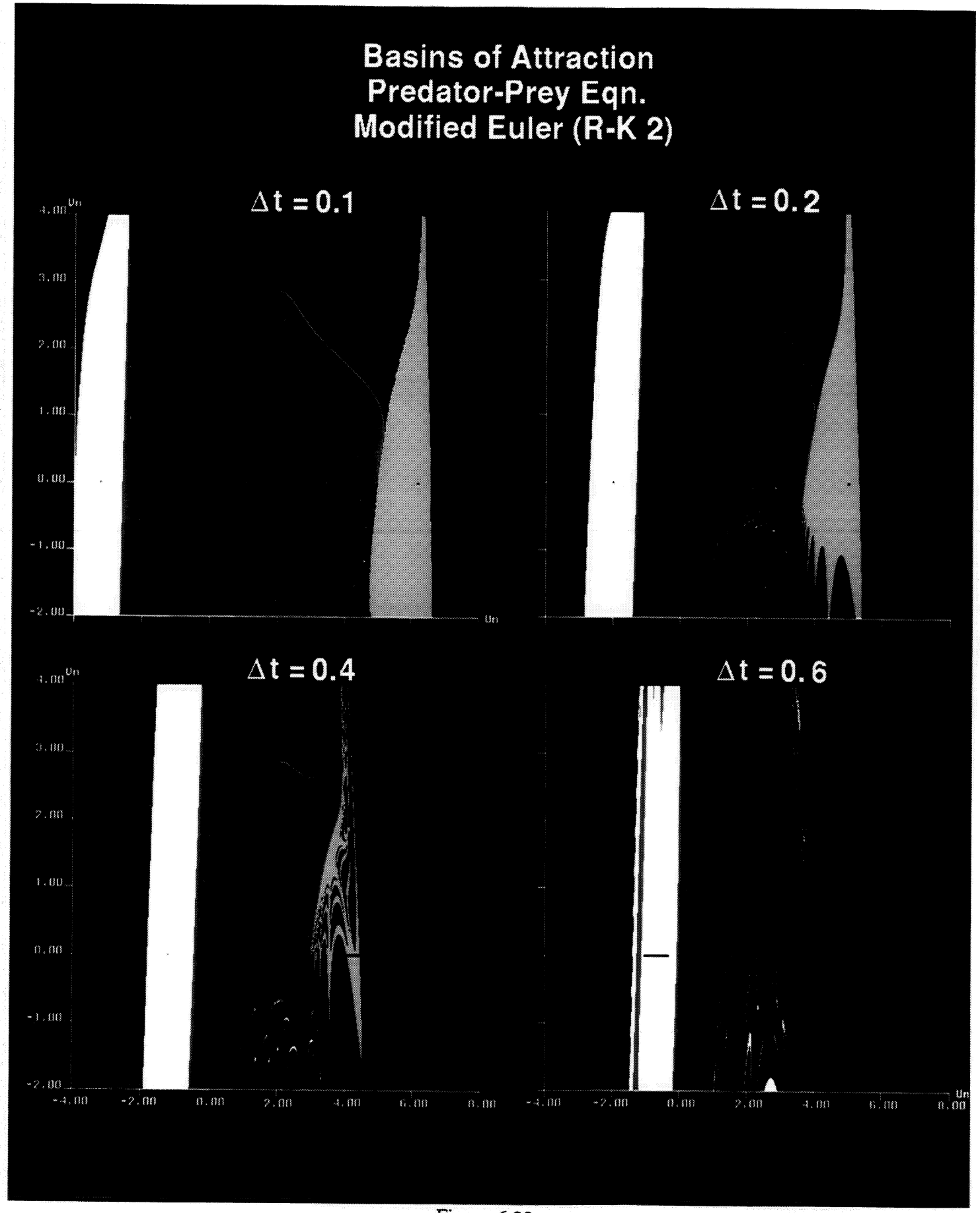
Basins of Attraction
Predator-Prey Eqn.
Modified Euler (R-K 2)
Δt = 0.1
Δt = 0.2
Δt = 0.4
Δt = 0.6
4.00
3.00
2.00
1.00
0.00
-1.00
-2.00
-4.00
-2.00
0.00
2.00
4.00
6.00
8.00

Figure 6.22

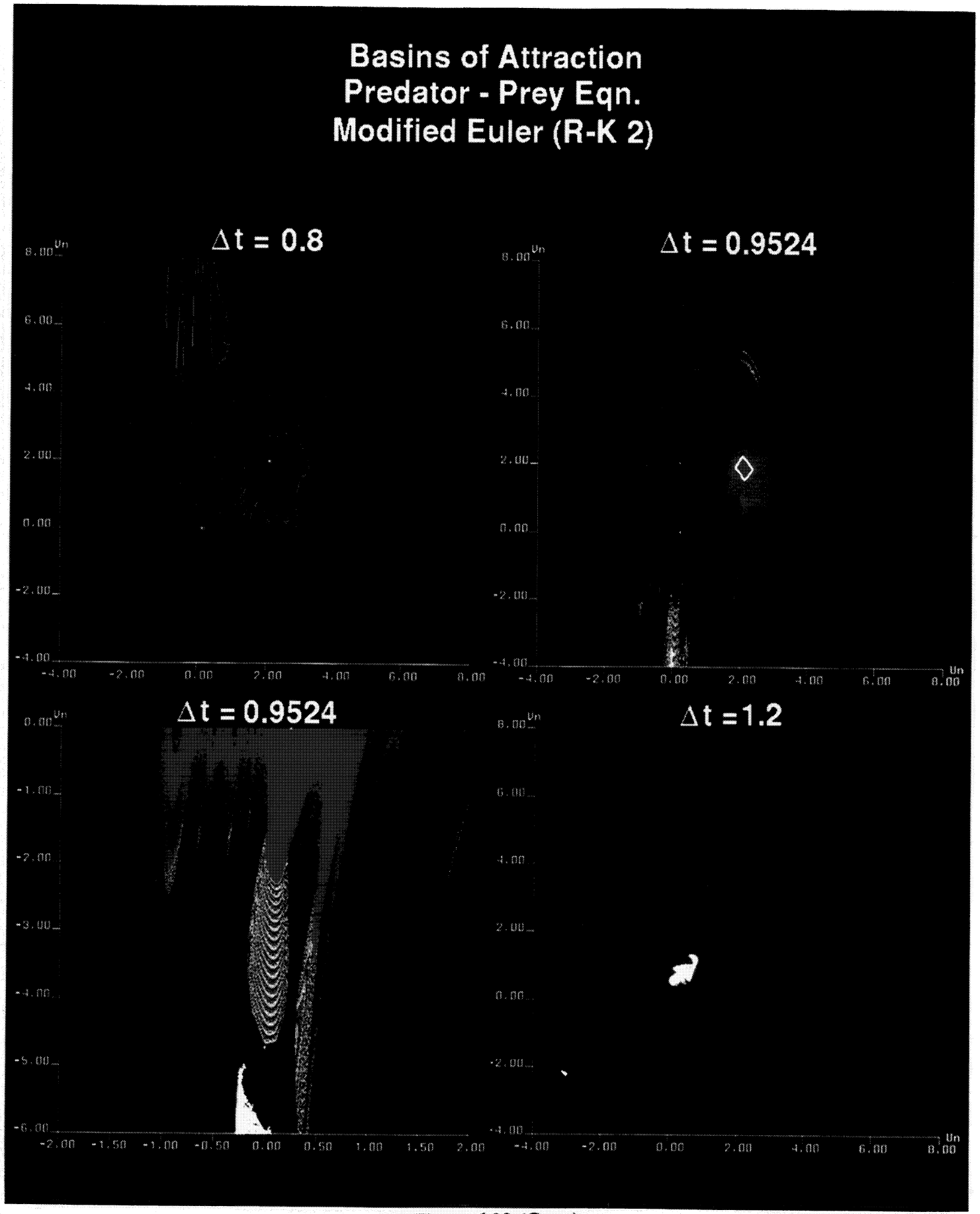

Figure 6.22 (Cont.)

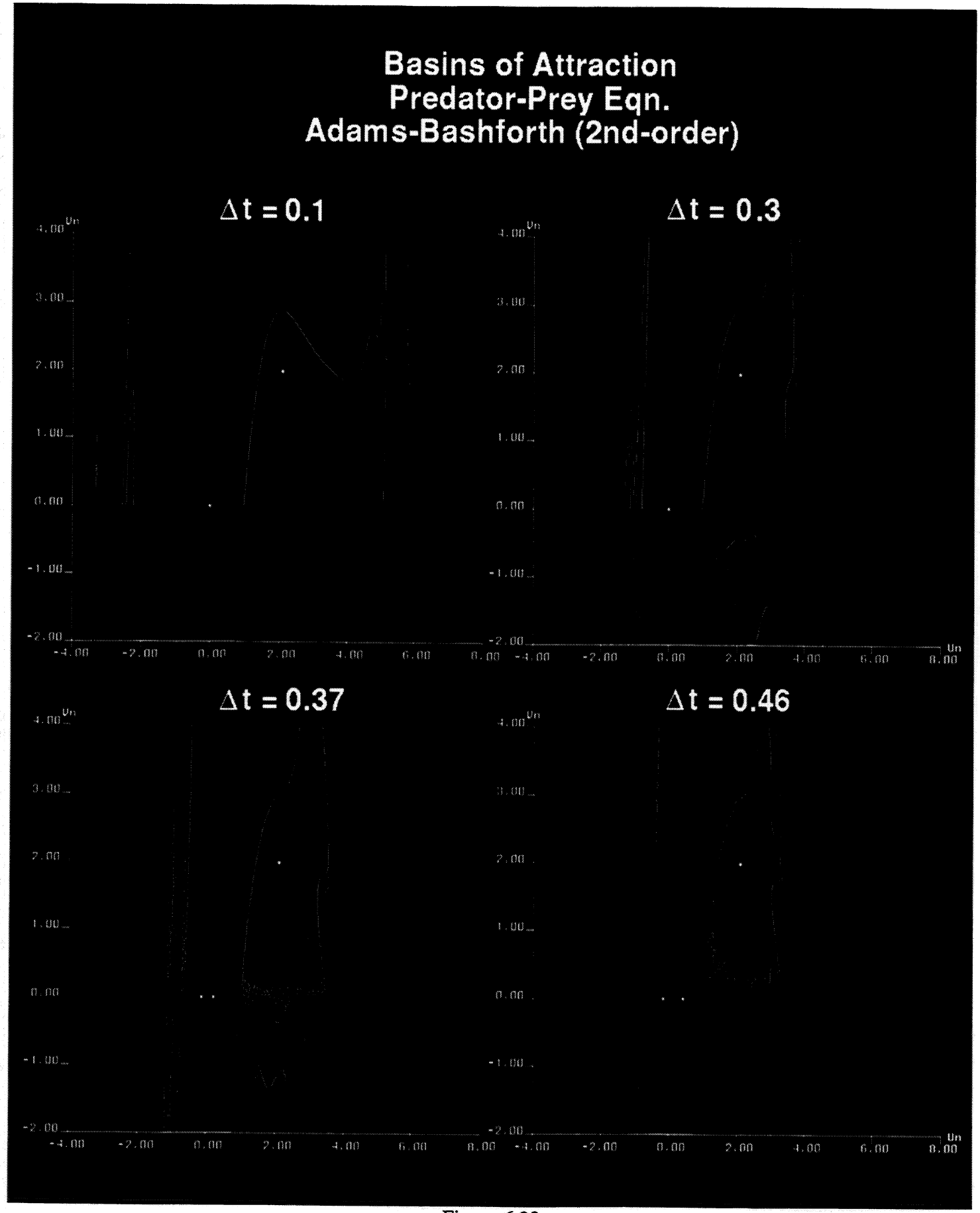
Basins of Attraction
Predator-Prey Eqn.
Adams-Bashforth (2nd-order)
Δt = 0.1
Δt = 0.3
Δt = 0.37
Δt = 0.46
Un
4.00
3.00
2.00
1.00
0.00
-1.00
-2.00
-4.00
-2.00
0.00
2.00
4.00
6.00
8.00

Figure 6.23

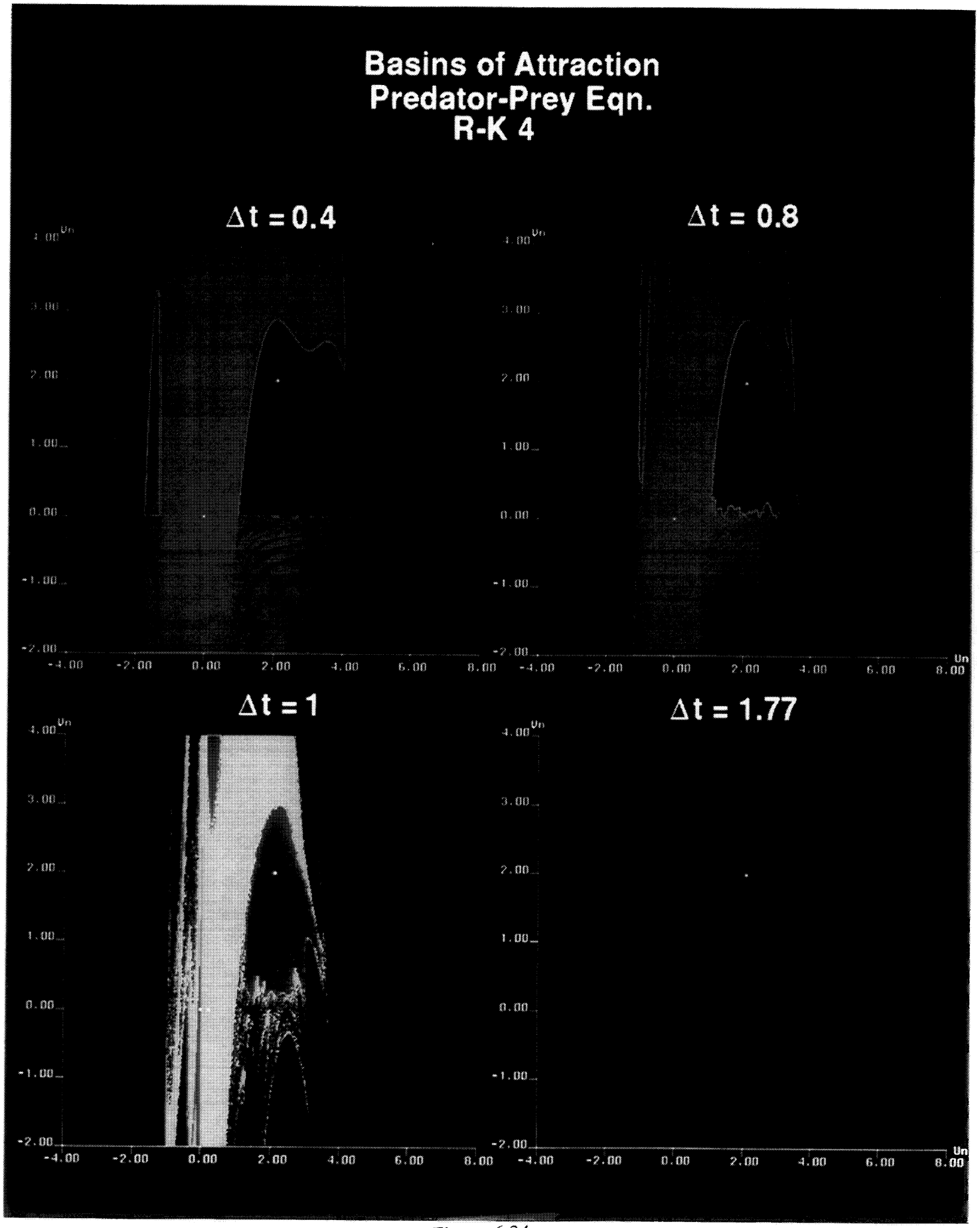
Basins of Attraction
Predator-Prey Eqn.
R-K 4
Δt = 0.4
Δt = 0.8
Δt = 1
Δt = 1.77
Un
4.00
3.00
2.00
1.00
0.00
-1.00
-2.00
-4.00
-2.00
0.00
2.00
4.00
6.00
8.00

Figure 6.24

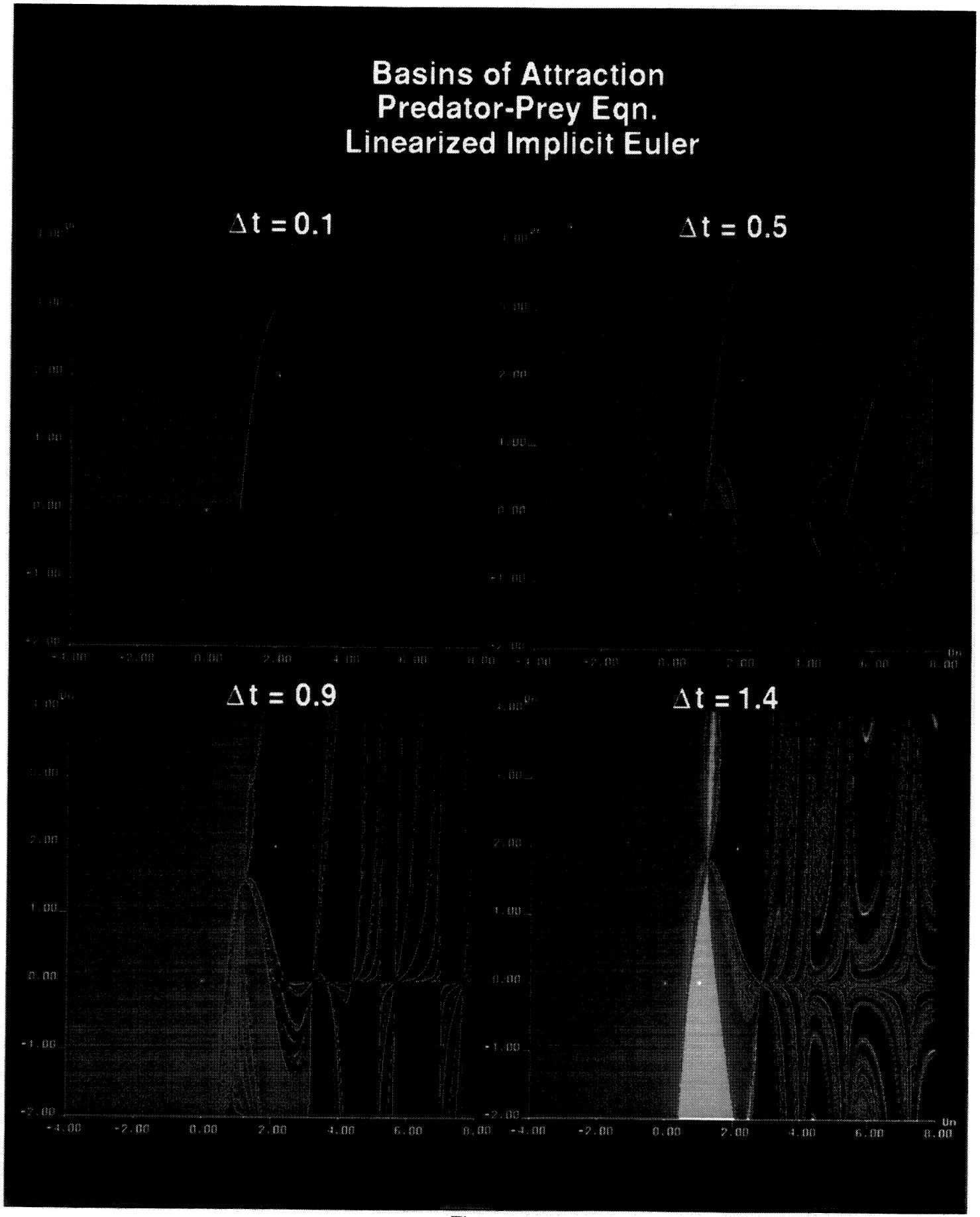
Basins of Attraction
Predator-Prey Eqn.
Linearized Implicit Euler
Δt = 0.1
Δt = 0.5
Δt = 0.9
Δt = 1.4

Figure 6.25

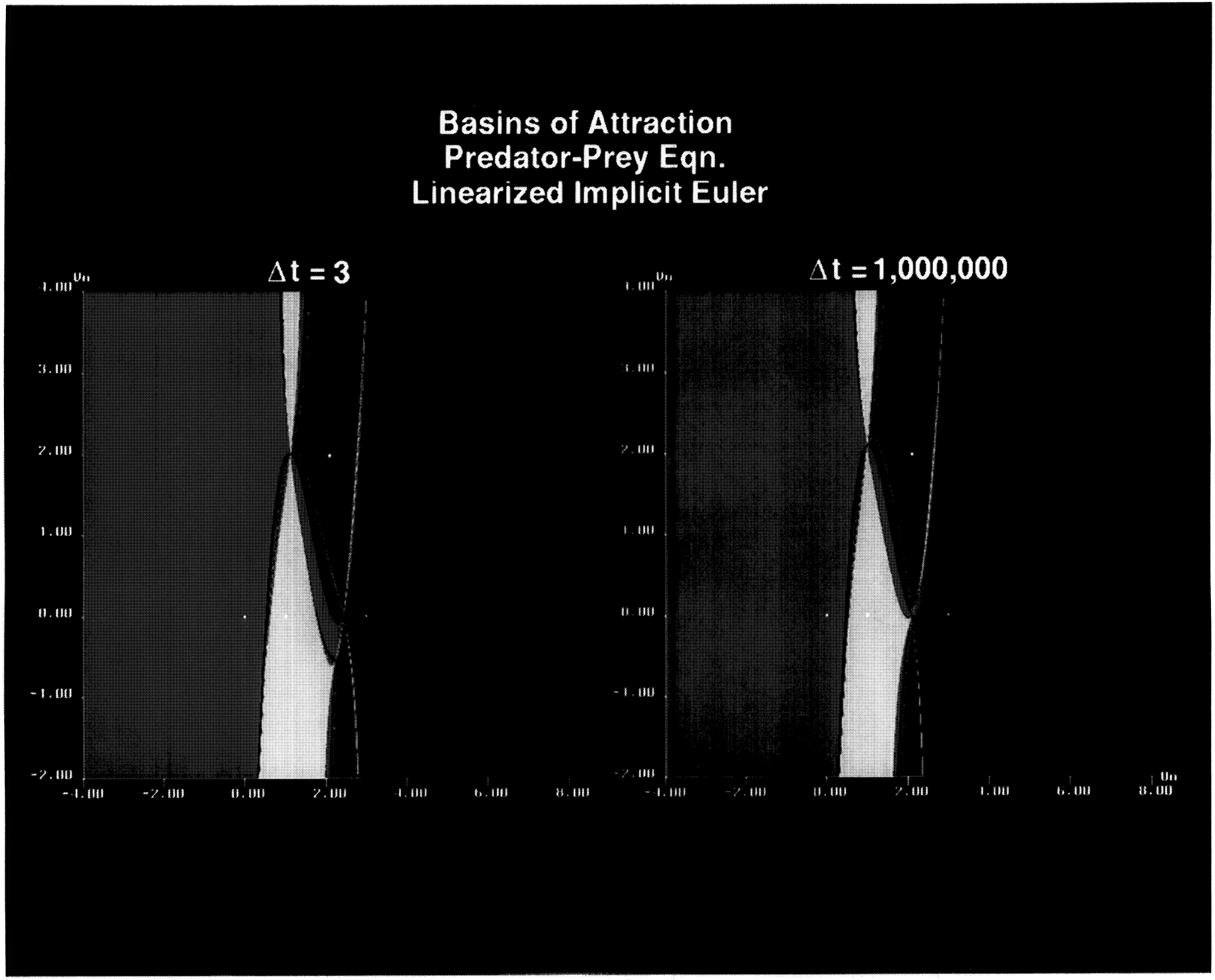

Figure 6.25 (Cont.)

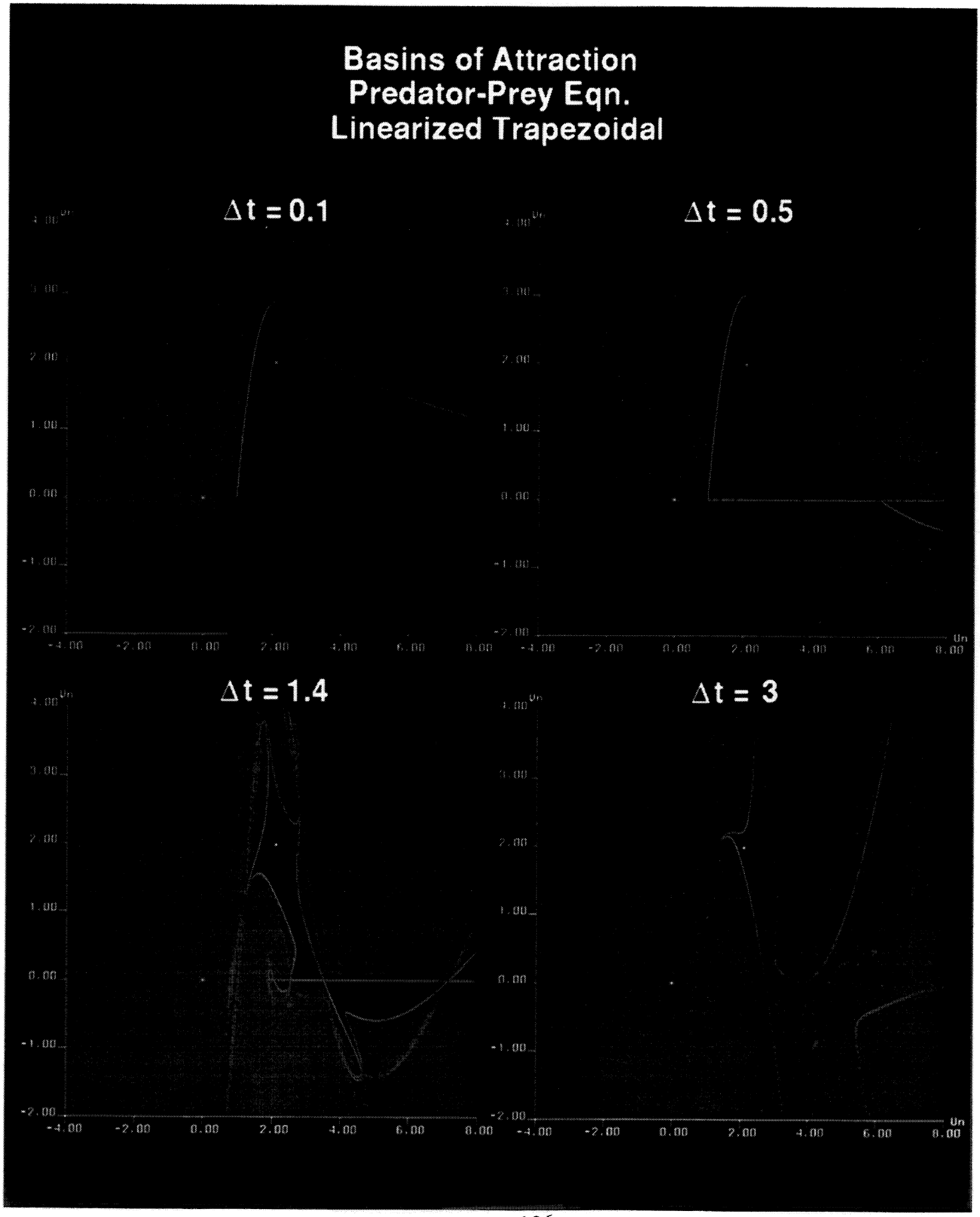
Basins of Attraction
Predator-Prey Eqn.
Linearized Trapezoidal
Δt = 0.1
Δt = 0.5
Δt = 1.4
Δt = 3
Un
4.00
3.00
2.00
1.00
0.00
-1.00
-2.00
-4.00
-2.00
0.00
2.00
4.00
6.00
8.00

Figure 6.26

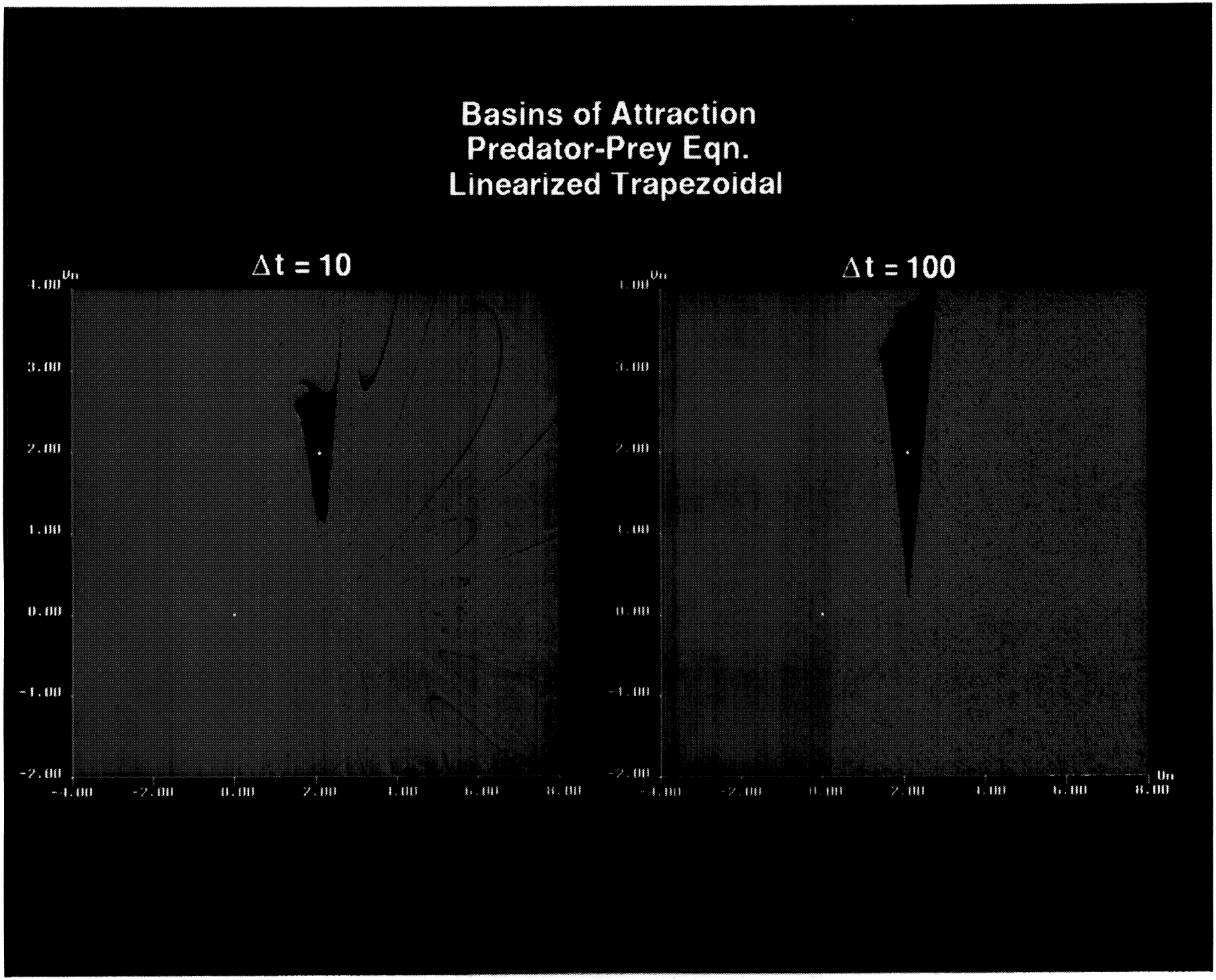

Figure 6.26 (Cont.)

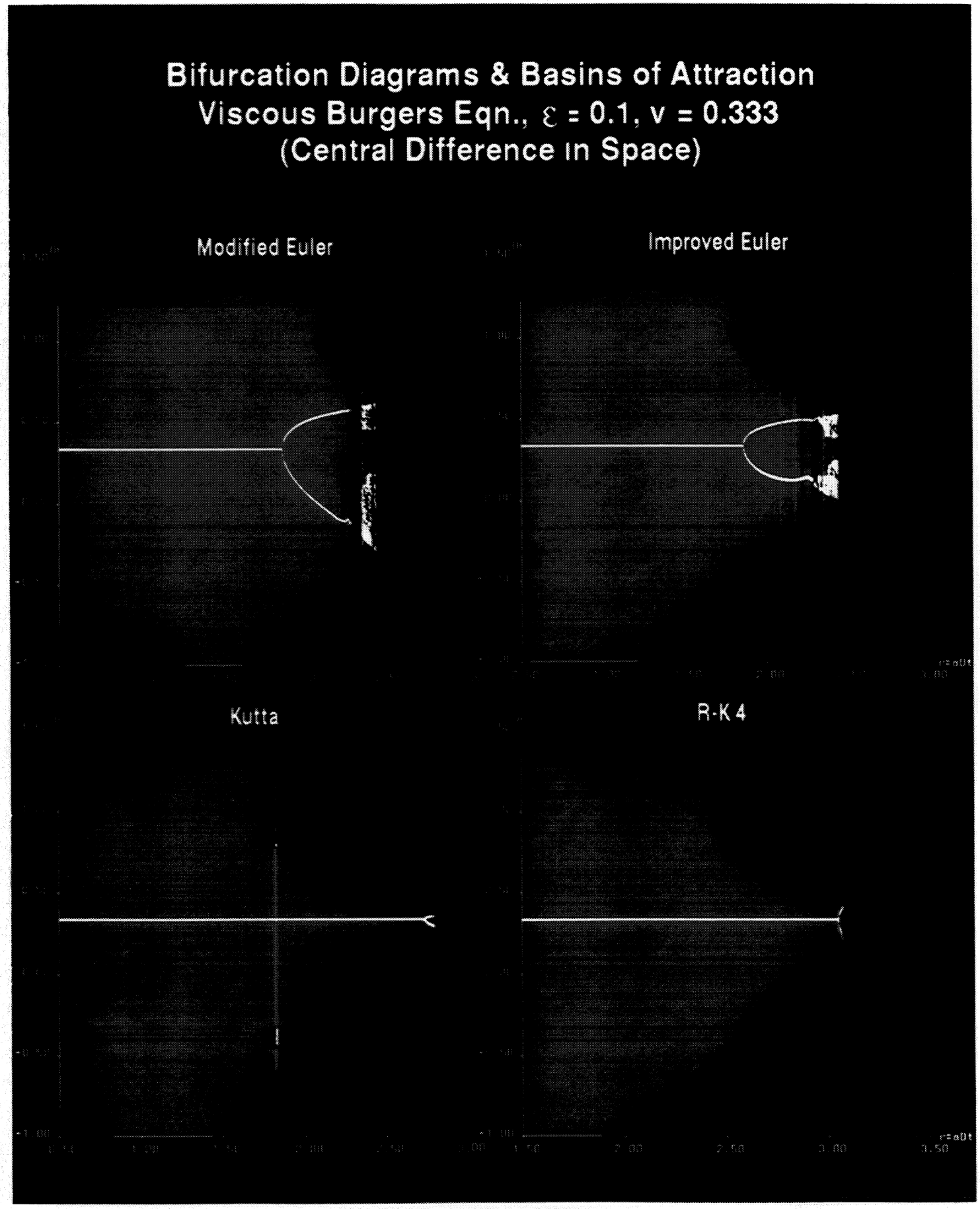
Bifurcation Diagrams & Basins of Attraction
Viscous Burgers Eqn., ε = 0.1, v = 0.333
(Central Difference in Space)
Modified Euler
Improved Euler
Kutta
R-K 4

Figure 6.27

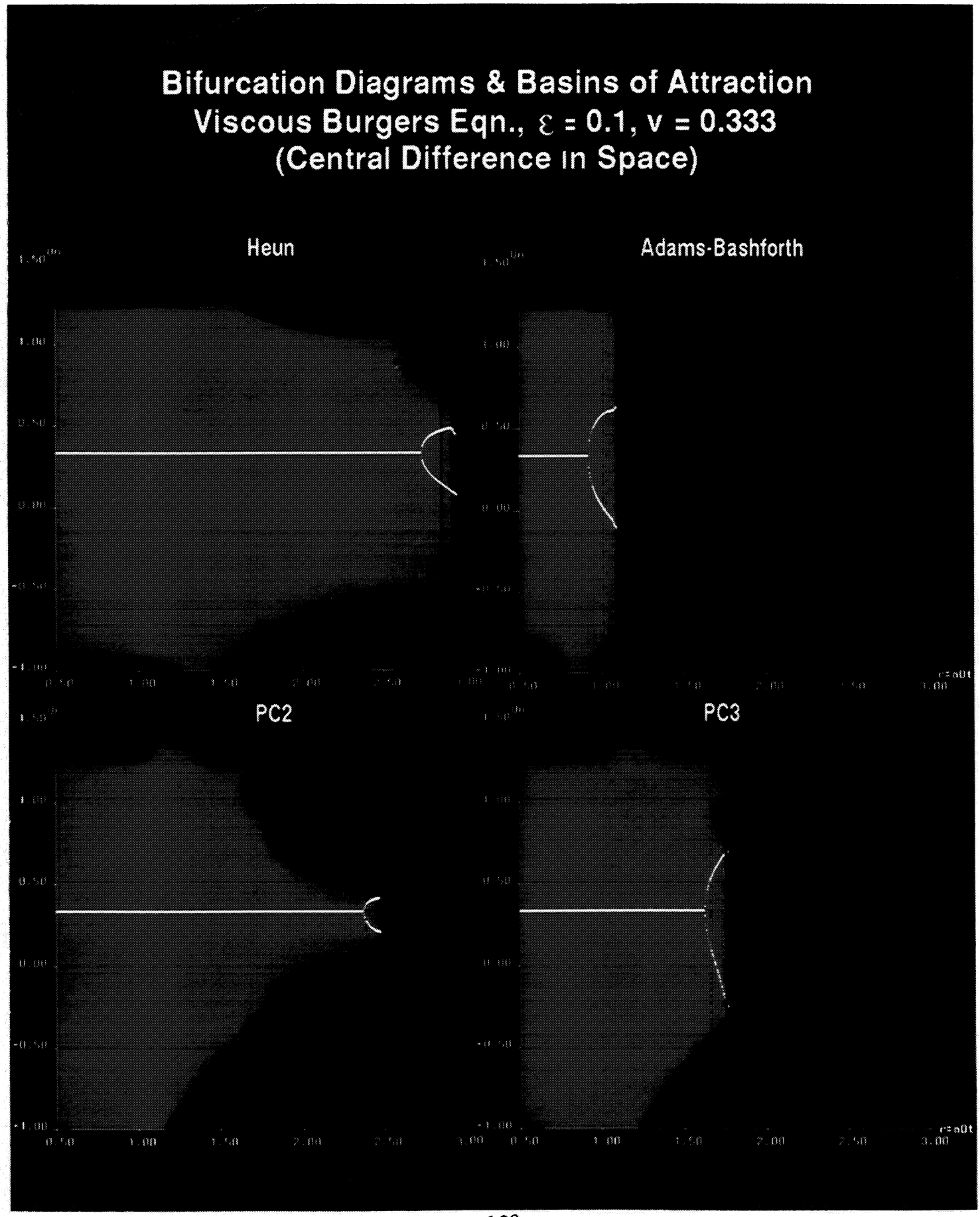
Bifurcation Diagrams & Basins of Attraction
Viscous Burgers Eqn., ε = 0.1, v = 0.333
(Central Difference in Space)
Heun
Adams-Bashforth
PC2
PC3

Figure 6.28

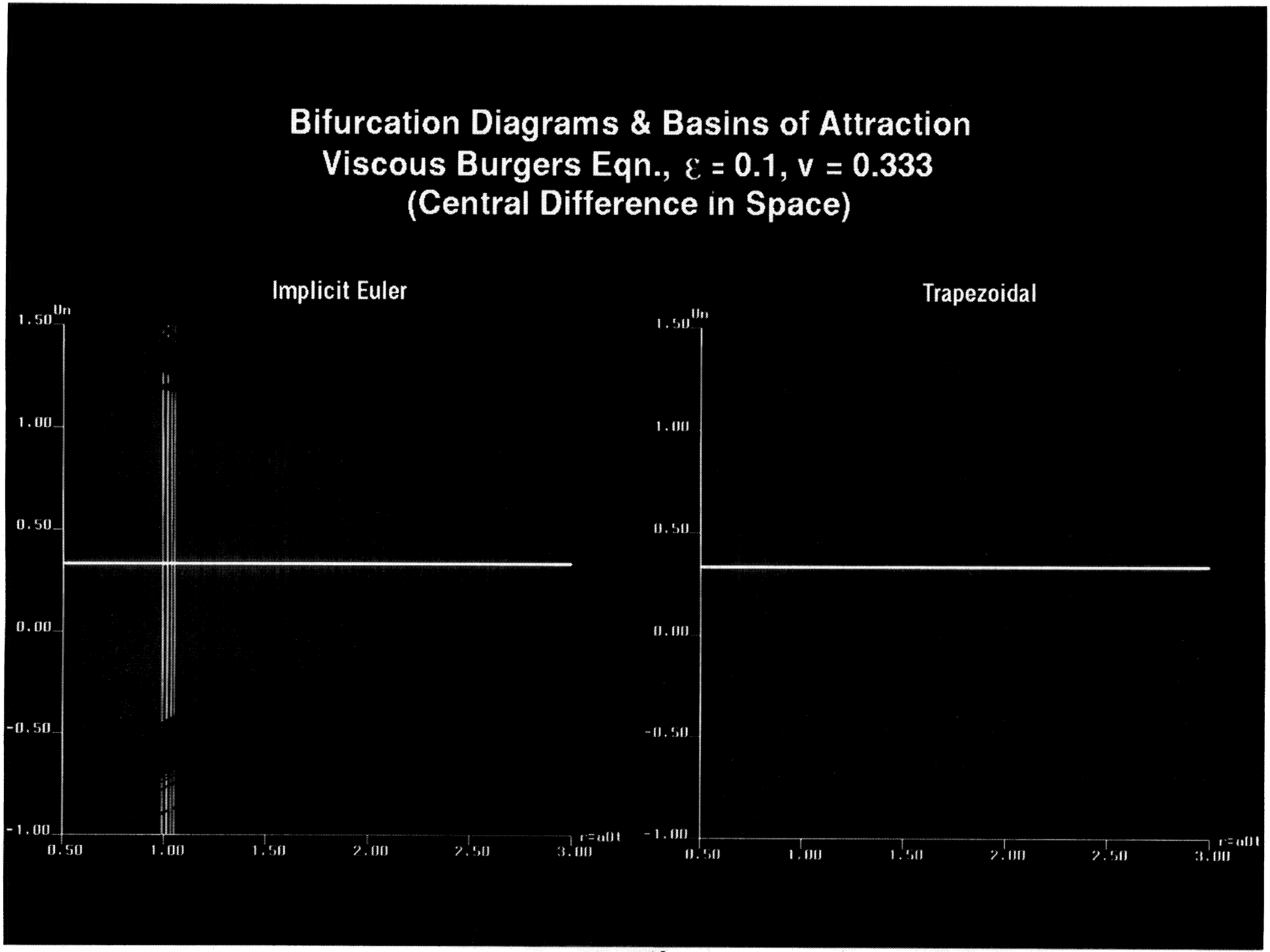
Bifurcation Diagrams & Basins of Attraction
Viscous Burgers Eqn., ε = 0.1, v = 0.333
(Central Difference in Space)
Implicit Euler
Trapezoidal
Un
1.50
1.00
0.50
0.00
-0.50
-1.00
0.50
1.00
1.50
2.00
2.50
3.00

Figure 6.29

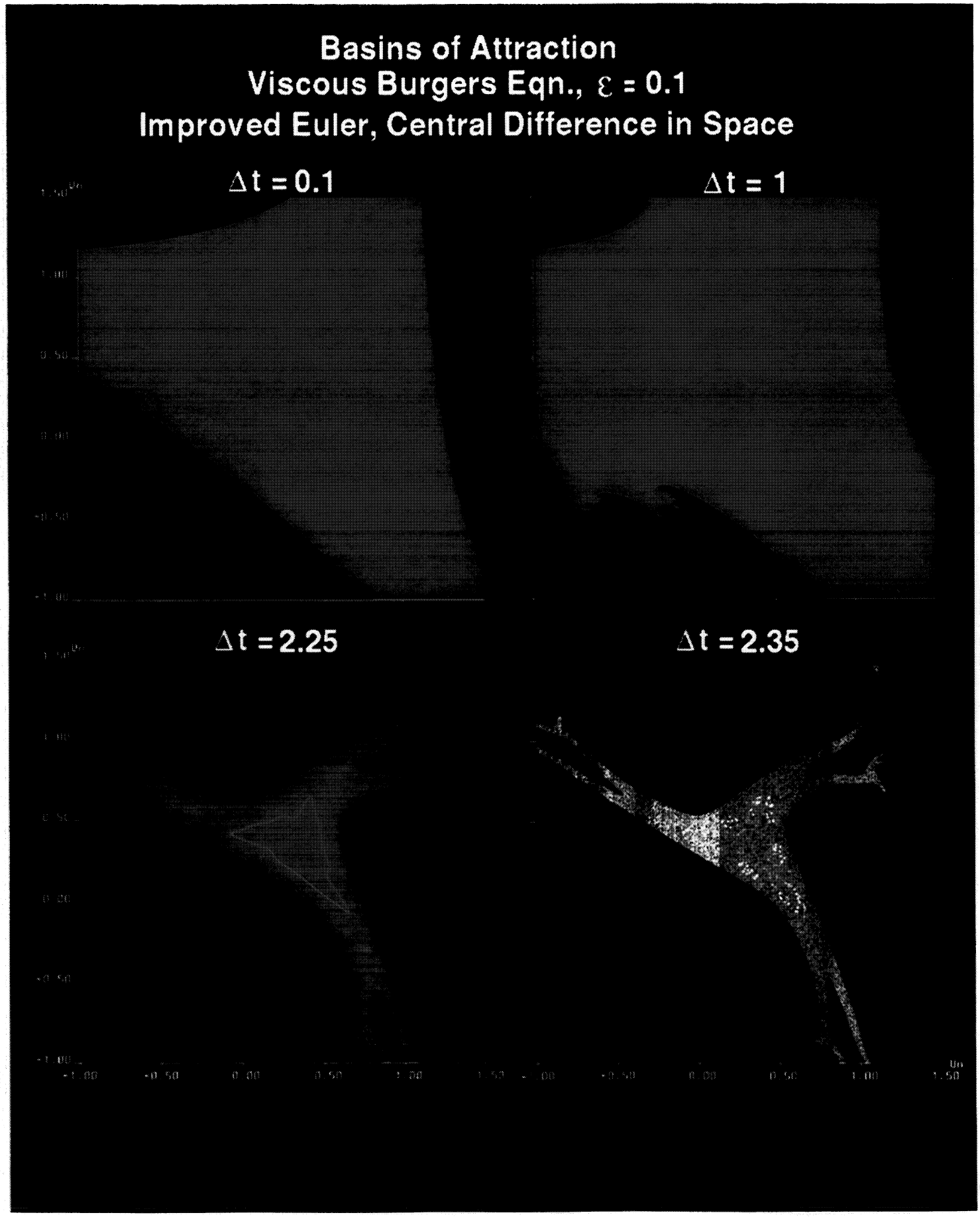
Basins of Attraction
Viscous Burgers Eqn., ε = 0.1
Improved Euler, Central Difference in Space
Δt = 0.1
Δt = 1
Δt = 2.25
Δt = 2.35

Figure 6.30

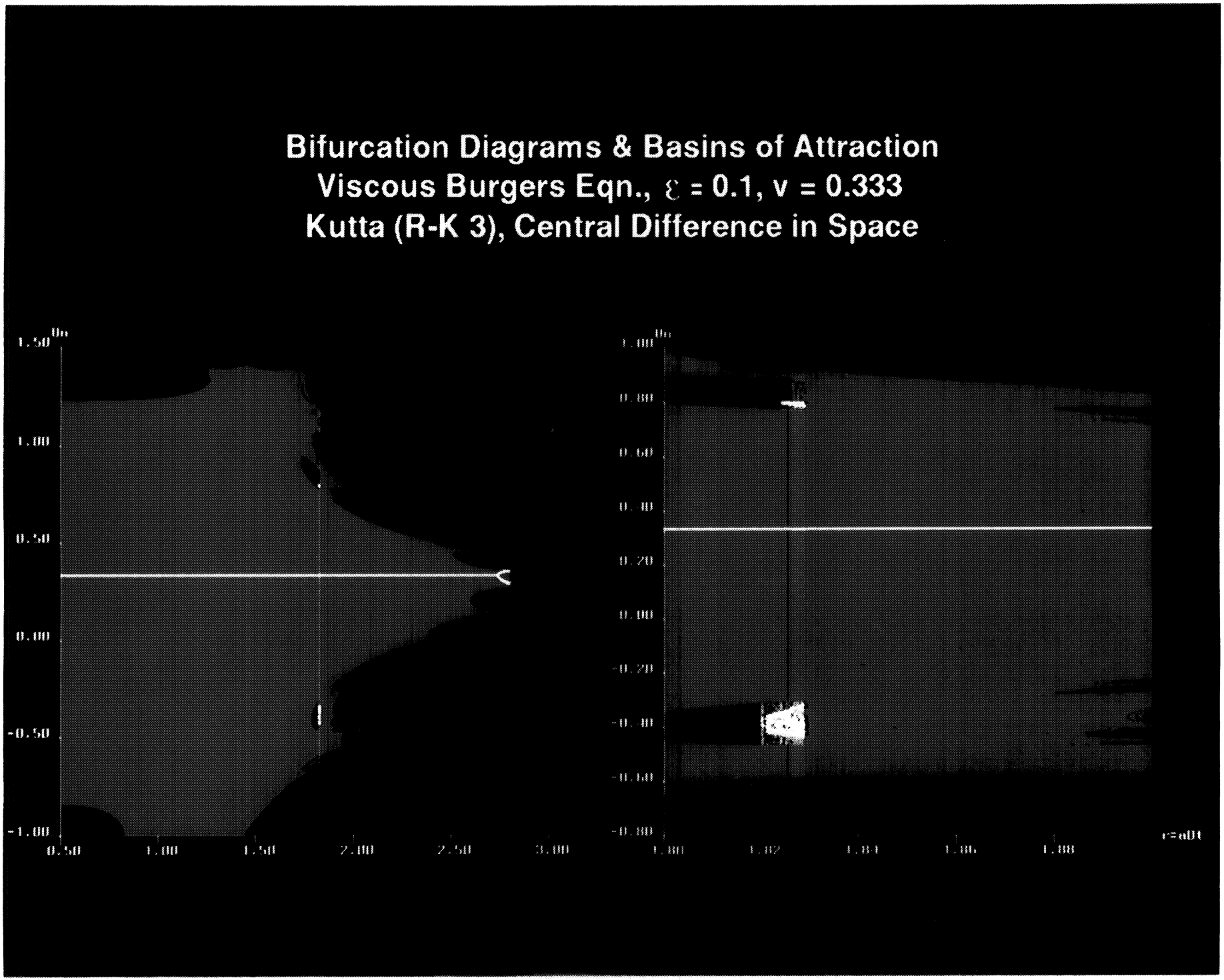
Bifurcation Diagrams & Basins of Attraction
Viscous Burgers Eqn., ε = 0.1, v = 0.333
Kutta (R-K 3), Central Difference in Space
1.50
1.00
0.50
0.00
-0.50
-1.00
0.50
1.00
1.50
2.00
2.50
3.00
1.00
0.80
0.60
0.40
0.20
0.00
-0.20
-0.40
-0.60
-0.80
1.80
1.82
1.84
1.86
1.88
r=a0t

Figure 6.31

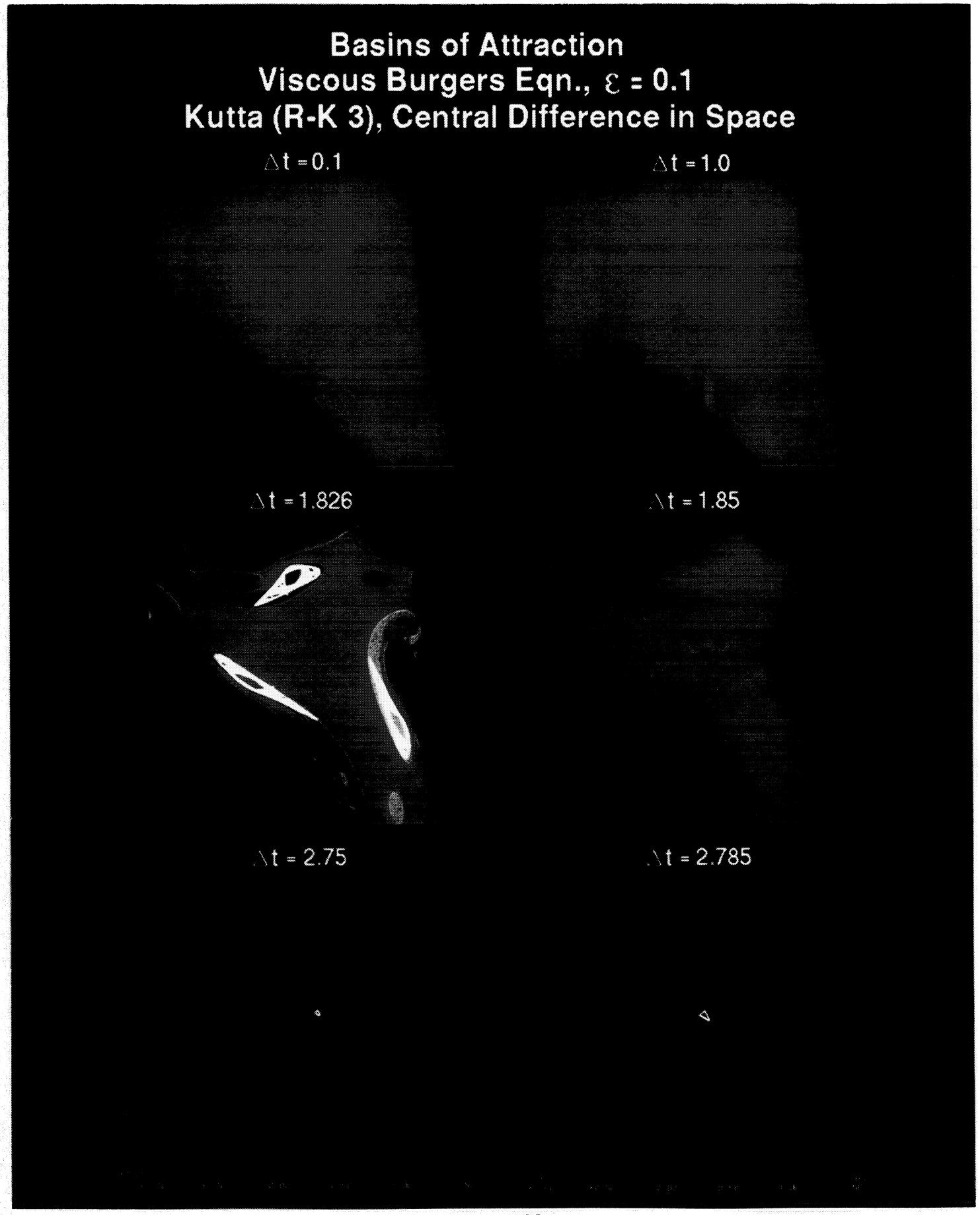
Basins of Attraction
Viscous Burgers Eqn., ε = 0.1
Kutta (R-K 3), Central Difference in Space
Δt = 0.1
Δt = 1.0
Δt = 1.826
Δt = 1.85
Δt = 2.75
Δt = 2.785

Figure 6.32

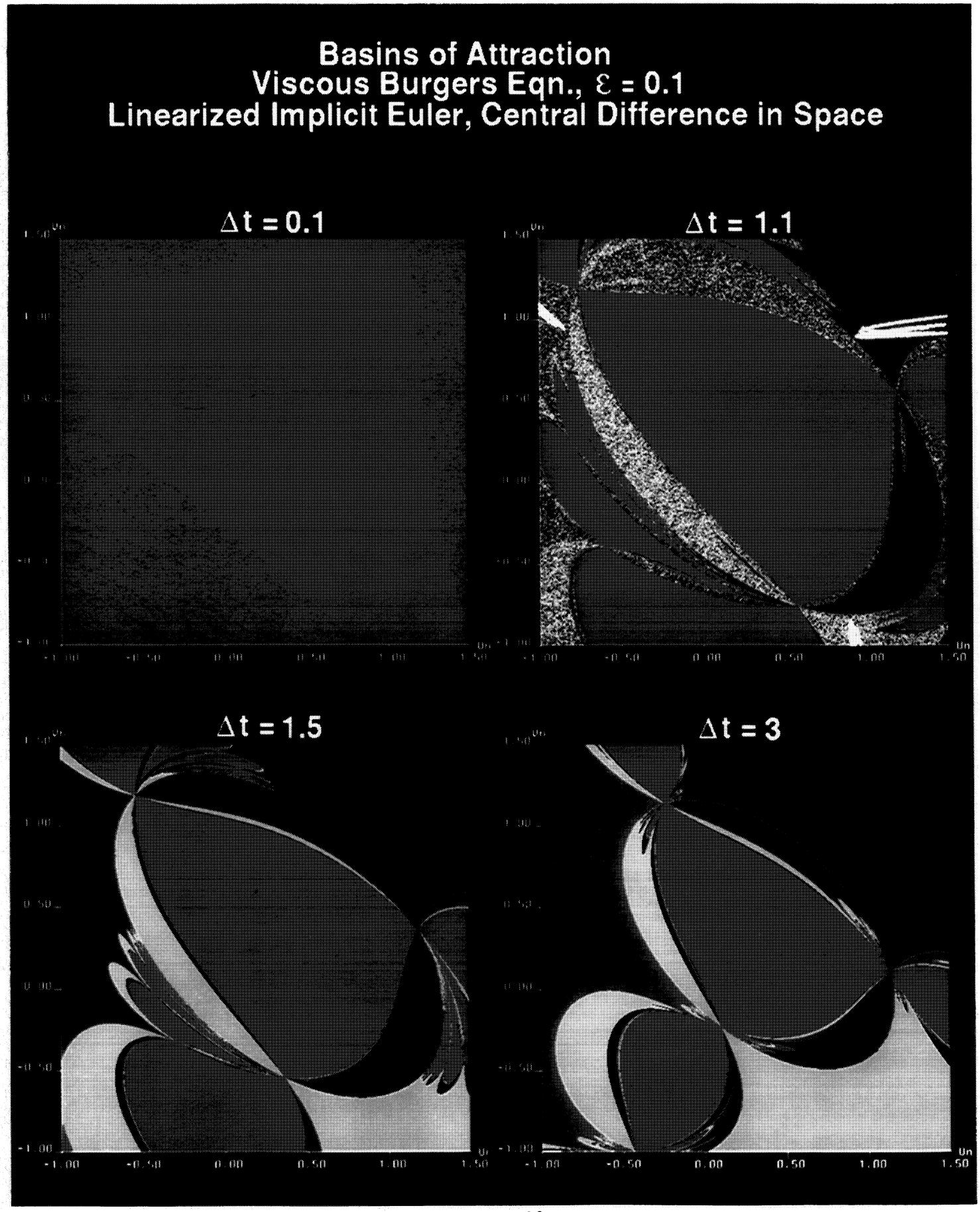
Basins of Attraction
Viscous Burgers Eqn., ε = 0.1
Linearized Implicit Euler, Central Difference in Space
Δt = 0.1
Δt = 1.1
Δt = 1.5
Δt = 3
Un
-1.00
-0.50
0.00
0.50
1.00
1.50

Figure 6.33

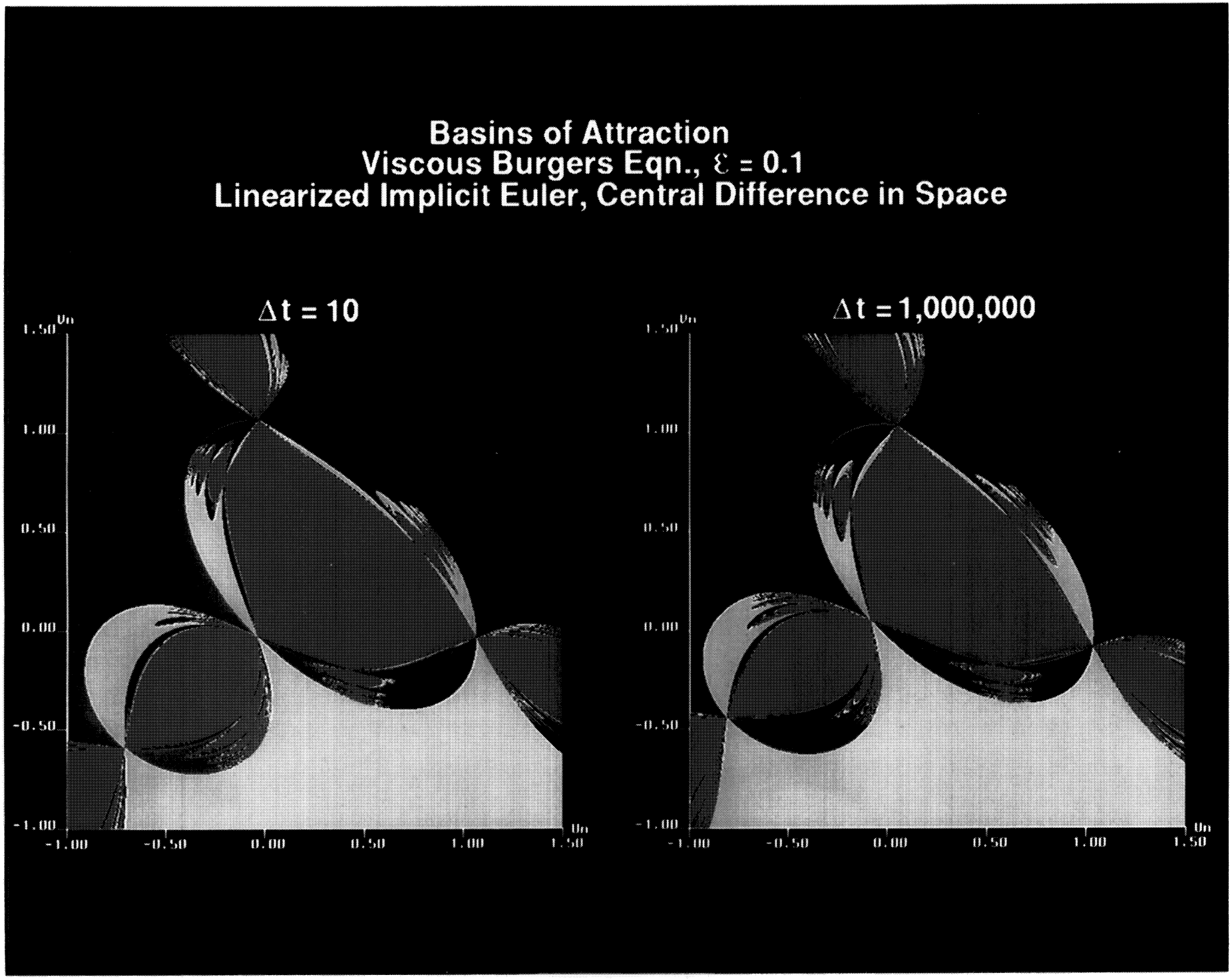

Figure 6.33 (Cont.)

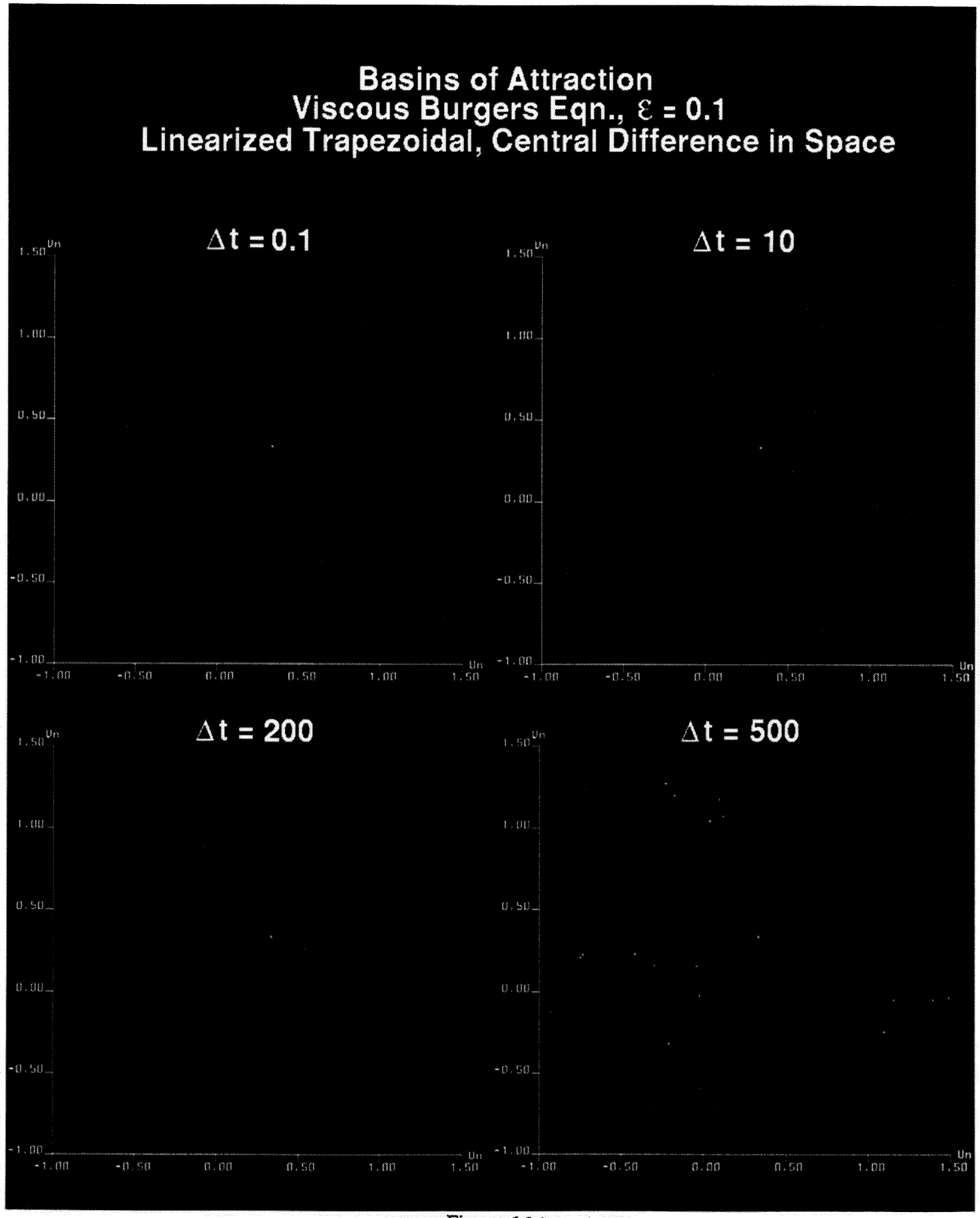
Basins of Attraction
Viscous Burgers Eqn., ε = 0.1
Linearized Trapezoidal, Central Difference in Space
Δt = 0.1
Δt = 10
Δt = 200
Δt = 500
Un
1.50
1.00
0.50
0.00
-0.50
-1.00
-1.00
-0.50
0.00
0.50
1.00
1.50

Figure 6.34

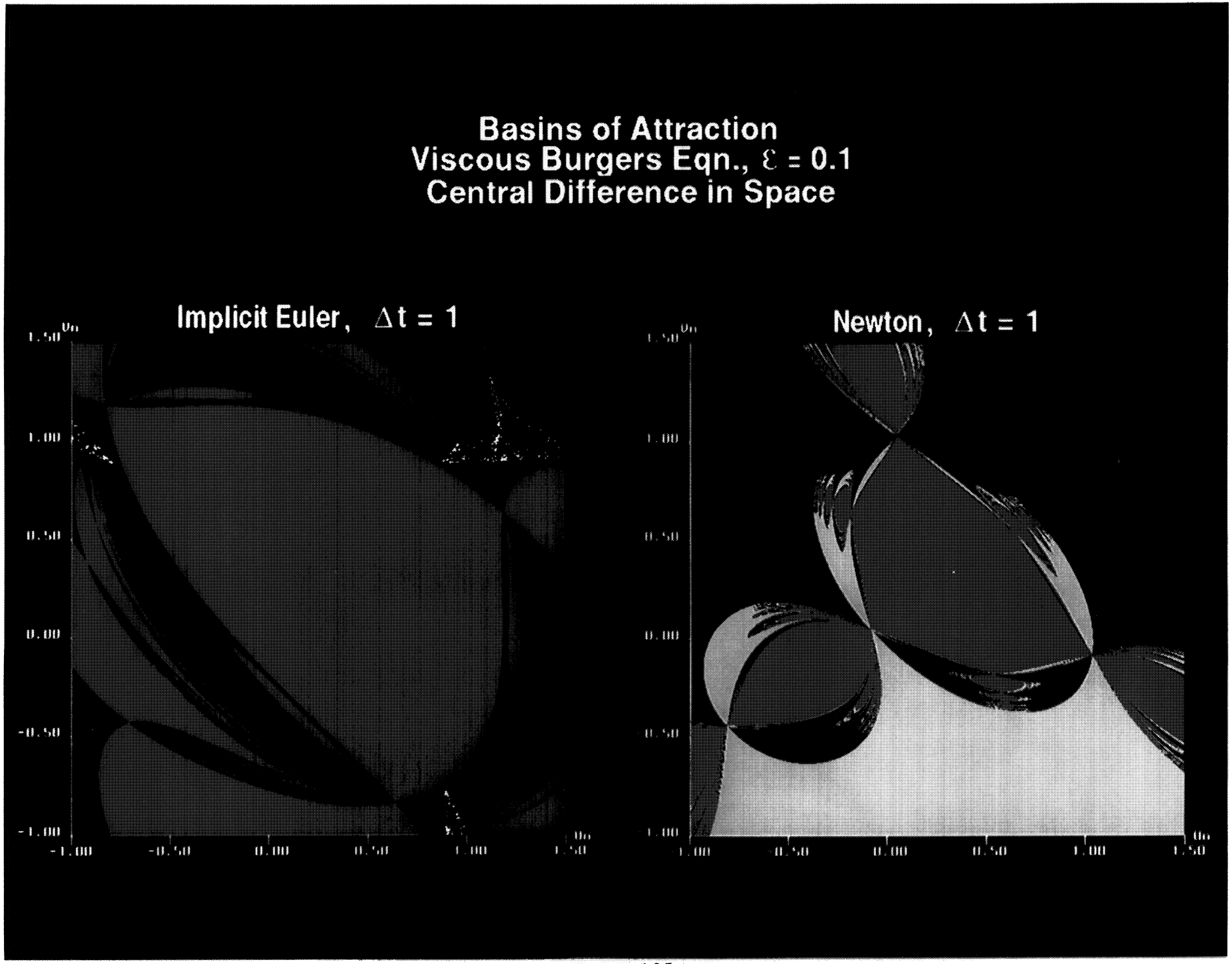
Basins of Attraction
Viscous Burgers Eqn., ε = 0.1
Central Difference in Space
Implicit Euler, Δt = 1
Newton, Δt = 1

Figure 6.35